SPACECRAFT RADIATORS FOR ADVANCED MISSION REQUIREMENTS

REPORT NO. 2-30320/9R-52212
23 APRIL 1980

FINAL REPORT
TASK 3.7
CONTRACT NAS9-14776

SUBMITTED TO
NATIONAL AERONAUTICS AND SPACE ADMINISTRATION
JOHNSON SPACE CENTER
HOUSTON, TEXAS

By
VOUGHT CORPORATION
P.O. BOX 225907
DALLAS, TEXAS 75265

VOUGHT CORPORATION

SPACECRAFT RADIATORS FOR ADVANCED MISSION REQUIREMENTS

REPORT NO. 2-30320/9R-52212

23 APRIL 1980

FINAL REPORT
TASK 3.7

CONTRACT NAS9-14776

SUBMITTED TO

NATIONAL AERONAUTICS AND SPACE ADMINISTRATION
JOHNSON SPACE CENTER
HOUSTON, TEXAS

By

VOUGHT CORPORATION

P.O. BOX 225907
DALLAS, TEXAS 75265

VOUGHT CORPORATION

SPACECRAFT RADIATORS FOR ADVANCED MISSION REQUIREMENTS

REPORT NO. 2-30320/9R-52212

23 APRIL 1980

FINAL REPORT
TASK 3.7

CONTRACT NAS9-14776

SUBMITTED TO

NATIONAL AERONAUTICS AND SPACE ADMINISTRATION
JOHNSON SPACE CENTER
HOUSTON, TEXAS

By

VOUGHT CORPORATION
P.O. Box 225907
Dallas, Texas 75265

PREPARED BY:	REVIEWED BY:	APPROVED BY:
J. W. Leach	J. A. Oren	R. L. Cox

F O R E W O R D

The work documented in this report was performed in the Advanced Space area of Vought Corporation for the NASA Johnson Space Center under Contract NAS9-14776, Task 3.7 "Technology Assessment." The purpose of the work has been to identify design requirements for future spacecraft heat rejection systems and to evaluate the impact of these requirements on the design of radiators. The study outlines development work needed to efficiently integrate heat rejection systems into future spacecraft having large heat rejection capacities and long mission durations. Emphasis is given to conceptual designs which will reduce the cost of the spacecraft.

TABLE OF CONTENTS

APPENDICES

LIST OF FIGURES

LIST OF FIGURES (CONT'D)

LIST OF TABLES

1.0 INTRODUCTION AND SUMMARY

The objectives of this study are to identify design requirements for future spacecraft heat rejection systems, to evaluate the impact of these requirements on the construction of conventional pumped fluid and hybrid heat pipe/pumped fluid radiators, and to conceptually design new heat rejection systems which may improve the performance or reduce the cost of the spacecraft. The study addresses heat rejection requirements which are large compared to those of existing systems and mission durations which are relatively long.

Heat rejection capacities addressed in this study range from 10 to 250 KW. The operating life goal is arbitrarily selected as 5 years. The major impact of this on the construction of radiator panels is that tubing wall thicknesses are sized so that there is only a small probability of meteoroid penetration in a 5 year mission. The radiator panel can be made to survive longer missions with little weight or cost impact by simply increasing the wall thickness or by employing meteoroid bumpers. Other guidelines for designing the heat rejection system are: transport fluid inlet temperature range from 100°F to 200°F, transport fluid return temperature range from 0°F to 40°F, and 200 lb/KW electrical power penalty for transport fluid pumping.

The study includes analyses of conventional pumped fluid and hybrid heat pipe/pumped fluid radiators which determine the optimum values of radiator fin thicknesses, spacing of heat pipes or transport tubes, Reynolds numbers, and other radiator design parameters. Data necessary for the selection of transport fluids and radiator surface coatings are also analyzed in relation to future mission requirements. In addition, new radiator concepts are presented which are expected to be applicable to these requirements. Groundrules for deriving and evaluating the new concepts give less emphasis to traditional weight and deployed area than is current practice, and more emphasis to other features such as stowage volume, user interface convenience, growth potential, adaptability to heat load variations, and reliability.

The part of the study concerned with the evolution of large heat rejection systems involves the specific construction of the elements of the system; whether the radiators contain heat pipes, for example, as well as procedures for constructing the system from the elements. A large system built up from independent subsystems with oversizing, redundant components, and/or scheduled maintenance to compensate for element failures is signifi-

cantly lighter and more feasible technically than one with a single transport loop having the same capacity and reliability. Therefore, this study evaluates alternative ways to build up large systems from modules by computing the system size and probability of success taking account of the construction and reliability of the components.

In summary, the following approach is taken to improve future heat rejection systems:

1) elements of the system are selected and designed for optimum weight, cost, and reliability,
2) new radiator concepts are introduced that are uniquely designed for future mission requirements,
3) procedures for constructing large long-life systems are proposed that take advantage of modular construction, oversizing, and component redundancy to improve performance and reliability.

2.0 OPTIMIZATION OF CONVENTIONAL RADIATORS

This section discusses design details for improving conventional spacecraft radiators. It includes data relevant to the selection of transport fluids and radiator coatings, reliability information on pump loop components, and details of radiator panel construction for traditional parallel flow panels and for hybrid heat pipe/pumped fluid panels.

2.1 FLUID SELECTION

Technical issues and property data for evaluating transport fluids in pumped fluid or hybrid heat pipe/pumped fluid radiator systems and working fluids in heat pipes are presented in this section.

Transport Fluids

The selection of transport fluids is important since the fluid properties affect the radiator area, system weight, pressure drop, and component life. Of primary interest are: (1) pumping power penalty (a function of viscosity, specific heat, and density), since this affects the pump design and electrical power requirements, (2) heat transport characteristics which determine the size of radiators and heat exchangers, (3) materials compatibility and lubricity, which affect operating life, and (4) contamination threat. Also of importance are availability, freeze or pour point for low load or quiescent operation, flash point, toxicity, and flow stability.

In previous studies pump power and conductance parameters have been developed[1] which are useful in assessing the relative merits of fluids for both laminar and turbulent flow regimes. These parameters were developed from basic fluid flow and heat transfer correlations by holding the boundary temperature, heat load, and system geometry constant. For these conditions, the pumping parameter and conductance were found to be dependent only on the transport fluid properties. The pump power parameters are:

$$\psi_L = \frac{\mu}{\rho^2 \, Cp^2} \qquad \text{for laminar flow}$$

$$\psi_T = \frac{\mu^{.25}}{\rho^2 \, Cp^{2.75}} \qquad \text{for turbulent flow}$$

and the conductance parameters are:

$$\eta_L = K^{.67} \qquad \text{for laminar flow}$$

$$\eta_T = \frac{K^{.2}}{P_r^{.47}} \qquad \text{for turbulent flow}$$

where: μ = viscosity
ρ = density
Cp = specific heat
K = thermal conductivity
P_r = Prandtl number

Computer values of the performance parameters of typical coolants are compared in Figures 1 and 2.

Fluids with low conductance parameters and high pump power parameters are poorly suited for spacecraft cooling system applications, and would be selected only if other fluids failed because of other considerations. The fluid selected usually is not straight-forward because fluids with desirable pumping power parameters (such as Freon 21) may have lower conductance parameters than fluids with poor pump parameters (such as glycol water). Also, fluids which operate efficiently in the turbulent regime must be compared with fluids which favor laminar flow. Therefore, to evaluate the adaptability of candidate fluids to a particular spacecraft it is usually necessary to give detailed consideration to the radiator construction and the weight increase required with the selection of fluids with poor thermal conductance, as well as the impact on the electrical power system and the pump design with the selection of fluids with high pump power parameters.

Properties of fluids which are candidates for future mission applications are listed in Table I. An optimum radiator design will exist for each fluid which minimizes the system weight including the weight of the power source for driving the pump. To illustrate how the choice of the transport fluid affects a typical system design, calculations were made to determine optimum system configurations for several candidate fluids assuming a weight penalty factor of 245 Kg/KW, typical values of pump motor efficiencies (30%), and an assumed radiator environment of 0°F. The results, presented in Table II, show that several fluids can be considered without seriously impacting the

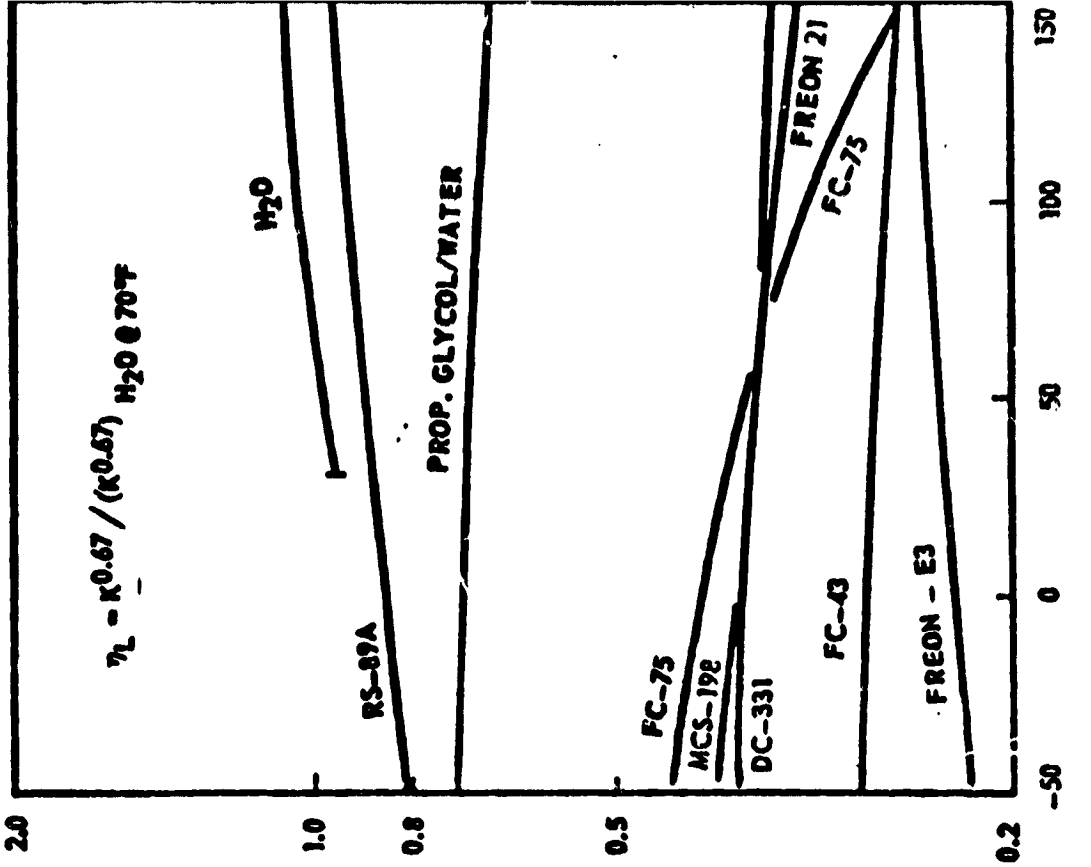

Figure 1 Laminar Pump Power and Conductance

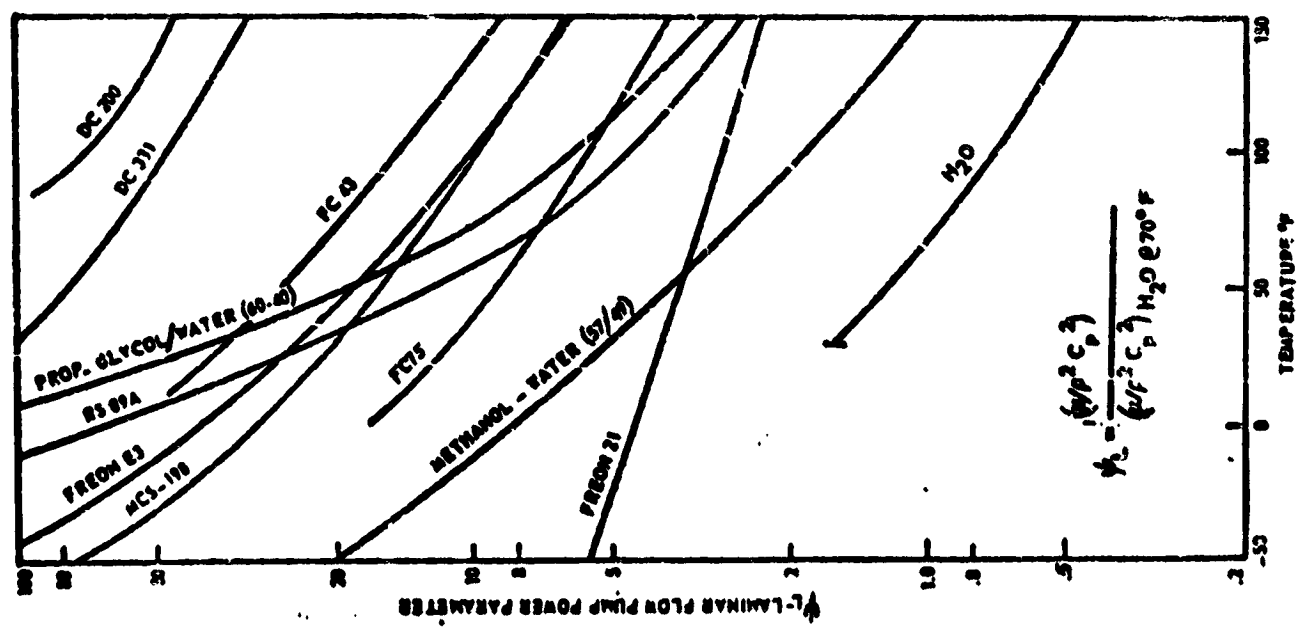

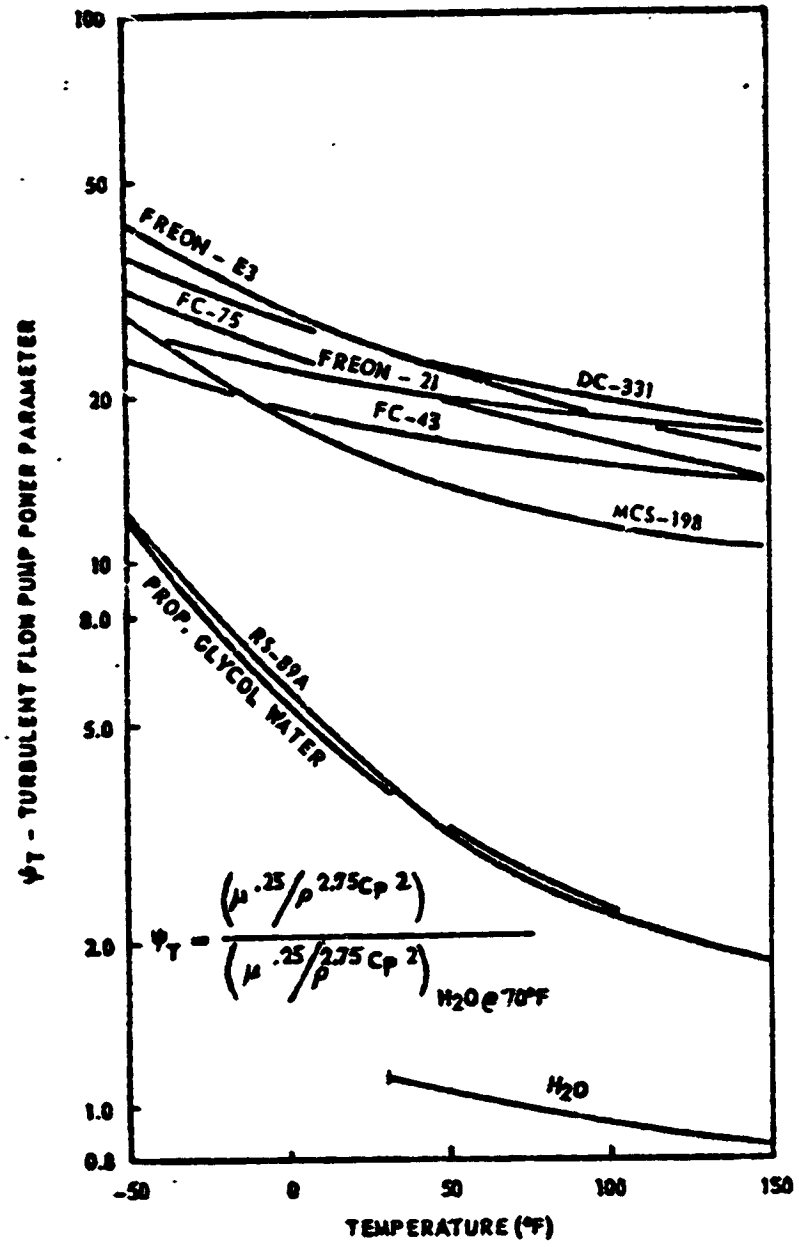

TURBULENT PUMP POWER

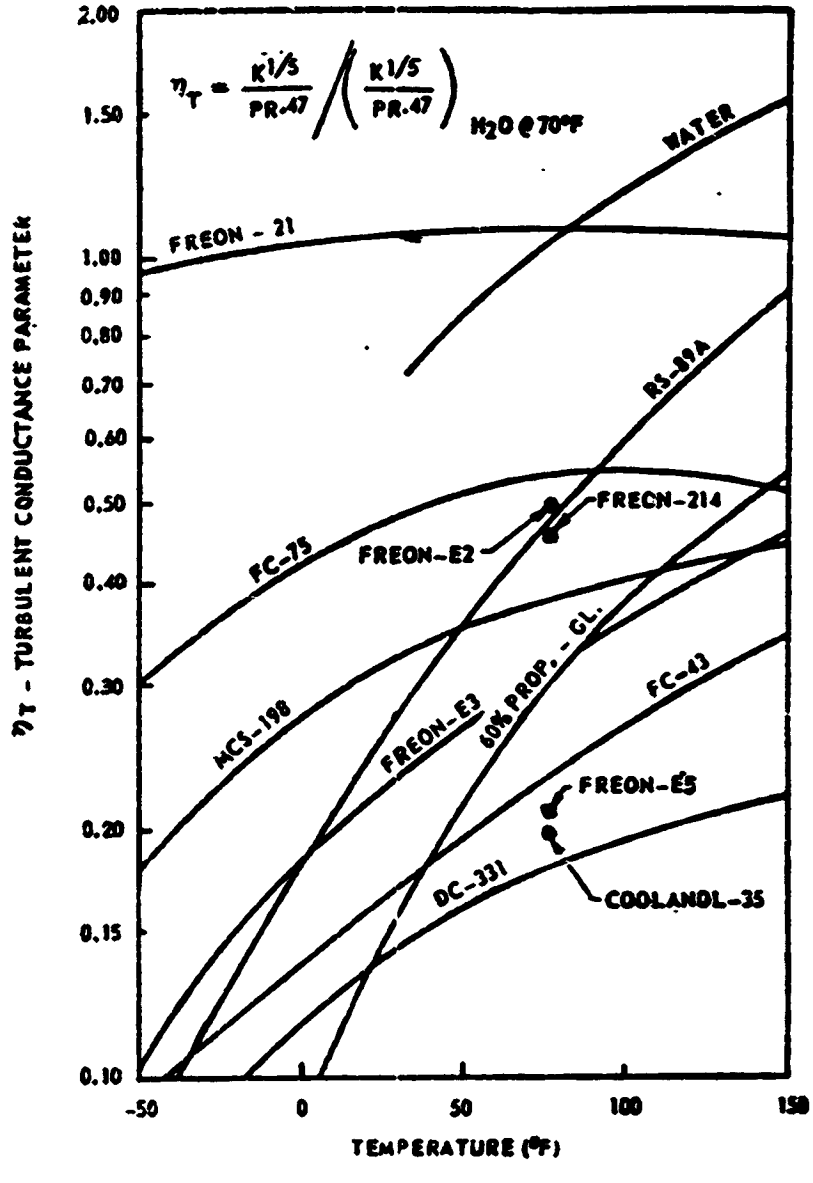

TURBULENT CONDUCTANCE

Figure 2 Turbulent Pump Power and Conductance

TABLE I

PROPERTIES OF CANDIDATE FLUIDS

FLUID	P_v (PSIA)	ρ (LBM/FT^3)	C_p (BTU/LB-°R)	μ (LB/FT-HR)	K (BTU/HR-FT-°F)	POUR PT. (°F)	FLASH PT. (°F)
CRONITE FC-100	< .1	56.0	0.45	6.1	.057	- 100	200
CRONITE 70	< .1	59.5	0.37	72.6	.080	- 100	430
DOW CORNING DC 331	< .1	58.6	0.36	24.2	.050	- 130	420
GENERAL ELECTRIC SF 96	< .1	57.1	0.36	12.1	.067	- 120	275
GENERAL ELECTRIC SF 81	< .1	60.6	0.36	120	.087	- 120	None
ETHYLENE GLYCOL-WATER (RS-89a)	0.3	67.1	0.73	11.8	.219	- 80	240
DuPONT FREON 21	25	85.3	0.25	0.83	.071	- 21	None
DuPONT FREON 11	16	92.1	0.208	1.01	.050	- 168	None
DuPONT FREON E-1	8	96	0.245	1.2	.036	- 246	None
DuPONT FREON E-2	0.6	105	0.240	2.6	.041	- 190	None
3-M FC-88	4.4	101	0.244	1.19	.037	- 150	None
3-M FC-75	0.5	111	0.24	3.6	.037	- 135	None
3-M FC-77	0.8	113	0.24	3.6	.038	- 150	None
MONSANTO COOLANOL 15	< .1	56.0	0.43	4.5	.062	- 140	170
MONSANTO COOLANOL 20	< .1	55.2	0.47	5.2	.067	- 100	230

TABLE II

EFFECT OF TRANSPORT FLUID ON WEIGHT AND SURFACE AREA FOR A 4 KW SYSTEM

TRANSPORT FLUID	WEIGHT DELTA RELATIVE TO R-21 (KG)	AREA RATIO RELATIVE TO R-21 (%)
FREON 21	0	1.000
FREON 11	1.3	1.006
FREON E-1	0.5	1.018
FREON E-2	2.1	1.140
FC-88	0.5	1.018
FC-75	2.0	1.068
FC-77	3.1	1.155
COOLANOL 15	1.0	1.082
ETHYLENE GYLCOL/WATER (R8-89a)	- 0.2	1.012
ORONITE FC-100	1.5	1.090

weight or geometric configuration of the vehicle, and that the fluid selection can be based on other considerations such as materials compatibility, operating temperature range, vapor pressure, lubricity, and vehicle contamination in case of leakage.

A property that is extremely important in applications to pumped fluid or hybrid heat pipe/pumped fluid radiators is the fluid's susceptibility to flow instabilities. This property is a function of how the fluid viscosity varies with temperature.

In improperly designed spacecraft cooling systems flow instabilities may originate in the radiator panel where large changes in the transport fluid temperature occur at low heat load conditions. For serpentine flow radiators with no parallel flow passages the flow instability causes the pump to stall, and is usually accompanied by subsequent freezing of the transport fluid. This may damage the pump or motor, and in some orbit configurations, the system may be permanently disabled because the transport fluid will not re-thaw when the operating conditions change.

Space radiators with parallel fluid transport passages are also susceptible to flow instabilities at low heat load conditions. When the difference between the fluid inlet and outlet temperatures is too large, the flow distribution in the parallel tubes changes abruptly from being uniform, where each tube carries approximately the same flow, to non-uniform, where the flow in one or more of the parallel radiator tubes completely stagnates. Flow instabilities are undesirable when accompanied by freezing of the fluid in the non-flowing tubes since this may prohibit the flow from returning to the uniform distribution when the operating conditions change. Also, metal tubing may eventually fail due to stresses caused by the freezing and thawing of the transport fluid. To prevent flow instabilities the heat rejection system should be equipped with heaters or other methods of control which prevent unfavorable operating conditions from occurring, and a transport fluid should be selected which is resistent to flow instabilities.

The properties of the transport fluid determine the range of operating conditions for which stable flow occurs. An equation from Ref. (2) gives the approximate operating limits for stable flow in terms of the transport fluid properties. The criteria for stable flow is:

$$\nu(To) < 2 \frac{\int_{T_i}^{T_o} \nu Cp \left[1 + \frac{4\eta w \varepsilon \sigma T^3}{\pi K N_u} \right] dT}{T^4 - T_\infty^4} \Bigg/ \frac{\int_{T_i}^{T_o} Cp \left[1 + \frac{4\eta w \varepsilon \sigma T^3}{\pi K N_u} \right] dT}{T^4 - T_\infty^4} \qquad (1)$$

Where:

T_o = fluid outlet temperature
T_i = fluid inlet temperature
T_∞ = environment temperature
ν = fluid viscosity
k = fluid thermal conductivity
Cp = fluid specific heat
w = radiator fin width
ε = radiator fin emittance
σ = Stefan Boltzmann constant
Nu = Nusselt Number

Figure 3 gives the minimum outlet temperature for stable flow computed from Equation (1) for some candidate TCS transport fluids. The figure shows that RS-89a (ethylene glycol-water) has the more restricted operating range. This has been a significant factor which has limited the usage of ethylene glycol-water in space radiators. It does not eliminate the fluid from consideration for all applications because the thermal control system can often be designed to operate in the stable regime. However, the selection of a fluid such as Freon 21 would allow more freedom in the design of the control system.

Heat Pipe Fluids

The first consideration in the selection of a suitable working fluid for heat pipes is vapor temperature range. A variety of characteristics must be examined in order to determine the most acceptable fluid for a proposed

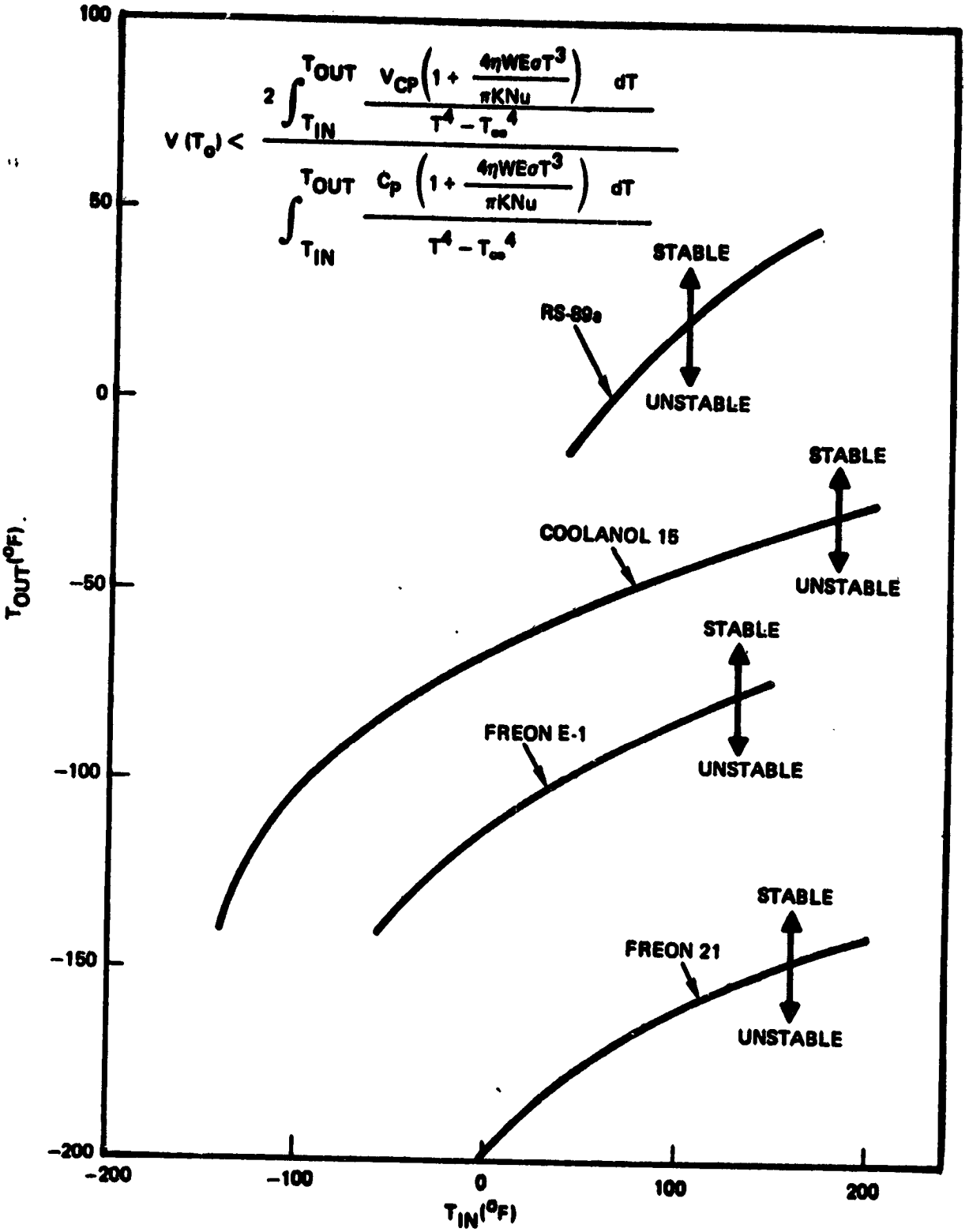

FIGURE 3 APPROXIMATE STABILITY CURVES FOR CANDIDATE RADIATOR FLUIDS

application. Some of the prime requirements are:

1) Fluid/material compatibility
2) Fluid thermal stability
3) Wetability of wick and wall materials
4) Thermal properties (vapor pressure, latent heat, conductivity, viscosity, and surface tension)

A convenient means for quickly comparing working fluids is provided by the liquid transport factor defined as:

$$N_\ell = \frac{\sigma_L \cdot \lambda \cdot \rho_L}{\mu_L}$$

where:
- N_ℓ = liquid transport factor
- σ_L = liquid surface tension
- λ = latent heat of vaporization
- σ_L = liquid density
- μ_L = liquid viscosity

Curves of N_ℓ versus temperature are available in the literature for a number of candidate fluids. Data for candidate fluids for the temperature range studied here are given in Figure 4. At any selected operating temperature the fluid which exhibits the highest liquid transport factor will generally yield the best heat transfer characteristics.

Contamination Threat of Fluids

Evaluation of the contamination threat of a heat pipe or transport fluid involves several considerations. One is the condensation temperature and energy associated with desorption or evaporation. This would be a factor in considerations of deposition rates on cold surfaces. Another could be the fluid's infrared absorption spectrum, which would influence the tolerable contamination of infrared sensors in some applications. A third is the potential of the fluid vapor for chemical reaction with other spacecraft materials. Table III gives materials compatibility data for several candidate fluids, and is taken from Reference 19.

Selection of Fluids for Radiator Design Optimization Studies

In following sections, detailed radiator optimization analyses are performed which require fluid property data. Freon 21 is the coolant employed

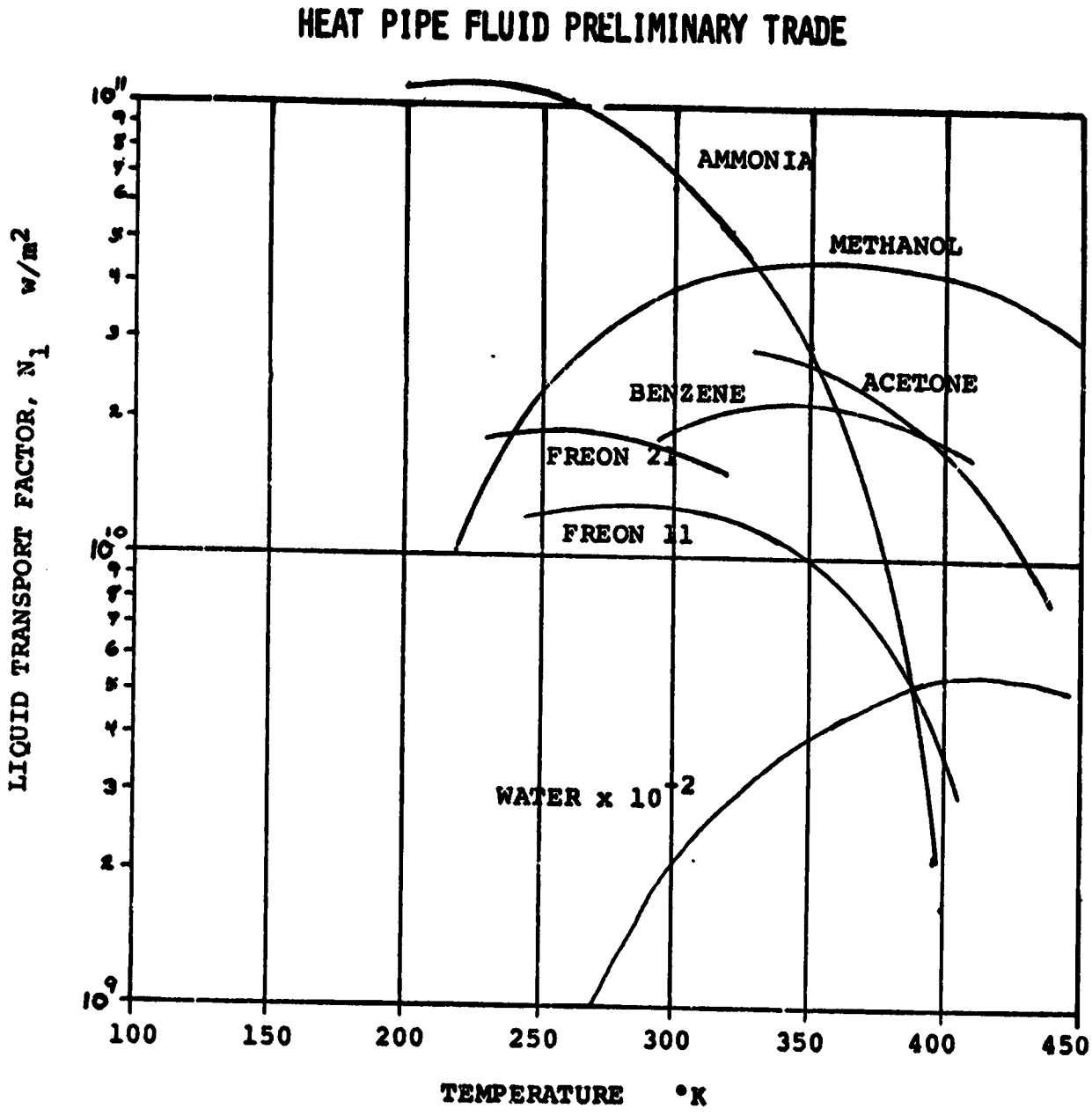

FIGURE 4 HEAT PIPE FLUID TRANSPORT PARAMETER DATA

TABLE III MATERIALS COMPATIBILITY SUMMARY

COOLANTS					COMPATIBILITY																
									SEALS (7)						BEARINGS						
PUMPED FLUIDS	HEAT PIPE		STABILITY		ALUMINUM	STAINLESS STEEL	TITANIUM		TEFLON	VITON A	BUTYL RUBBER	BUNA N	KALREZ		CARBON	TEFLON		NONVOLATILE CONTENT (OR LOW) %	HEAT OF VAPORIZATION, CAL./G	MOLECULAR WEIGHT	VAPOR PRESSURE @ 100°F, PSIA	REMARKS
X	X	FREON 11	S		S	S	S		4.5	4	41	6	U		S	S		<0.01	43.10	137.4	23.5	
X	X	FREON 21	S		S	S	S		3.5	26	24	48	4		S	S		<0.05	57.86	102.9	46.0	
X		COOLANOL 20	(2)		S	S	S		S	S	-	S	-		S	S		0.50	-		0.016	AVAILABILITY
X		FC-75	S		S	S	S		0	0.7	0	0.7	-		S	S		0	20.9	500.08	0.60	VAPOR PRESSURE AT 77°F
X		FLO TEC 3350																		288.05	19.3	
	X	ACETONE	S		S	S	S		S	U	S	U	O		(8)	(8)		0	124.5	58.08	7.5	
	X	AMMONIA	S		(5)	S	S		S	U	S	F	O		(8)	(8)		0	327.1	17.03	211.9	
	X	METHANOL	S		S	S	(6)		S	U	S	S	S		(8)	(8)		0	262.8	32.04	4.1	
	X	WATER	(3)		(4)	S	S		S	S	S	S	S		(8)	(8)		0	595.5	18.02	0.94	
X		GLYCOL/WATER	(4)		(4)	S	S		S	2	1	S	S		S	S		1.7 (9)		(62.07)	0.58	MOLECULAR WEIGHT OF GLYCOL ( )
X		METHANOL/WATER	(4)		(4)	S	S		S	0.6	0	S	O		U	S		0.1			1.45	VAPOR PRESSURE AT 77°F
	X	BENZENE	S		S								S					0	94.3	78.11	3.4	

(1) S = Satisfactory, F = Fair, U = Unsatisfactory
(2) Coolanol 20 is sensitive to water contamination. Hydrolysis yields a gel.
(3) Water will freeze at the lower operating temperature
(4) An inhibitor is required if there are dissimilar metals in the system. The inhibitor probably would not last 5 yrs.
(5) There is no effect on aluminum if the ammonia is dry. There may be slight attack at the upper operating temperature if wet.
(6) Anhydrous methanol has been found to cause stress corrosion cracking of titanium. 1% or more water acts as an inhibitor.
(7) Numbers are percent linear swell.
(8) Heat pipe fluids - bearings not required.
(9) Additive in RS 89a coolant.
(10) Additive used in methanol/water for Saturn IU.

for the transport fluid in these studies. It's thermal properties result in minimum system weight, and its operating temperature range is broader than most other fluids. It has good chemical stability, and low nonvolatile content. For heat pipes, ammonia is baselined as the working fluid. It has the highest liquid transport factor of the fluids applicable to the temperature range of this study. Other trade study criteria such as chemical stability and material compatibility appear to be acceptable.

2.2 THERMAL CONTROL COATINGS

Thermal control coatings are an important issue in this study because of the required operating life of 5-10 years, and the emphasis is placed on high radiator performance and minimum cost. Good thermal control coatings should have the following properties: low solar absorptance (for sun viewing surfaces), high emittance, low outgassing, stability in space environment, and avoidance of static charge buildup (high altitude orbits). The discussion presented in this section is a summary of appropriate prior studies, and is based mainly on Reference 19.

Candidates considered include: silver and aluminum backed Teflon, optical solar reflectors, astroquartz fabric, front surface coated Kapton film, aluminum oxide coated aluminum, zinc orthotitonate paint, and a NASA-Goddard inorganic conductive yellow paint. Initial values of the emissivity and solar absorptivity, and degraded values of solar absorptivity are given in Table IV for some of the coatings.

Silver backed Teflon has become a very popular thermal control coating because of low absorptivity (about 0.1), high emissivity (about 0.8) and purported stability in the space environment. Numerous spacecraft and probes have flown with this material. Figure 5 presents test and flight data for silver Teflon showing an initial rapid degradation (probably due to contamination) followed by minimal further increase in solar absorptivity in low earth orbit. For high altitude flights where significant fluxes of electrons and protons are present in combination with solar ultraviolet, degradation continues at a rate that would appear unacceptable for a five year mission even if an asymptotic tailing off occurs. Research for the Air Force[3] has shown that silver Teflon loses its mechanical integrity and degrades such that its solar absorptivity increases by a factor of about 3 for a simulated 5 year exposure to high altitude orbits. There is also an indication that low earth orbit degradation (solar ultraviolet only) may also be more severe for a 5 year mission that would be anticipated. Work with astroquartz fused silica fabric coatings[4] indicates that when used in

TABLE IV THERMAL CONTROL COATINGS SUMMARY

- **SEVEN POTENTIAL RADIATOR COATINGS EVALUATED FOR LONG TERM STABILITY**

POTENTIAL COATING	INITIAL α/ε	ASYMPTOTIC Δα	FINAL α
OPTICAL SOLAR REFLECTORS	0.066/0.75	0.035 CLEAN @ GEO 0.26 DIRTY @ GEO	.10 .33
SILVER BACKED TEFLON	.085/.78	.15 @ GEO .05 @ LEO	.24 GEO .13 LEO
ASTROQUARTZ	.16/.86 TO .2/.86	.035 (TESTS) .06 in 6 MO (FLT)	.2 TO .26
ANODIZED ALUMINUM	.14/.75	-	-
ZINC ORTHOTITANATE	.11/.9	0.04 (1 YEAR)	-
GODDARD INORGANIC CONDUCTIVE YELLOW PAINT	.21/.9	0.09 (2 YEAR)	.30

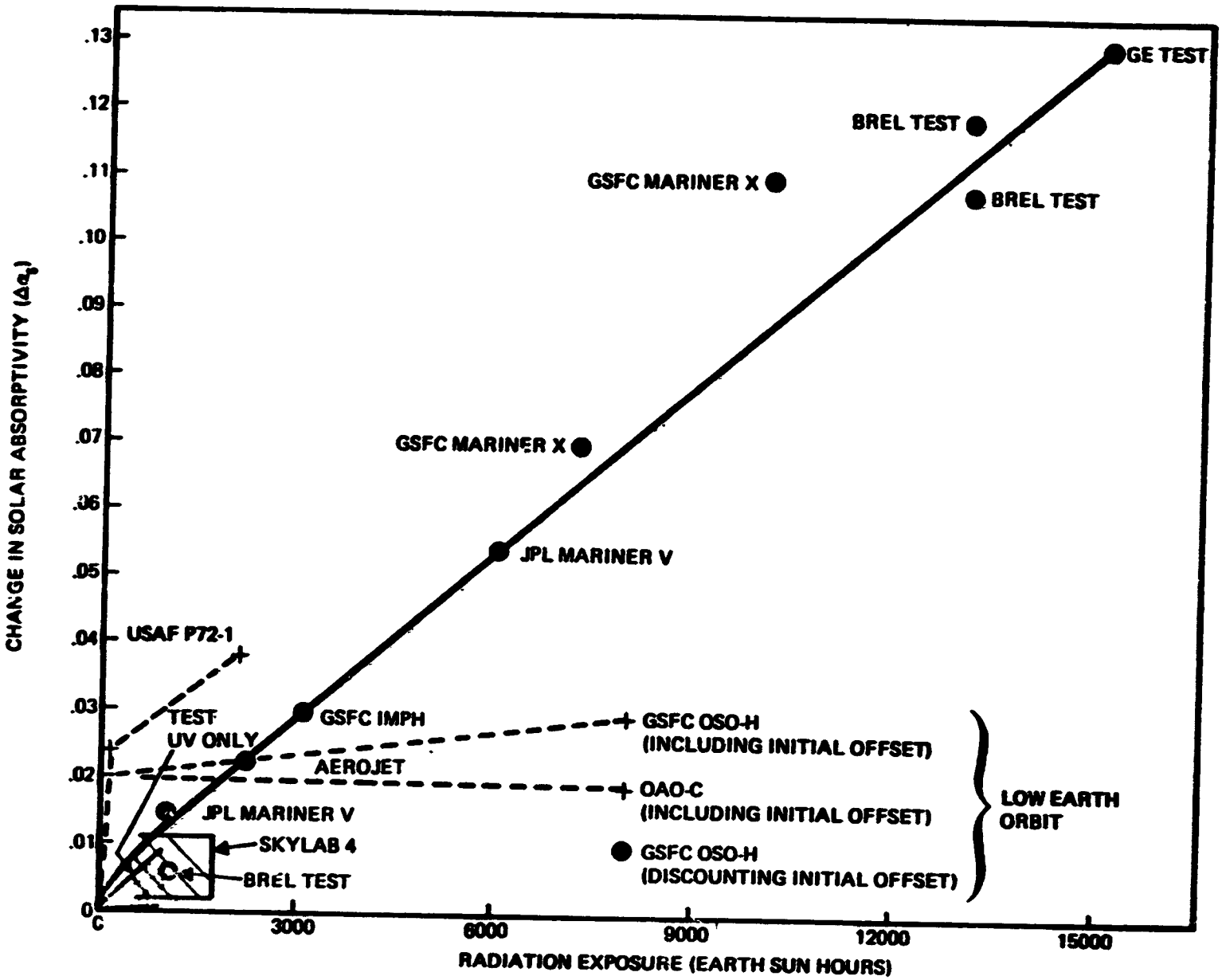

FIGURE 5 CORRELATION OF SILVER/TEFLON DEGRADATION DATA

conjunction with a silver Teflon substrate a reasonably low solar absorptivity of about 0.18 is obtained, and improved environmental stability is expected. Although the use of astroquartz is not an established technology and it has the disadvantage of being difficult to clean, silver Teflon with astroquartz is a candidate for both low and high orbits because of its unique promise of long life. Bare silver Teflon is probably suitable for low orbits. Additional information and performance data for metallized Teflon and for astroquartz fabric are given in Tables V and VI respectively.

Another candidate coating for direct solar exposure at high altitude is the Optical Solar Reflector (OSR) described in Table VII, consisting of silver or aluminum backed quartz tiles about one inch square. Because these tiles are expensive, heavy, and must be bonded to the radiator they are basically undesirable and not suited for large radiator systems. However, data indicates they have the lowest solar absorptivity available and are stable in the combined ultraviolet, proton and electron environments of deep space. Thus these coatings should be considered in concepts which entail small radiators with significant solar exposure. Their contamination threat from the adhesive must be evaluated.

No paint coatings (organic or inorganic) are know which are stable in high altitude orbits. A new coating, zinc orthotitanate, is under development[5] but insufficient data are available to assess its applicability at this time. An inorganic yellow paint is also being developed by Goddard for high altitudes. The only other known potentially stable high altitude coatings are evaporated silicon or aluminum oxides over metallized substrates. Table VIII gives data for these coatings. Figure 6 compares solar absorptivity data for candidate high altitude coatings.

An alternate approach which offers greatly improved confidence is to orient the radiator such that very little solar irradiation is present. This would not only retard degradation but would minimize, if not eliminate, degradation effects. In this case a simple durable coating such as anodized aluminum could be used (to provide a high emissivity). An added advantage would be the elimination of any contamination threat from either the coating itself or an adhesive securing it.

Data obtained during the past few years indicates that film surfaces, such as multilayer insulation or silver Teflon, can obtain a large

TABLE V ADDITIONAL METALLIZED TEFLON DATA

HEMISPHERICAL EMITTANCE

$\varepsilon_H \doteq .66$ (2 MIL)

$\varepsilon_H \doteq .78$ (5 MIL)

INITIAL SOLAR ABSORPTANCE

AG/FEP	AL/FEP
2 MIL: $\alpha = 0.06$	$\alpha \doteq 0.13$
5 MIL: $\alpha = 0.085$	$\alpha \doteq 0.14$

RECENT GEOSYNCHRONOUS SPINNING SATELLITE DATA (AEROJET)

- 2 MIL AG/FEP:
  - GROUND PROPERTIES $\alpha \doteq 0.063$
  - AFTER FEW WEEKS $\alpha \doteq 0.08$
  - AFTER 0.5 YR $\alpha \doteq 0.08$
  - AFTER 1.75 YRS $\alpha \doteq 0.12$

  } $\Delta\alpha \doteq 0.02$

- 5 MIL AL/FEP:
  - GROUND PROPERTIES $\alpha \doteq 0.144$
  - AFTER FEW WEEKS $\alpha \doteq 0.16$
  - AFTER 0.5 YR $\alpha \doteq 0.175$

  } $\Delta\alpha \doteq 0.02$

RECENT LABORATORY SIMULATIONS OF GEOSYNCHRONOUS EXPOSURES (BOEING, GE)

5-MIL SILVER TEFLON

- NON-SUBSTROM CONDITIONS: $\Delta\alpha = 0.078$ @ 4000 ESH UV + 6×10^{15} e^- & p^+ at 2×10^8 $e^-, p^+/cm^2$-sec
- SUBSTORM CONDITIONS: $\Delta\alpha = 0.302$ @ 100 ESH UV + 2×10^{15} e^- & p^+ at 3×10^9 $e^-, p^+/cm^2$-sec (SEVERE DIELECTRIC BREAKDOWN)

2- VS 5-MIL TEFLON

- 2-MIL FEP ABOUT HALF DEGRADATION AS 5-MIL FOR HIGH ENERGY PARTICLES

STATIC CHARGE RELIEF

- 100 Å OVERCOAT OF INDIUM/TIN OXIDE INDICATED TO RELIEVE CHARGE
- MINIMAL SOLAR ABSORPTANCE EFFECTS: $\Delta\alpha \doteq 0.02$ (INITIAL)
- DEGRADATION OF OVERCOAT $\Delta\alpha \doteq 0.02$ IN 3000 ESH

TABLE VI ASTROQUARTZ FABRIC

- PREPARED BY HEAT LAMINATING 11-MIL PURIFIED SILICA FABRIC TO 1-MIL FEP TEFLON AND ALUMINUM FOIL
  - ALTERNATE DIRECT APPLICATION OF FABRIC WITH DOUBLE-BACKED ALUMINIZED KAPTON TAPE
- INITIAL OPTICAL PROPERTIES (GE, AEROJET)
  - α/ε = 0.16/0.86 TO 0.2/0.86
- ASYMPTOTIC $\Delta\alpha \triangleq 0.035$ FROM COMBINED UV/ELECTRON LABORATORY SIMULATION
- FLIGHT DATA (AEROJET) INDICATED $\Delta\alpha \triangleq 0.06$ IN 1/2-YEAR AT GEOSYNCHRONOUS ALTITUDES (GREATER THAN METALLIZED TEFLON)
- LABORATORY TESTS INDICATE NO STATIC CHARGE BUILDUP
- MINIMAL SOURCE OF OUTGASSING PRODUCTS
- DISADVANTAGES
  - DIFFICULT TO AVOID OR REMOVE GROUND CONTAMINATION
  - APPARENT GREATER SENSITIVITY TO ORBITAL CONTAMINATION THAN METALLIZED SILICA TILES OR TEFLON

TABLE VII OPTICAL SOLAR REFLECTOR

SILVER BACKED FUSED SILICA TILES PROVIDE LOW SOLAR ABSORPTANCE, HIGH EMITTANCE, EXCELLENT NATURAL ENVIRONMENT STABILITY

$\alpha/\epsilon \triangleq 0.066/0.75$ (10 MIL SILICA)

DEGRADATION STRONGLY RELATED TO CONTAMINATION ENVIRONMENT

ASYMPTOTIC $\Delta\alpha \triangleq 0.035$ IN "CLEAN" AREA AT GEOSYNCHRONOUS ORBIT

ASTMPTOTIC $\Delta\alpha \triangleq 0.26$ IN "DIRTY" AREA AT GEOSYNCHRONOUS ORBIT

INDIUM OXIDE STATIC CHARGE RELIEF COATING

$\alpha/\epsilon \triangleq 0.082/0.75$ (10 MIL SILICA)

NO OBSERVABLE DIFFERENCE IN REPORTED DEGRADATION AT GEOSYNCHRONOUS ORBIT

TABLE VIII OTHER THERMAL COATING CANDIDATES

GODDARD INORGANIC CONDUCTIVE YELLOW PAINT (NON-CHARGING)

- HIGH TEMPERATURE FIRED ZINC OXIDE PIGMENT IN SILICATE BINDER-SPRAY PAINT

  α/ε = 0.21/.9 TYPE NS 43C
- TWO-YEAR COMBINED ENVIRONMENT SIMULATION, GEOSYNCHRONOUS: $\Delta\alpha$ = 0.09
- FLYING ON ISEE -A, -B, -C ; SCATHA
- POROUS CHARACTER (LIKE Z-93) DIFFICULT TO PROTECT/CLEAN

FRONT SURFACE COATED KAPTON

- ALUMINUM OXIDE/ALUMINUM COATED ¼-MIL KAPTON FILM REMAINED HIGHLY REFLECTIVE UNDER 13,000 ESH + 3 x 10^{16} p^+/cm^2 SOLAR WIND SIMULATION
- INDICATIONS THAT COATED KAPTON FILM IS NON-CHARGING
- ADDITIONAL DATA AND EMITTANCE IMPROVEMENT REQUIRED

ZINC ORTHOTITANATE IN INORGANIC BINDER

- SOLAR ABSORPTANCE UNDER 0.2
- COATING SIMILAR TO Z-93 ONLY BETTER PROPERTIES
- MORE DATA REQUIRED

ALUMINUM OXIDE COATED ALUMINUM

- ANODIZED ALUMINUM OR EVAPORATED ALUMINUM OXIDE
- POTENTIAL FOR NON-CHARGING DUE TO CONDUCTIVE NATURE OF OXIDE (ANODIZED CHARGES)
- INITIAL $\alpha/\varepsilon \doteq 0.14/0.75$
- ADDITIONAL EVALUATION NEEDED OF DEGRADATION AND CHARGING

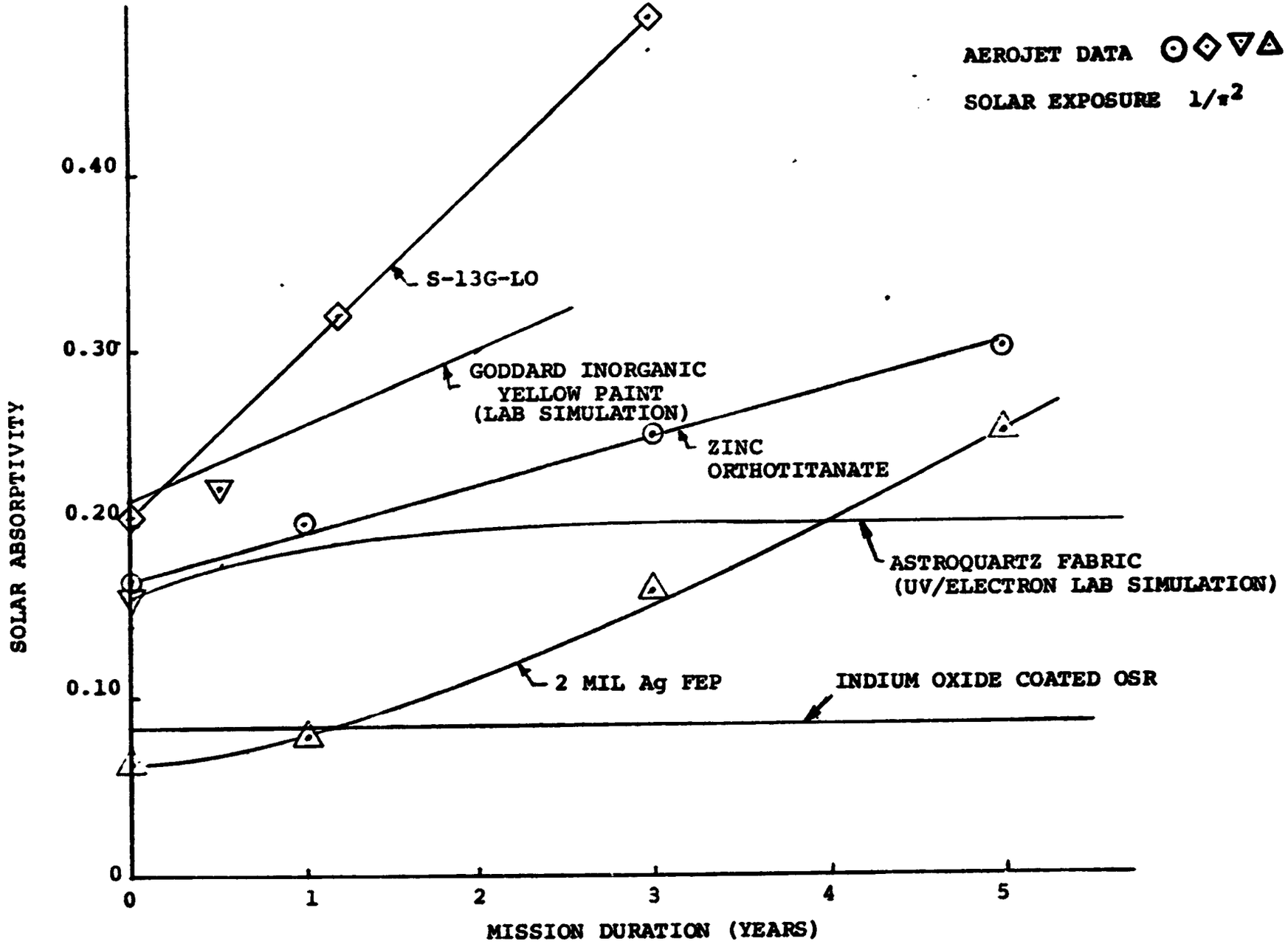

FIGURE 6 SIMULATED DEGRADATION OF RADIATOR COATINGS IN GEOSYNCHRONOUS ORBITS

static charge buildup during solar substorm activity with high altitude spacecraft. A static discharge can occur which damages the coating and provides spurious signals to the spacecraft. A significant amount of research has been directed toward alleviating static buildup in coating materials. A potential inherent advantage of the flexible radiator fin material also being developed under this contract is its potential to dissipate static charge. Since the fin consists of a fine silver wire mesh embedded in the Teflon film, it is conceivable that this fin material, perhaps covered with astroquartz for stability, would offer a lightweight advanced technology approach to obtain a satisfactory high altitude radiator. Other countermeasures which may be taken to avoid static charge buildup include:

- Addition of transparent conductive film to coating surface (induim/tin oxide, others)
- Metal grid applied to surface
- Inherently conductive coating (astroquartz, conductive paint)

Selection of Thermal Control Coatings

The following recommendations are made for selecting radiator coatings for long duration missions:

1) Low Earth Orbits - Metallized Teflon is the best currently qualified choice based on initial α, ε, and degraded properties. Contamination of the coating has the most adverse effect on α degradation. The radiators should be oriented away from thrusters and other sources of contamination when possible.

2) High Earth Orbits - No satisfactory coating available, although astroquartz is probably acceptable with design allowances for degradation. Laboratory data indicate metallized Teflon is unacceptable without an overcoat to avoid static charging, although some satellite flight data suggest the problem may not be as severe as would be expected. Optical solar reflectors have less severe degradation than Teflon, but weight and cost make them unattractive for large areas. Astroquartz fabric and Goddard conductive yellow inorganic paint have high initial values of solar absorptivity, are difficult to clean, and would be expected to degrade to $\alpha \approx 0.3$ in 5 years. More data is needed for other coatings such as the flexible radiator fin material, front surface Kapton film, zinc orthotitanate paint and aluminum oxide coated aluminum.

2.3 COMPONENT LIFE STUDY

The objectives of the component life study were to establish the current state-of-the-art component lifetimes, to identify component designs which are capable of 5-10 year operating lives, and to identify components which will require further development. The approach taken was to survey the long-life component technology. Much of the information presented in this section was obtained from Reference 19.

Table IX summarizes operating life data obtained for typical spacecraft coolant system components. The table shows that, with the exception of thermal control coatings, all components have projected life times of 5 years or greater. However, except for the fluid accumulator, five year lifetimes have not been demonstrated. Therefore, based on projected component performance and design allowances for coating degradation, 5 year operating life is achievable. The probability of success for 5-10 year missions depends on how the system is designed; whether it has been oversized or contains redundant elements for example. The details of how to design thermal control systems is discussed in Section 5.0. This section addresses only the operating characteristics of components of the system.

Pumps

Contacts with the major manufacturers of aerospace pumps indicate that the development of pump motor assemblies capable of operating continuously for more than five years will challenge the state-of-the-art. Pump motor assemblies applicable to spacecraft thermal control systems have been tested for more than 20,000 hours without failure, and several designs have projected operating lifetimes greater than 5 years (Table X).

Figure 7 presents a typical pump selection curve which indicates regions of best efficiency for gear, vane and centrifugal pumps. The curve shows that centrifugal pumps favor low pressure rise and high flowrates. Often environmental control systems require a higher pressure rise, which could be met more efficiently by a gear or vane pump. However, gear and vane pumps generate contaminants and have more moving parts in contact and are thus undesirable from life considerations. In addition they create pressure pulsations

TABLE IX CRITICAL COMPONENT LIFE SUMMARY

COMPONENT	SUPPLIERS CONTACTED	PROJECTED LIFE	DEMONSTRATED LIFE
PUMP/MOTOR/INVERTER	SUNSTRAND	> 5 YEAR (43,800 HRS)	17,000 HRS 20,000 HRS
	AIRESEARCH	> 5 YEAR (43,800 HRS)	17,000 HRS
	FAIRCHILD	> 40,000 HRS	10,000 HRS ON SIMILAR DESIGN
FLUID ACCUMULATOR (GAS PRECHARGED)	METAL BELLOWS	100,000 FULL CYCLES (15,000 REQUIRED)	100,000 FULL CYCLES
THERMAL CONTROL VALVE	AIRESEARCH	5 YEARS	NOT DEMONSTRATED
	SUNSTRAND	5 YEARS	NOT DEMONSTRATED
FLUID SWIVEL	VOUGHT DESIGN	5 YRS W/DEVELOPMENT (2.6×10^6 ROTATIONS)	1100 ROTATIONS
FLEX HOSES	METAL BELLOWS	5×10^5 CYCLES (2×10^6 CYCLES REQD)	
HEAT PIPES	HUGHES	> 5 YEARS	10 YEARS
	LOCKHEED	> 5 YEARS	
RADIATOR COATING	LITERATURE	INDEFINITE WITH DEGRADED PROPERTIES	15,000 EARTH SUN HOURS

TABLE X VENDOR INFORMATION ON PUMPS

I. SUNSTRAND CORPORATION

- **APPLICATION** - SHUTTLE ORBITER ACTIVE THERMAL CONTROL SYSTEM (ATCS)
- **DESIGN** - TWO STAGE CENTRIFIGAL
  HYDRODYNAMIC CARBON SLEEVE BEARINGS
  COMPLETE WELDED ASSEMBLY, HERMETICALLY SEALED CANNED ROTOR AND STATOR
- **COOLANT** - FREON 21
- **TESTING** - ONE UNIT AT 17,000 HRS AND ANOTHER FOR 20,000 HRS
  COMPLETE DISASSEMBLY WITH ALL DIMENSIONS WITHIN NOMINAL
- **PERFORMANCE** - FLOWRATE = 3.7 GPM
  PRESSURE RISE = 69 PSI
  EFFICIENCY = 33%
  POWER = 350 WATTS
- **FLUID/MATERIAL COMPATIBILITY** - CURRENTLY SUNSTRAND TECHNOLOGY CAN SUPPORT PUMP DESIGNS FOR OTHER FLUIDS SUCH AS COOLANOL 20, METHANOL/WATER AND WATER BY PROPER SELECTION OF MATERIALS
- **CURRENT LIFETIME** - ESTIMATED TO BE 5 YEARS MINIMUM

II. GARRETT - AIRESEARCH

- **APPLICATION** - EXPERIMENTAL
- **DESIGN** - SINGLE STAGE CENTRIFIGAL
  HYDOSTATICALLY PRESSURIZED CONICAL BEARINGS
  BEARING MATERIAL INCONEL WITH TEFLON COATING
  MAGNETICALLY COUPLED MOTOR

TABLE X VENDOR INFORMATION ON PUMPS (CONT'D)

II. GARRETT - AIRESEARCH (CONTINUED)

- COOLANT - FREON 21
- TESTING - 17,000 HOURS WITH NO APPRECIABLE WEAR
- PERFORMANCE - FLOWRATE = 3.2 GPM
  PRESSURE RISE = 55 PSI
  EFFICIENCY = 27%
  POWER = 300 WATTS
- CURRENT LIFETIME - 5 YEAR LIFE IS ACHIEVABLE

III. FAIRCHILD-STRATOS DIVISION

- APPLICATION - EXPERIMENTAL
- DESIGN - DOUBLE ENDED CENTRIFIGAL
  ALL CARBIDE BEARINGS AND IMPELLER SHROUD
  AC CANNED MOTOR
- COOLANT - FREON 21
- TESTING - 10,000 HOURS ON DESIGN SIMILAR TO ABOVE
- PERFORMANCE - FLOWRATE = 3 GPM
  PRESSURE RISE = 60 PSI
  EFFICIENCY = 29%
  POWER = 270 WATTS
- FLUID/MATERIAL COMPATIBILITY - NO TECHNOLOGY FOR METHANOL/WATER
- CURRENT LIFETIME - ESTIMATED TO BE 40,000 HOURS

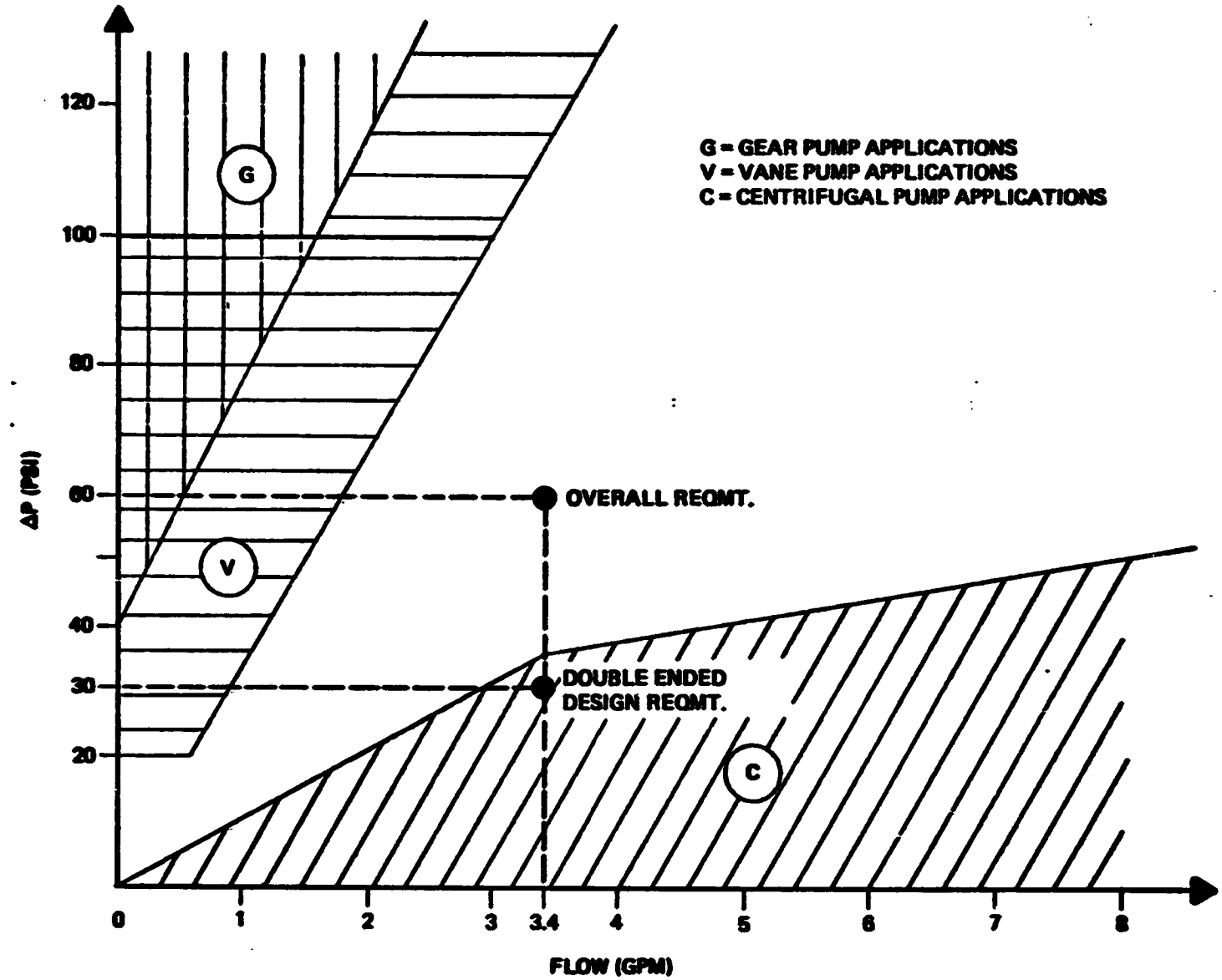

FIGURE 7 MINIATURE PUMP APPLICATION ZONES-OPTIMUM EFFICIENCY SPEEDS (SPACE HARDWARE ONLY)

and vibrations. To avoid these problems and still obtain satisfactory efficiencies (on the order of 50%) double ended centrifugal pumps have been devised. These halve the pressure rise per stage enhancing overall efficiency. The double ended feature not only increases efficiency but also unloads axial thrust increasing lifetime potential. Further gains in lifetime may be possible through the use of carbide bearings, with a good prospect for achieving the 5 year (44,000 hours) desired lifetime.

Pump Motors

Submerged canned stator AC motors have been proven reliable on space programs such as Apollo, Biosatellite, Shuttle Orbiter, and Saturn over a number of years. The technique of enclosing the motor stator in a sealed stainless steel can has been fully developed, to the point that the difference of efficiency between this and other designs is usually unmeasurable. The submerged motor has the inherent advantage of direct heat transfer to the fluid for efficient dissipation of motor heat, continual lubrication of the bearings, and the ability for hermatic sealing of the unit if necessary. Since the possibility of motor failure is generally associated with stalled pumps or motor overheat, and since the possibility of stalling a centrifugal pump is very remote, and the likelihood of motor overheat is also remote with direct fluid cooling, the integral submerged motor concept appears to be a leading long life choice. Solid state DC to AC inverters facilitate the use of canned stator AC motors on satellites.

Accumulators

The functions of the accumulator are to provide system pressure adequate to prevent transport fluid vaporization at any temperature encountered, to provide positive pump suction pressure, and to accommodate fluid volume changes due to temperature excursions and leakage. Two types of accumulators might be considered: bladderless accumulators and metal bellows. Two pressurization techniques, a gas pre-charge system and a regulated accumulator temperature system might be considered. The gas pre-charge system will require a larger overall volume but will not require power. Vendor information on accumulators is given in Table XI.

Coolant Loop Bypass Valves

The life of the coolant loop bypass valves is not considered to be a significant problem area. Because of the relatively steady heat load

TABLE XI VENDOR INFORMATION ON ACCUMULATOR

METAL BELLOWS CORPORATION

- **DESIGN**
  - GAS PRE-CHARGED
  - WELDED METAL BELLOWS
  - COMPLETE WELDED ASSEMBLY (NO "O" RINGS)
- **FLUID** - COMPATIBLE WITH ALL FLUIDS UNDER CONSIDERATION
- **LEAKAGE** - RATE CHECKED AND MAINTAINED TO 10^{-9} SCC/SEC He BEFORE AND AFTER GAS CHARGING PROCEDURE
- **LIFETIME**
  - EXISTING TECHNOLOGY CAN SATISFY 5 YEAR REQUIREMENT
  - HAS BEEN DEMONSTRATED FOR 100,000 CYCLES

typical of spacecraft, the valve will probably have to cycle less than 50,000 times in a 5 year mission. Space qualified electronically controlled valves have been tested by Vought for the Space Shuttle program without difficulty for comparable durations over 30,000 cycles. The design life of the Shuttle valve on the Flow Control Assembly (FCA) is 20,000 cycles. Elements of the valve which might fail include metal bellows, Teflon seats, and stepper motors. The bellows have been extensively tested past 50,000 cycles whereas Teflon seats have been tested to 500,000 cycles. Bypass valve stepper motors are capable of more than 30,000,000 steps in a vacuum environment. Thermostatically actuated valves with very low failure rates are also under development for such programs as the Satellite Infrared Experiment (SIRE).

Fluid Swivels

The operating life depends strongly on the external loading and the selection of seals to compensate for fluid temperature variations. With proper designs to account for side and axial loading, an operating life of five years should be possible. However, it is difficult to provide system redundancy for rotating fluid swivels because it is necessary for all of the swivels to be located on the axis of rotation.

Heat Pipe Life

The majority of published literature on heat pipe life tests indicates that lifetimes on the order of 5 years are possible. However, the design of a heat pipe that is capable of continuous operation over a 5-year period requires meticulous attention to several critical details. Some of the basic heat pipe design details which can affect useful lifetime include: fluid chemical stability, fluid/material compatibility, fluid purity, and metal cleanliness. Quality control during heat pipe manufacture also cannot be over-emphasized in its relationship to continuous heat pipe performance.

All of the above items must be addressed in order to insure against the primary causes of failure - corrosion and generation of non-condensable gases. If the wall or wick material is soluble in the working fluid,mass transfer is likely to occur between the condenser and evaporator. Solid material will be deposited in the evaporator resulting in local hot spots or blocking of the pores in the wick. Non-condensable gas generation is probably the most common cause of heat pipe failure as the non-condensables accumulate in the condenser section blocking fluid transfer.

Other important life considerations in high performance heat pipes include survival of the wick when subjected to the launch vibroacoustic spectrum.

Fatigue life of the wick is important in designs requiring flexing, such as a gimbal section. The topic of accelerated life testing and extrapolation to predict long term performance is also significant to long life heat pipe assessments.

2.4 MICROMETEOROID PROTECTION

When designing thermal control systems for long duration missions, micrometeoroid considerations have a significant impact on the design of the radiators and the coolant loop lines exposed to the space environment. In heat pipe radiator designs the transport fluid manifolds must be shielded, and the radiator panel must be oversized to account for the loss of heat pipes by meteoroid puncture. In pumped fluid radiators the manifolds and parallel flow cross tubes must be designed to withstand micrometeoroid impacts. Typically the exposed cross section of the transport loop is about the same for pumped fluid or hybrid heat pipe/pumped fluid designs, so that the mass of armor or meteoroid bumper required is essentially independent of the radiator design.

The transport loop wall thickness must be sufficient to retain the transport fluid pressure after being struck by a micrometeoroid. The depth of the crater left by the most damaging meteoroid expected to strike the tubing during the designed operating life of the radiator is computed from a ballistic equation which is based on ground test data, and a meteoroid flux model derived from penetrations of metal foils in near earth orbits.

The mechanics of hypervelocity impacts are not completely understood. An equation given in Reference (6) correlates the existing data reasonably well. The equation is

$$t = 0.65 \left(\frac{1}{\varepsilon_t}\right)^{1/8} \left(\frac{\rho_m}{\rho_t}\right)^{1/2} (V_m)^{7/8} (d_m)^{19/18} \qquad (2)$$

where:
- t = thickness of material penetrated (cm)
- ε_t = percentage elongation of target material
- ρ_t = mass density of sheet material (gm/cc)
- ρ_m = mass density of meteoroid (gm/cc)
- V_m = normal impact velocity (km/sec)
- d_m = meteoroid diameter (cm)

Equation 2 generally predicts greater depths of penetration than other equations[7,9] derived for penetration of metals, and will therefore provide for a conservative thermal control system design when applied in conjunction with standard meteoroid environment models.

The radiator panel tubing wall thickness needed for survival of a given system design depends on the projected target area, the exposure time, and the required probability of success for the mission. The probability of no meteoroid penetrations is given by

$$P_o = e^{-\zeta A \tau N} \qquad (3)$$

where:
- ζ = shielding factor (% of area exposed)
- A = projected area (m^2)
- τ = time of exposure (sec)
- N = meteoroid flux for particles capable of penetrating tubing (Particles/m^2-sec)

The tube wall thickness is computed from Equation (2) so that the number of particles determined from the meteoroid flux model having sufficient energy to penetrate the tubing gives the desired probability of success from Equation 3.

For a five year mission the tubing must be designed so that only relatively large meteoroids are capable of penetration. For large meteoroids the cumulative meteoroid flux model for sporadic and stream meteoroids is[9]

$$\log_{10} N = -14.37 - 1.213 \log_{10} m \qquad (4)$$

Where N is the flux density for meteoroids having mass greater than or equal to "m". The meteoroid mass may be expressed in terms of quantities in Equation 2 as follows:

$$m = \frac{\pi}{6} \rho_m d_m^3 \qquad (5)$$

Equations 2 - 5 may be solved to give the tubing wall thicknesses required for a given design and required probability of success.

Because of the danger of possible contamination by leaking thermal control system fluids, the tube wall thickness should be selected so that there

is only a very small probability of a single meteoroid puncture.

To minimize the contamination threat emphasis should be placed on designing the system to minimize the possibility of a single meteoroid penetration with the least system weight and complexity. Table XII compares meteoroid penetration characteristics data for two typical 150 ft^2 radiator designs as calculated from Equations 2 - 5. The results show that high probabilities of mission success are possible with moderate radiator tube wall thicknesses.

A significant weight savings is possible if plastic meteoroid barriers are employed so that the wall thickness of the transport tubing or heat pipes may be reduced. The elongation term in Equation 2 is much larger for plastics ($\varepsilon = 300$) than for metals ($\varepsilon = 3$). Limited experimental data in the literature substantiates the importance of this term.

Qualitative data for plexiglas and polycarbonate[10] shows that polycarbonate ($\rho = 1.2$, $\varepsilon = 5$) for retarding meteoroids. Hypervelocity test results for polyethylene ($\rho = 0.9$, $\varepsilon = 500$) in Ref. (7) are predicted conservatively by Equation (2). The equation predicts slightly greater depths of penetration than are measured at velocities below 12 Km/sec, and much greater depths of penetration than Ref. (7) indicates will occur at velocities typical of micrometeoroids, viz. 20 Km/sec.

Tests were conducted at Texas A&M University[8] in support of this contract to substantiate that Equation 2 gives the correct depth of penetration for FEP Teflon tubing. The results given in Figure 8 show that the penetration depths of nylon projectiles, $\rho = 1.15$, are predicted adequately by Equation 2 whereas steel projectiles, $\rho = 8.0$, penetrate greater depths than the equation predicts. This indicates that the exponent of the projectile density in Equation 2 may be too small. If this is the case the equation is conservative for predicting damage by micrometeoroids ($\rho = 0.5$).

Table XII shows that the weight of the radiator panel may be reduced by more than 20 lb_m if Teflon meteoroid barriers are used. An alternative procedure for reducing weight involves the application of meteoroid bumpers. Multiple wall, or bumper type meteoroid protection systems are known

TABLE XII

COMPARISON OF MICROMETEOROID PROTECTION REQUIREMENTS
FOR TYPICAL PUMPED FLUID AND HEAT PIPE RADIATOR DESIGNS

DESIGN VARIABLE (5 Year Life)	PUMPED FLUID RADIATOR	HEAT PIPE RADIATOR
Radiator Tube Spacing	6"	12"
Tubing I.D.	0.1875"	0.50"
Radiator Surface Area (Each Side) (2-Sided)	150 Ft^2	150 Ft^2
Tubing Target Area	14.73 Ft^2	19.64 Ft^2
Probability of no Penetration	0.99	0.99
Tubing Wall Thickness Required	0.139"	0.151"
Tubing Weight	51.3 lbm	55.6 lbm
Weight with Teflon Meteoroid Barrier	29.6 lbm	31.4 lbm

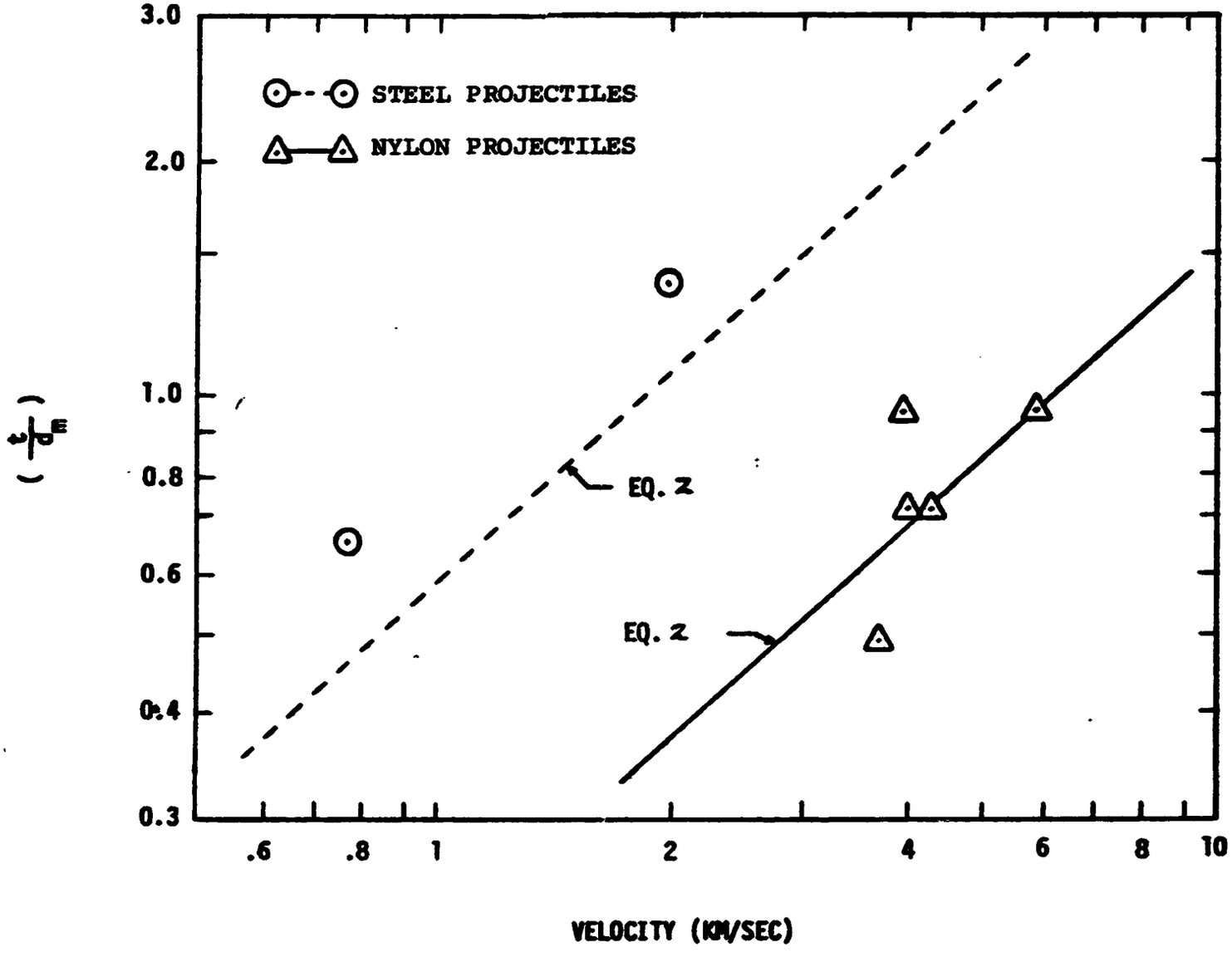

FIGURE 8 HYPERVELOCITY IMPACT TEST OF FEP TEFLON

to have significant weight advantage over single wall or armor type systems, but complicate the radiator design such that they have not been employed in short mission duration applications where the mass associated with meteoroid protection is not significant.

Ground test data have shown that the optimum multiple wall system contains a thin first wall called a bumper, and a second or main wall which is spaced at a sufficient distance from the bumper to permit a meteoroid striking the bumper to be dispersed before making contact with the main wall. Systems with more than two sheets do not provide as much protection as those with two properly designed sheets[16]. Honeycomb or other filler materials between the walls is less effective than a vacuum or air gap. The thickness of the bumper should be sufficient to cause damage to the meteoroid, but should not be so thick that material broken loose from the bumper has enough mass to damage the main wall. The optimum thickness of the bumper is approximately one-tenth the diameter of the projectile.

Several emperical equations have been proposed to represent the relationship of the required thicknesses of the first and second walls, the spacing between the walls, the target material properties, and the projectile properties. A general form of the equation for the thickness of the main wall is

$$t_2 = K V_m^{\alpha} S^{\beta} \rho_m^{\gamma} d_m^{\delta} \qquad (6)$$

where K, α, β, γ, and δ are empirical constants, and S is the spacing between the plates. Table XIII lists the values of the exponents in Eq. 6 from various correlations in the literature. The table shows that there are significant

TABLE XIII EXPONENTS IN EQUATION 6

REFERENCE NO.	α	β	γ	δ	(tl/dm)
11	1	- 2	2	4	?
12	0	- 2	1	3	0.1
13	1	- .5	0.5	1.05	0.3 to 0.5
14	.278	- 1.39	?	2.92	0.25 to 0.4
15(a)	?	- 0.75	0.6	1.0	0.25
15(b)	?	- 1.4	0.6	1.0	0.10

differences in the forms of the proposed equations. Part of the discrepancy is due to variations in the thicknesses of the bumper sheets which have a large influence on the type of damage to the main wall. The equations from Ref. (12) and Ref. (15-b) are for optimum front sheet thicknesses, and therefore should not be applied to more general cases. Of the remaining equations, the one from Ref. (14) gives the most conservative estimate of the material thickness required to prevent penetration of the main wall. This equation also predicts depths of penetration measured in Refs. (15) and (17). Therefore, Eqs. 7 and 8 below, from Ref. (14), are employed in this work to design radiators with meteoroid bumpers.

$$t_2 = 5.33 \left(\frac{\rho_m}{\rho_t}\right)^{1/2} \frac{V^{0.278} d_m^{2.92}}{t_1^{0.578} S^{1.39}} \tag{7}$$

$$0.1 d_m \leq t_1 \leq 0.4\, d_m \tag{8}$$

The materials constant, K, which was originally measured for 2024-T3 aluminum targets and pyrex-glass projectiles, has been modified to account for density variations of the target and projectile.

When applying Eq. 7 to design radiators, there are two variables, t_2 and S, which may be adjusted to provide meteoroid protection, whereas in single wall radiator designs, there is only one variable, the tubing wall thickness. The thickness of the bumper layer is fixed by Eq. 8 and the diameter of the smallest meteoroid that will penetrate the double wall system. Since there are two variables defined in Equation 8, one of the variables can be arbitrarily selected to minimize radiator fabrication difficulties, or to reduce weight. The radiator optimization computer routine described in Section 2.5 is programmed to minimize weight by solving Eq. 8 simultaneously with

$$\frac{d(wt)}{dS} = 0 \tag{9}$$

non-linear expressions are obtained for t_2 and S which must be solved iteratively.

2.5 OPTIMIZATION OF PUMPED FLUID SPACE RADIATORS

Manifold Configurations

Typically, pumped fluid space radiators are designed with parallel flow passages which are joined together by manifolds at the edges of the radiator. This design has been shown to be effective for ECS radiators with heat rejection capacities of the order of 10 KW. For large radiators, the system weight can be reduced if the flow routing is modified so that the lengths of the manifolds and crosstube are not constrained by the overall radiator dimensions.

For the configuration shown in Figure 9, the physical dimensions of the cross tubes are not tied directly to the radiator size so that the designers have more freedom to select the tube diameter, the Reynolds number, and other radiator parameters when optimizing heat transfer, pressure drop, and exposed cross section to the micrometeoroid environment. In effect, an arbitrarily large radiator is constructed from a number of optimum sized, parallel connected panels having common manifolds.

Very large radiator systems might require a more general panel configuration with parallel headers. In this case the manifold dimensions are independent of the radiator size, and may be varied to obtain an optimum design. This generality is not required for the radiators considered in this study. Statistical analyses presented in Section 4.0 show that very large radiator systems should be constructed from smaller subsystems having independent pumped fluid loops.

The parallel manifold configuration of Figure 9 is justifiable for the radiator sizes considered herein. The optimum cross tube diameters are relatively small because of micrometeoroid considerations so that close manifold spacing is necessary to minimize fluid pressure losses. Figure 10 gives the percentage radiator weight reduction that occurs with multiple manifolds for typical ECS operating conditions.

The minimum radiator weight in Figure 10 occurs when the panel has four manifolds. This is typical of all the systems analyzed in this work. The weight of the headers becomes large in radiators with more than four manifolds, and effects the advantage of the smaller tube diameters which are possible with additional manifolds. The radiator weight is relatively insensitive to the number of manifolds for heat rejection rates of the order of

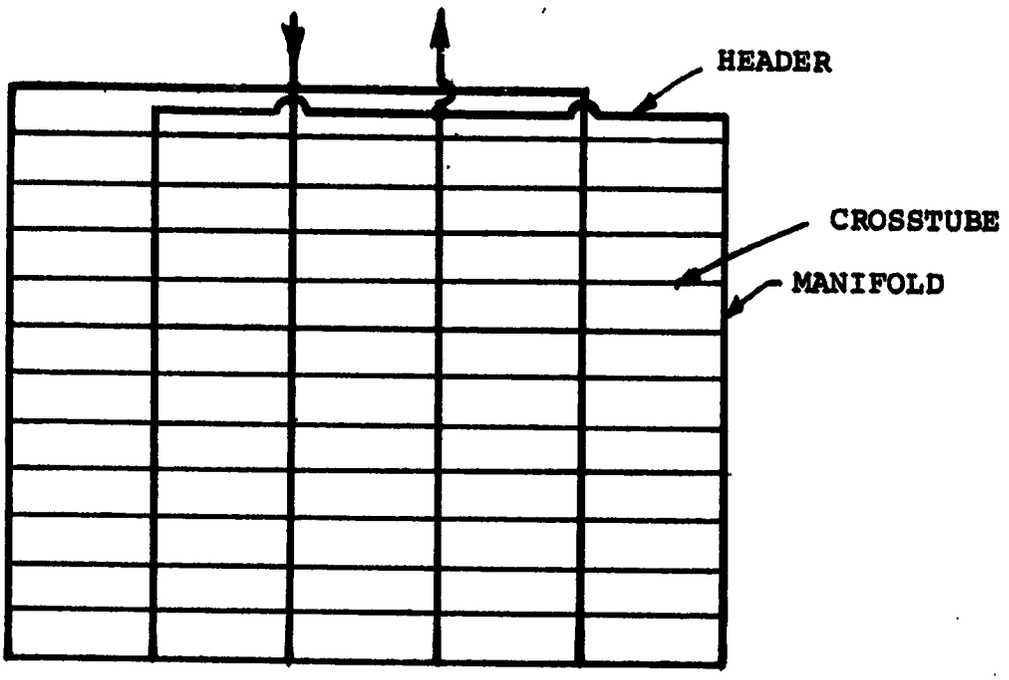

FIGURE 9

PARALLEL MANIFOLD RADIATOR CONFIGURATION

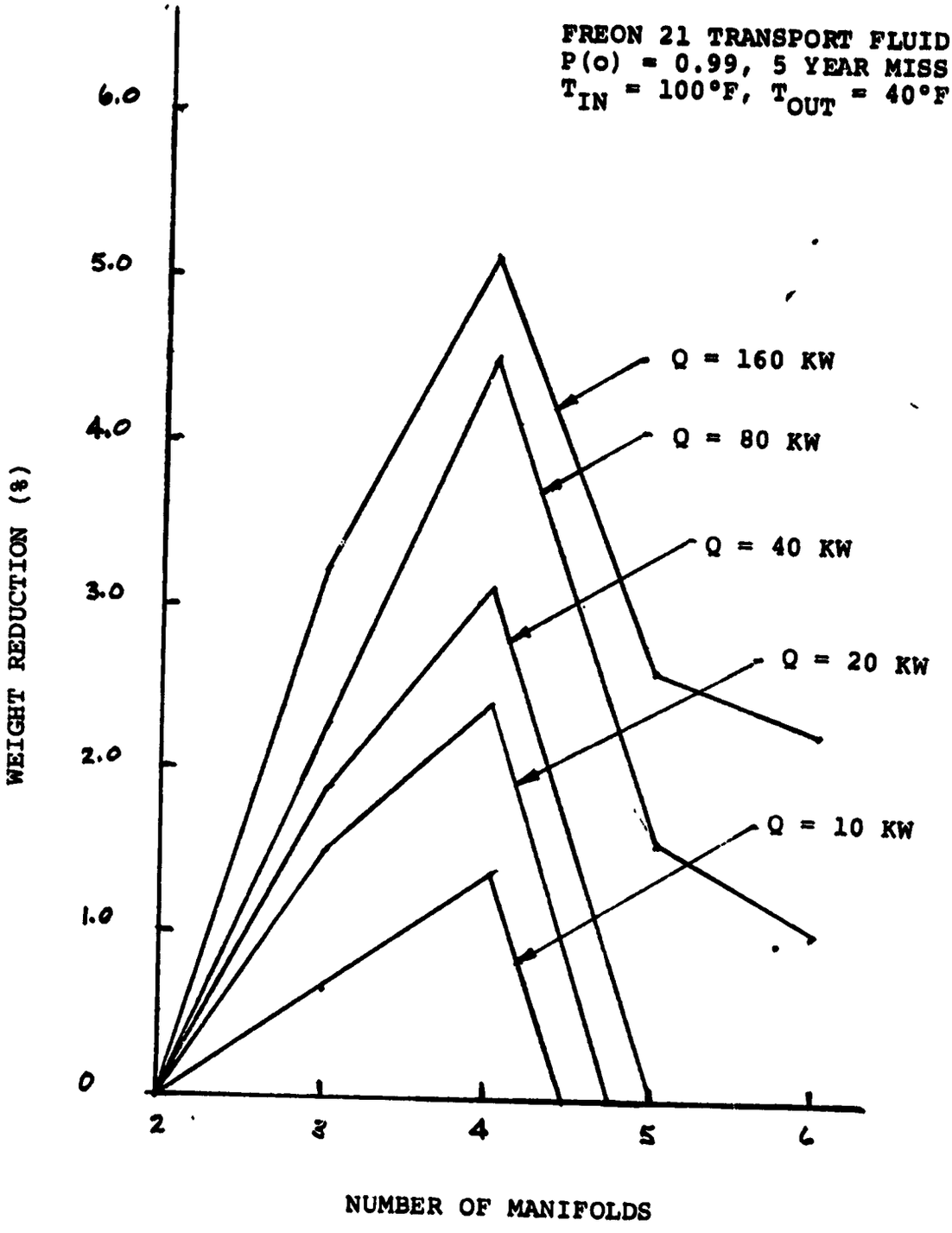

FIGURE 10
WEIGHT REDUCTION FOR TYPICAL PUMPED FLUID
SPACECRAFT RADIATORS WITH MULTIPLE MANIFOLDS

10 KW, so that the panel design can be biassed without weight penalty by constraints such as would occur when adapting the panel to an existing deployment mechanism for example.

Radiator Optimization Calculations

Table XIV lists the design variables for the radiator panel of Figure 9. To determine the best radiator design, one must select an optimization criterion in the form of some function of the design variables which is to be minimized, establish the relationship between the dependent and independent variables, and then determine the values of the independent variables which minimize the criterion function. In this section a procedure is described for minimizing a function of radiator panel weight and area

$$F = wt + C_1 A \tag{10}$$

The weight of the radiator is considered to be the sum of the weights of the manifolds, headers, cross tubes, radiator fin and coating, radiator fluid, and weight penalty for pressure drop.

$$wt = W_M + W_H + W_{LT} + W_{FC} + W_{FL} + W_P \tag{11}$$

Other associated radiator system component weights can be included in the analysis by modifying constants in Eqs. 10 and 11. For example, the weight of the deployment system is proportional to the radiator area, and can be accounted for by increasing the constant C_1 in Eq. 10.

The manifolds and headers must be sized to give a uniform flow distribution. This is done by requiring that the pressure drop in the headers and manifolds be small in comparison to the pressure drop in the cross tubes.

$$\Delta P_M = C_2 \Delta P_{CT} \tag{12}$$

$$\Delta P_H = C_2 \Delta P_M \tag{13}$$

For turbulent flow in the manifolds and cross tubes Eq. 12 becomes

$$\frac{S}{d_m^{4.8}} \left[\left(\frac{2\dot{m}W}{S}\right)^{1.8} + \left(\frac{2\dot{m}W}{S} - 2\dot{m}\right)^{1.8} = \ldots (2\dot{m})^{1.8} \right] = C_2 \frac{\ell}{d_{ct}^{4.8}} \dot{m}^{1.8} \tag{14}$$

TABLE XIV

GENERAL PUMPED FLUID RADIATOR DESIGN PARAMETERS

FIXED PARAMETERS	INDEPENDENT PARAMETERS	DEPENDENT PARAMETERS
REQUIRED HEAT REJECTION	NUMBER OF MANIFOLDS	RADIATOR AREA
MISSION TIME	CROSS TUBE SPACING	RADIATOR WEIGHT
PROBABILITY OF NO METEOROID PENETRATION	CROSS TUBE DIAMETER	LENGTH OF CROSS TUBES
FLUID PROPERTIES	REYNOLDS NUMBER	MANIFOLD DIAMETER
FLUID INLET TEMPERATURE	FIN EFFICIENCY	HEADER DIAMETER
FLUID OUTLET TEMPERATURE	$\Delta P(\text{MANIFOLD})/\Delta P(\text{CROSS TUBES})$	FIN THICKNESS
ENVIRONMENT TEMPERATURE		TUBE WALL THICKNESS
RADIATOR COATING PROPERTIES		TOTAL PRESSURE DROP
PUMPING POWER PENALTY FACTOR		FLOWRATE PER CROSS TUBE
PUMP EFFICIENCY		
FUNCTION OF RADIATOR WEIGHT AND AREA TO BE MINIMIZED		

The sum in Eq. 14 may be approximated as follows

$$(2\dot{m})^{1.8}[1 + 2^{1.8} + 3^{1.8} + \ldots (\frac{W}{S})^{1.8}] \quad (2\dot{m})^{1.8}\frac{(\frac{W}{S})^{2.8}}{2.8} \quad [1 + 1.4\,\frac{S}{W}] \qquad (15)$$

Equation 14 becomes

$$(\frac{d_m}{d_{ct}}) = (\frac{1.243}{C_2} \quad \frac{W^{2.8}}{S^{1.8\ell}})^{0.2083} \qquad (16)$$

The exterior manifolds carry only half as much flow as the interior manifolds, and therefore have smaller diameters

$$d_m(\text{EXTERIOR}) = 0.772\, d_m \qquad (17)$$

For laminar flow in the manifolds and cross tubes,

$$(\frac{d_m}{d_{ct}}) = (\frac{W^2}{C_{2S\ell}})^{0.25} \qquad (18)$$

For turbulent flow in the manifold and laminar flow in the cross tubes

$$(\frac{d_m}{d_{ct}}) = (\frac{.00357\, W^{2.8}\, R_{e(\text{CROSS TUBE})}^{0.8}}{C_2 S^{1.8} \ell})^{0.2083} \qquad (19)$$

The weight of the manifolds per unit area is

$$W_M^1 = \frac{\rho\pi\, t_m}{144\, L}\,[t_m(\frac{L}{\ell} + 1) + d_m(\frac{L}{\ell} + .544)] \qquad (20)$$

The diameter of the header is the same as the diameter of the manifold for designs with up to four manifolds. When there are more than four manifolds,

$$(\frac{d_4}{d_m}) = 0.5146\,(\frac{(L - \ell)^{1.8}(L + 4.6\ell)}{C_2\, W\, \ell^{1.8}})^{0.2083} \qquad (21)$$

The weight of the headers per unit area is

$$W_H^1 = \frac{\rho \pi t_H}{144\ell} (d_h + t_H)^2 (1/W - \ell/A) \qquad (22)$$

The weight of the cross tubes per unit area is

$$W_{CT}^1 = \frac{\rho \pi t_{CT}}{144S} (d_{CT} + t_{CT})(1 + S/W) \qquad (23)$$

The wall thickness required to prevent failure by micrometeoroid puncture is computed from the meteoroid environment model, a ballistic equation for depth of penetration of the tubing material, and the required probability of survival. For long duration missions the tubing wall is sufficiently thick that only relatively large meteoroids are capable of penetration. The environment model[9] for large meteoroids is

$$\log_{10} N = -14.37 - 1.213 \log_{10} M \qquad (24)$$

Where N is the average number of micrometeoroids with mass greater than on granes which will strike 1 m^2 of radiator area per second. Equation 24 assumes an average meteoroid density of 0.5 gm/cc. Thus the meteoroid diameter is

$$d_M = 1.7578 \cdot 10^{-4} N^{-0.2748} \qquad (25)$$

A ballistic equation[6] for depth of penetration of the radiator tubing is

$$t = 6.32 \frac{d_M^{19/18}}{\varepsilon^{1/8} \rho^{1/2}} \qquad (26)$$

The probability of no meteoroid penetration is

$$P(0) = e^{-\zeta A N \tau} \qquad (27)$$

Where ζA is the total exposed cross section and τ is the time of exposure. The relative thicknesses of the cross tubes, manifolds, and headers are determined by minimizing the radiator weight for constant survivability. The weight of the flow passages is

$$wt = A_{CT} t_{CT} + A_M t_M + A_H t_H \qquad (28)$$

From Eqs. (25), (26), and (27), the probability of no penetration is

$$P(0) = \exp\left[-c\left[\frac{A_{ct}}{t_{ct}^{3.45}} + \frac{A_m}{t_m^{3.45}} + \frac{A_H}{t_H^{3.45}}\right]\right] \quad (29)$$

For minimum weight

$$d(wt) = A_{ct}dt_{ct} + A_m dt_m + A_H dt_H = 0 \quad (30)$$

For constant survivability,

$$dP(o) = \frac{A_{CT}}{t_{ct}^{4.45}}\, dt_{CT} + \frac{A_M}{t_m^{4.45}}\, dt_M + \frac{A_M}{t_H^{4.45}}\, dt_H = 0 \quad (31)$$

Multiplying Eq. 31 by an arbitrary constant (a Lagrangian multiplier) and subtracting Eq. 30

$$A_{CT}\left[1 - \frac{\lambda}{t_{ct}^{4.45}}\right]dt_{CT} + A_M\left[1 - \frac{\lambda}{t_m^{4.45}}\right]dt_M + A_H\left[1 - \frac{\lambda}{t_H^{4.45}}\right]dt_H = 0 \quad (32)$$

For Eq. 32 to be satisfied for all values of the multiplier

$$t_{ct} = t_m = t_H = \lambda^{1/4.45} \quad (33)$$

Thus the minimum weight occurs when the cross tubes, manifolds, and headers have equal thicknesses. The required thickness is

$$t = \frac{0.1088}{\rho^{1/2} c^{1/8}}\left[\frac{\zeta A\tau}{n\ell n(P(o))}\right]^{0.29} \quad (34)$$

Where the exposed cross section is related to the radiator area by

$$A = \pi A_R\left[\frac{d_{CT}}{S} + \frac{d_M}{L}\left(\frac{L}{\ell} + 0.544\right) + \frac{2d_H}{A_R}(L - \ell)\right] \quad (35)$$

Similar equations derived for the main wall thickness and bumper spacing in meteoroid bumper designs are programmed into the radiator optimization computer routine listed in Appendix A. The radiator area is computed by summing the radiating areas of each cross tube

$$A_R = \Sigma \left(\int_0^{\ell} S dx \right) = \left(\frac{L}{\ell}\right)\left(\frac{W}{S} + 1\right) \int_{T_{in}}^{T_{out}} \frac{s dT}{\left(\frac{dt}{dx}\right)} \tag{36}$$

where

$$\frac{dT}{dx} = \left(-\frac{1}{\dot{m}Cp} \right)\left(\frac{\eta \varepsilon \sigma S (T^4 - T_\infty^4)}{1 + 4\eta\varepsilon\bar{\sigma} S R T^3} \right) \tag{37}$$

and R is the resistance to heat transfer between the transport fluid and the base of the radiating fin. If the resistance to conduction through the tube wall is negligible,

$$R = \frac{1}{\pi K_f Nu} \tag{38}$$

Combining Eqs. 36 and 37

$$A_R = \frac{\dot{m}Cp \left(\frac{L}{\ell}\right)\left(\frac{W}{S} + 1\right)}{\eta\varepsilon\sigma} \left\{ \int_{T_{out}}^{T_\infty} \frac{dT}{T^4 - T_\infty^4} + 4\eta\bar{\varepsilon}\sigma S R \int_{T_{out}}^{T_\infty} \frac{T^3 dT}{T^4 - T_\infty^4} \right\} \tag{39}$$

substituting $Q = \left(\frac{L}{\ell}\right)\left(\frac{W}{S} + 1\right) \dot{m}Cp \left(T_{in} - T_{out}\right)$, and integrating

$$A_R = \frac{Q}{\eta\varepsilon\sigma(T_{in} - T_{out}} \left\{ \frac{1}{4T_\infty^3} \ell n \left[\left(\frac{T_{in} - T_\infty}{T_{in} + T_\infty}\right)\left(\frac{T_{out} + T_\infty}{T_{out} - T_\infty}\right) \right] \right.$$

$$\left. - \frac{1}{2T_\infty^3} \left[\tan^{-1}\left(\frac{T_{in}}{T_\infty}\right) - \tan^{-1}\left(\frac{T_{out}}{T_\infty}\right) \right] + \eta S \varepsilon \sigma R \, \ell n \left(\frac{T_{in}^4 - T_\infty^4}{T_{out}^4 - T_\infty^4} \right) \right\} \tag{40}$$

The weight of the radiator fin and coating per unit area is

$$W_{fc}' = \rho_f t_f + \rho_c t_c \tag{41}$$

The thickness of the radiator fin is a function of the radiator fin efficiency. For fin efficiencies greater than 0.7, the following equation represents the correlation obtained numerically by Lieblein[18].

$$t = \frac{3\sigma\bar{\epsilon}S^2T^3}{K(1-\eta)[.8307 + .7925(1-\eta) + .7050(1-\eta^2)]^2} \qquad (42)$$

The coating thickness is a function of the type of coating (e.g. silver backed Teflon) and the emissivity of the surface. In this study, silver backed Teflon coating with an emissivity of 0.8 is assumed. The coating thickness, including adhesive, for a two sided radiator is 0.012 inch.
The fluid weight per unit area is

$$WFL' = \frac{\rho_{FL}\pi}{576}\left[\frac{d_{ct}^2}{S} + \frac{d_m^2}{\ell}\left(1 + 0.544\,\frac{\ell}{L}\right) + \frac{d_H^2}{w}\left(1 - \frac{\ell}{L}\right)\right] \qquad (43)$$

The pumping power weight penalty per unit area is

$$W_P' = 5.423.10^{-8}\,\frac{C_3\dot{m}\Delta P}{\rho_{FL}S\ell\eta_P} \qquad (44)$$

Where ΔP is computed from friction factor versus Reynolds number data, and C_3 is the pump power penalty factor (lb/KW).

Equation 44 is the final equation needed to determine the value of the function of weight and area that is to be minimized to obtain the optimum radiator design. To determine the best radiator design, trial values of the independent variables in Table XIV are substituted into the equations listed above until the minimum value of the function F is established. Since this involves many calculations and a logical search through the ranges of several independent variables, a computerized approach is necessary. Listings of the radiator optimization routines developed for meteoroid armor and bumper protected designs are listed in Appendices A and B.

2.6 OPTIMIZATION OF HYBRID HEAT PIPE/PUMPED FLUID RADIATORS

Manifold Configurations

The manifold design of hybrid heat pipe/pumped fluid radiators must take into account watt-inch limitations of heat pipes, temperature drop

across the interface from the transport fluid to the heat pipe working fluid, pressure drop in the transport fluid loop, and micrometeoroid protection requirements. Transport fluid flow routings such as are shown in Figure 11 provide large radiating surface consistent with watt-inch limits of heat pipes and minimum exposed manifold cross sections to micrometeoroids. The overall width and length of the radiator can be varied by changing the diameters of the heat pipes to adjust the allowable distance between manifolds, and by selecting an integral number of manifolds consistent with the approximate overall dimensions required.

To minimize the temperature drop from the transport fluid to the heat pipe, heat conducting fins such as shown in Figure 12 may be employed. In this design compact heat exchanger core is employed to transfer heat from the transport fluid to conductive fins attached to the heat pipes. The fins have a dual function as heat conductors and meteoroid armor for the transport fluid loop.

The manifold detail in Figure 12 is one of several analyzed in this work. It is competitive in performance for some heat rejection requirements with other designs studied, and would be relatively easy to fabricate. Other designs developed under Vought funding are considered proprietary, and, therefore, are not discussed in detail here. Performance characteristics of some of the proprietary designs are compared with those of the design of Figure 12 and of pumped fluid radiators in Section 4.0.

Heat Pipe Designs

Exotic heat pipe designs are not required or desirable for hybrid radiator applications. Since the cost of the heat pipes is a significant part of the total cost of the radiator, and high watt-inch capabilities are not required, the simplest possible heat pipe designs should be selected. Axial grooved ammonia heat pipes have acceptable thermal performance characteristics for most applications, are highly reliable, and can be fabricated at less cost than other types of heat pipes. Center core wick heat pipes have slightly better thermal performance and cost slightly more than grooved pipes. Artery type heat pipes should be avoided because of their poor reliability and high cost.

Since each heat pipe in a hybrid heat pipe/pumped fluid radiator operates at a different temperature, there is a slight performance advantage

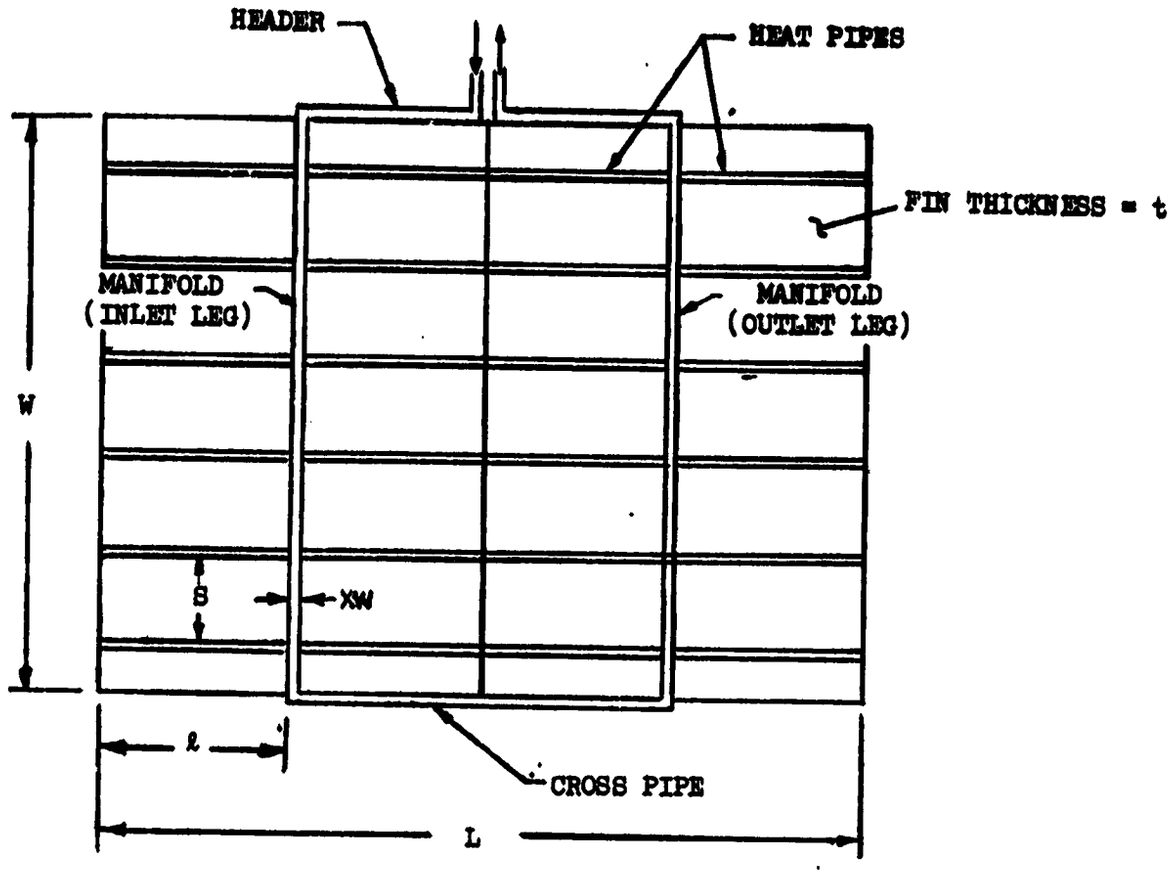

FIGURE 11 HEAT PIPE RADIATOR FLOW ROUTING CONFIGURATIONS

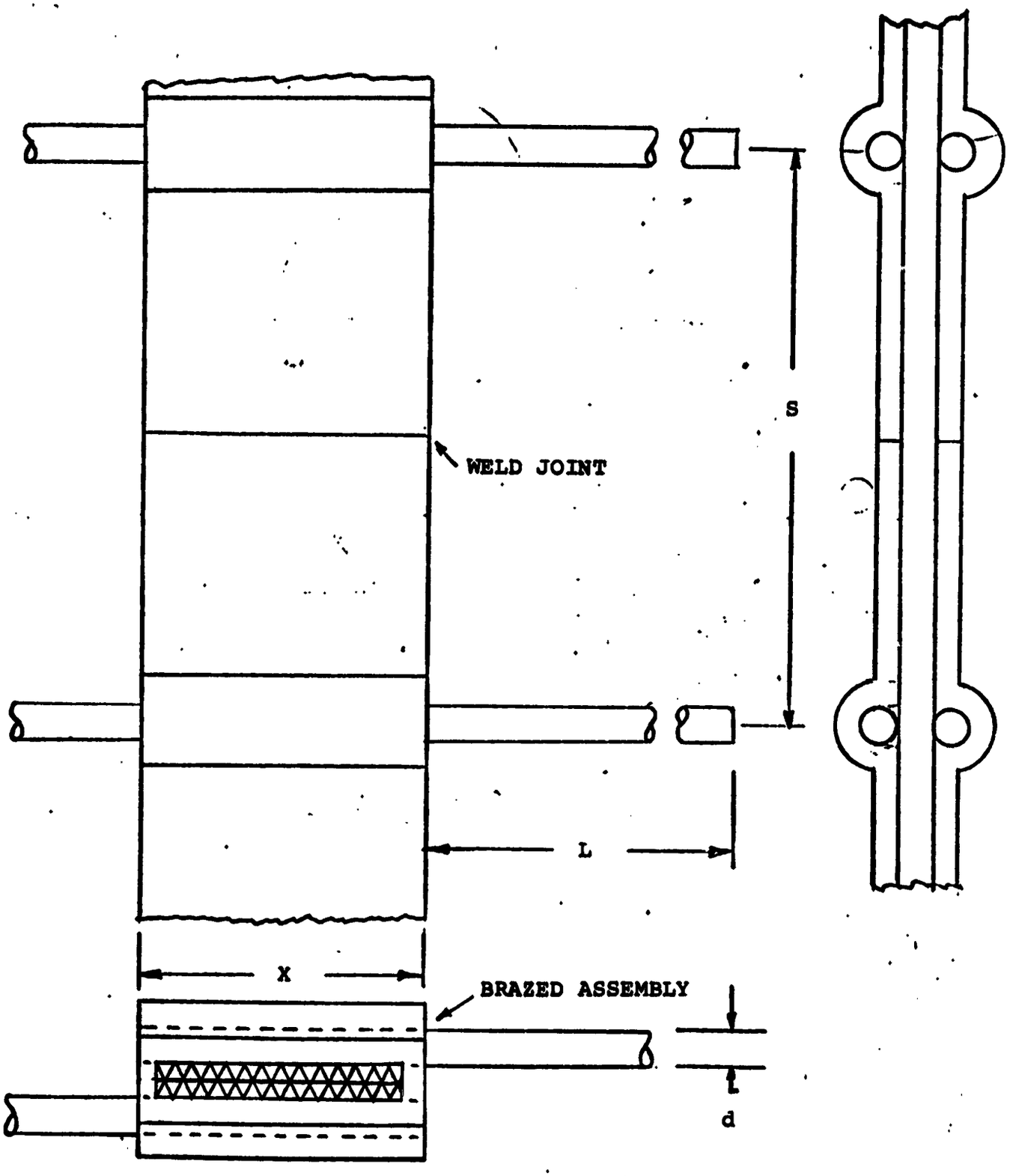

FIGURE 12 TYPICAL HEAT PIPE RADIATOR MANIFOLD DETAIL

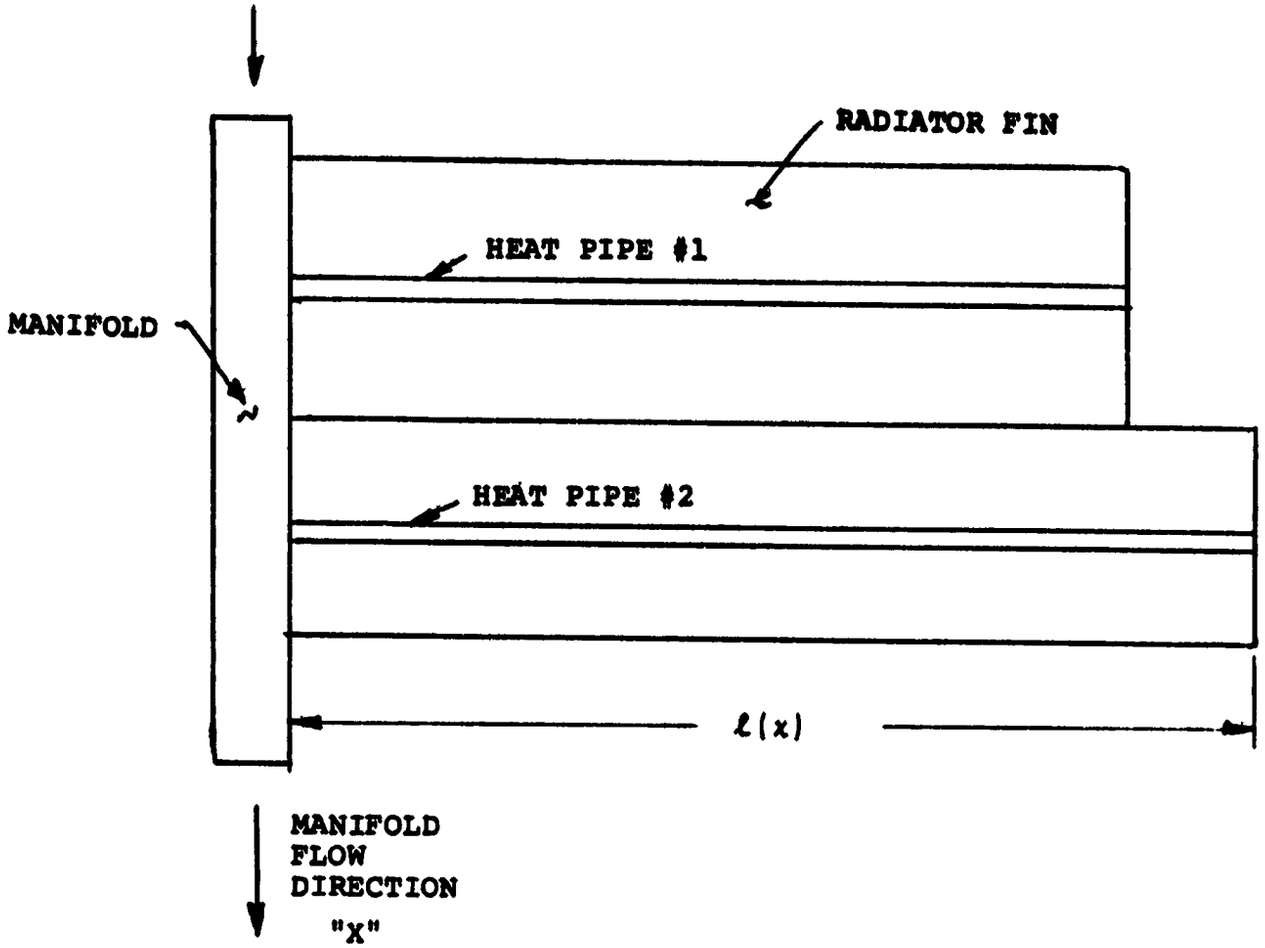

FIGURE 13 VARIABLE LENGTH HEAT PIPE RADIATOR

possible if the lengths of the heat pipes are adjusted in accordance with their heat rejection requirements. The problem to be solved in optimizing the design is to determine the length of the heat pipes in Figure 13 as a function in the flow direction (or fluid temperatures). The solution obtained by calculus of variations in Appendix C is

$$\ell = ct^{-3/2} \tag{45}$$

where C is a constant. Equation 45 shows that for minimum radiator area, the lengths of heat pipes near the transport fluid entrance to the radiator should be shorter than those near the outlet of the radiator. However, calculations in Appendix C show that the area of a radiator with optimum heat pipe lengths is less than 0.1% smaller than the area of a radiator with the same heat rejection capacity having constant length heat pipes. Thus, since variable length heat pipes complicate the radiator design, and do not significantly improve performance, only constant length heat pipes are considered in this work. Computer analyses performed under a separate contract show that variable spacing of heat pipes also complicates the radiator design with less than 0.1% increase in performance. Thus only constant spacing geometries are considered in this work.

The diameters of heat pipes must be sized so that they are capable of transporting heat at the maximum required rate. For minimum weight the heat pipe diameters should be as small as possible. Therefore, since the heat pipes near the transport fluid entrance are hotter, and reject more heat than those near the outlet, their optimum diameters should be larger. However, since variable heat pipe diameters also complicate the problem of fabricating the radiator panel, only constant diameter designs are considered here. If future designs should become so weight critical that variable heat pipe diameters would be considered, it is probable that an alternative approach of varying length or spacing in accordance with watt-inch requirements would be more attractive from a manufacturing viewpoint.

Hybrid Heat Pipe Radiator Optimization

The optimization of hybrid heat pipe radiators is similar to that of pumped fluid radiators in that values of independent variables such as heat pipe spacing, and radiator fin thicknesses are determined to minimize a

function of weight and area. An additional complication is involved in modeling the heat transfer in the manifold. For example, the thermal model of the manifold in Figure 12 must account for heat transfer in the compact heat exchanger core, the meteoroid shield, the joint between the manifold and the heat pipe, and the evaporative surface of the heat pipe. Pressure drop in the compact heat exchanger core must also be accounted for. A general thermal model is set up for each type of manifold design which includes adjustable parameters such as the heat exchanger core width "z" in Figure 12. In the optimization analyses the best values of the adjustable parameters are determined by computing the weight and area of the radiator for a range of permissable values of the parameters. The best manifold parameters and radiator fin parameters are determined simultaneously to obtain a true optimum design.

Computer routines were developed under Vought funding to optimize hybrid heat pipe radiator designs. These routines are considered to be proprietary, and are not discussed in detail here. Results of the optimization analyses are presented in Section 4.0 where candidate radiators based on pumped fluid and hybrid heat pipe designs are compared.

3.0 ADVANCED RADIATOR CONCEPTS

In this section advanced radiator concepts are presented that are expected to be applicable to the requirements of future spacecraft. These concepts give emphasis to adaptability, reliability, and growth potential for reduced development costs; and consider traditional weight and radiating area to be of secondary importance. Groundrules, desirable features, and technical issues for evaluating new concepts are listed in Tables XV, XVI, and XVII. Example applications of the advanced heat rejection systems are: the small power module, the large power module, and experiments for space processing, communications, solar power satellite demonstration, life sciences, and space construction demonstration.

3.1 Modular, Self Contained, Long Life Radiator System

The central idea of the modular, self-contained, long life radiator system shown in Figure 14 is to provide a modular deployable system with easily added or replaced modules. The heat rejection capacity can be easily expanded as requirements grow by adding additional modules. Refurbishment is accomplished by replacing modules, and development and qualification costs are reduced. The radiator panels could employ either flexible or rigid fins, and heat pipe or pumped fluid radiator panels could be used. The modules could be designed to fit into the Shuttle payload bay when retracted, as shown in Figure 15. For a 250 KW power module application, 8 to 10 modules could be joined together as shown in Figure 16.

3.2 Blanket Radiator System

The blanket radiator system consists of submodules of heat pipes joined by flexible radiator fin material as shown in Figures 17 and 18. The heat pipes may be joined to rigid pumped fluid manifolds by means of contact pressure to form large radiating areas as shown in Figure 19. This system has the advantages of modular designs described above, and may be stowed as a compact package.

3.3 Elemental Heat Pipe Radiator

The idea behind the elemental heat pipe radiator, shown in Figure 20, is to build up spacecraft radiators from the simplest possible elements. The element consists of a single heat pipe connected to a radiator fin. For

TABLE XV ADVANCED RADIATOR CONCEPTS

GROUNDRULES - PRELIMINARY REQUIREMENTS

PERFORMANCE

- 25 → 250 KW (GROWTH CAPABILITY - CAN BE MODULAR)
- LONG LIFE (5-10 YEARS INITIAL)
- 100°F TC 150°F FLUID INLET, 0°F TO 40°F FLUID OUTLET (INITIAL)
- WIDE HEAT LOAD RANGE (UP TO 100:1)
- POWER PENALTY 200 LB/KWe

INTERFACES

- SHUTTLE LAUNCH
- FREE FLYING
  - OR DOCKED TO POWER MODULE (OR OTHER HEAT SOURCE)
  - OR INTEGRAL WITH POWER MODULE (OR OTHER HEAT SOURCE)
- EXPECT TO INTERFACE WITH LARGE STRUCTURES
- INITIAL LOW EARTH ORBIT → LATER GEOSYNCHRONOUS

ERECTION

- DEPLOYABLE (DESIRED)
  - OR ASSEMBLE IN SPACE (NOT SPACE MANUFACTURED)

INITIAL OPERATIONAL CAPABILITY

- MID-TO-LATE 80'S

TABLE XVI ADVANCED RADIATOR CONCEPTS

GUIDELINES - DESIRABLE FEATURES

- SIMPLE STABILIZATION SYSTEM IF FREE FLYING (GRAVITY GRADIENT)
- MODULAR FOR
  - GROWTH POTENTIAL
  - OPTIMUM LIFE
  - PROXIMITY TO HEAT LOAD
  - VERSATILITY - APPLY TO VARIETY OF APPLICATIONS (LARGE OR SMALL)
- GROWTH POTENTIAL FOR HIGHER TEMPERATURES (TO 600°F)
- GROWTH POTENTIAL FOR 30 YEAR LIFE
- QUIESCENT STORAGE CAPABILITY
- SELF HEALING TO DAMAGE (COATING DEGRADATION, LEAKS)
- SIMPLE INTERFACES WITH USER HEAT SOURCE
- MINIMUM POWER CONSUMPTION, WEIGHT, STORAGE VOLUME
- SIMPLE/INFREQUENT MAINTENANCE (NONE PREFERRED)
- MINIMUM IMPACT TO USER HEAT SOURCE
  - ENVIRONMENT
  - STABILIZATION
  - VIBRATION

TABLE XVII ADVANCED RADIATOR CONCEPTS

GUIDELINES - TECHNICAL ISSUES

- **WEIGHT AND VOLUME**
  - TRADITIONAL WEIGHT AND VOLUME MAY NOT BE DRIVERS
  - MANY SHUTTLE PAYLOADS HAVE A SPARSE PACKING DENSITY
  - STOWED WEIGHT AND VOLUME MORE CRITICAL FOR LEO DEPLOYMENT
    - CONSTRAINED BY SHUTTLE CAPABILITIES
  - FOR LEO TO GEO TRANSFER WEIGHT IS A STRONG DRIVER
- **STATIC CHARGE AVOIDANCE**
  - IMPORTANT AT HIGH ALTITUDE ORBITS
  - CAUSES ARCING, SPACECRAFT & COATING DAMAGE
- **THERMAL COATING DEGRADATION**
  - SEVERE AT HIGH ALTITUDE ORBITS
  - CAN FORCE TO DESIGN AROUND OR MAINTAIN
- **LEAK DETECTION/ISOLATION**

FIGURE 14 DEPLOYABLE HEAT REJECTION MODULE ELEMENT

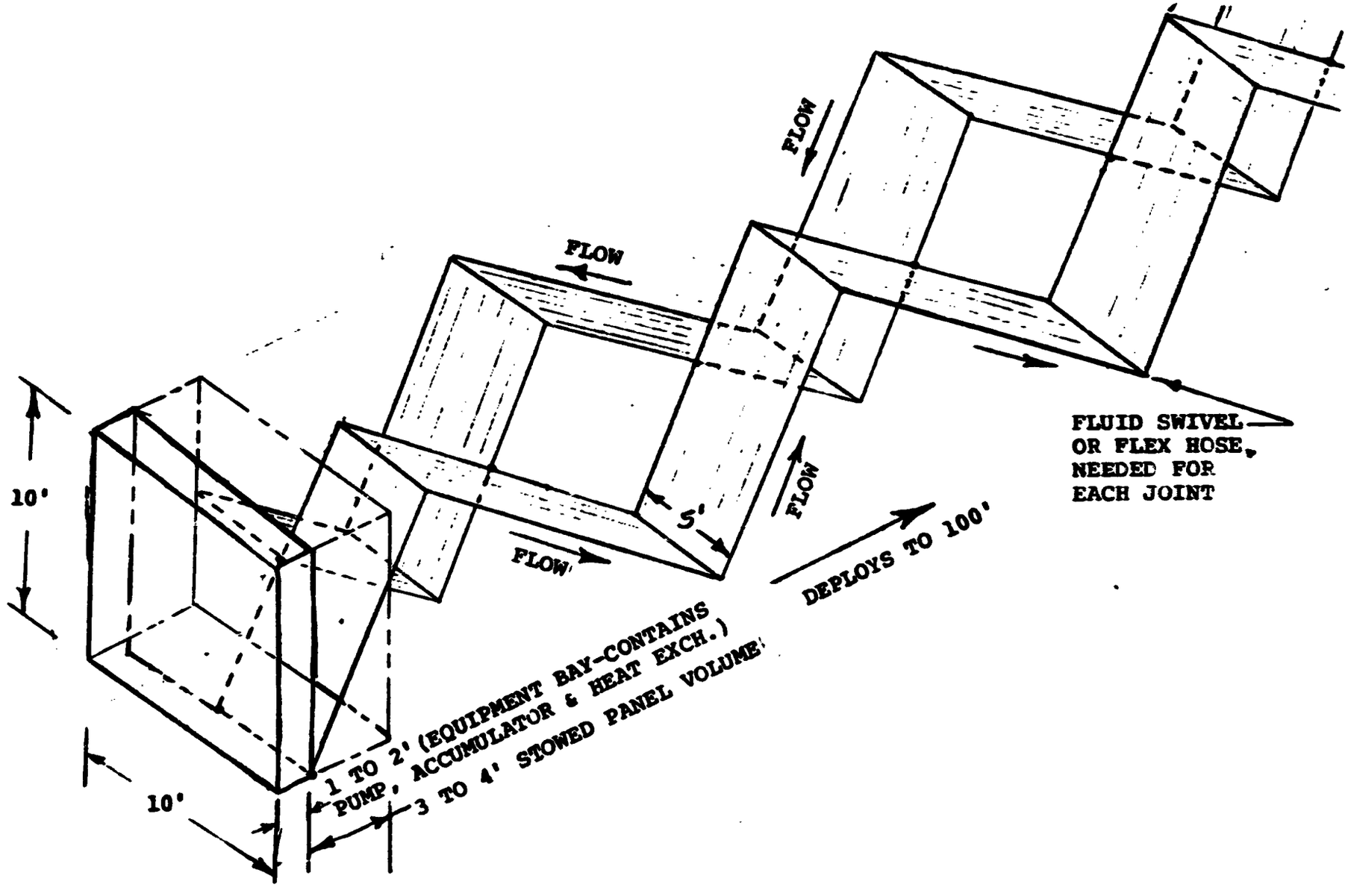

FIGURE 15 HEAT REJECTION MODULE STOWED IN SHUTTLE PAYLOAD BAY

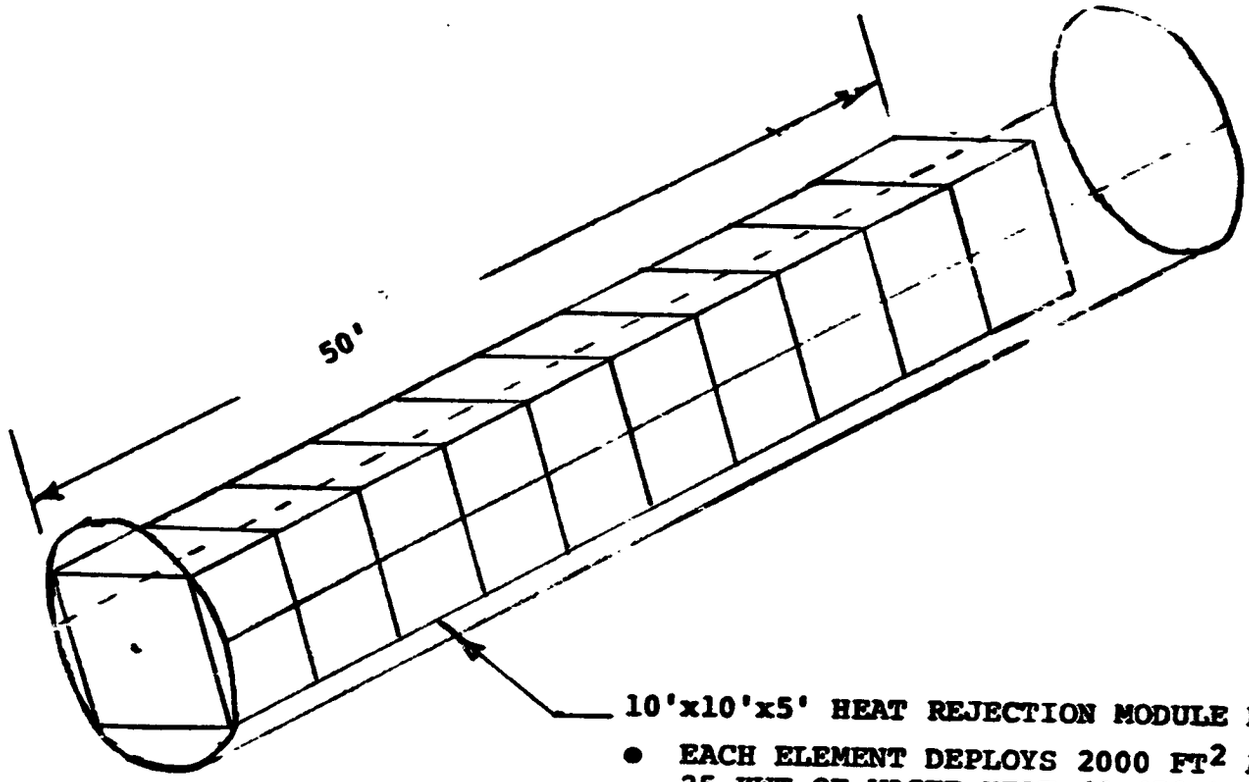

FIGURE 16 HEAT REJECTION MODULE APPLICATION TO TYPICAL 250 KW POWER MODULE

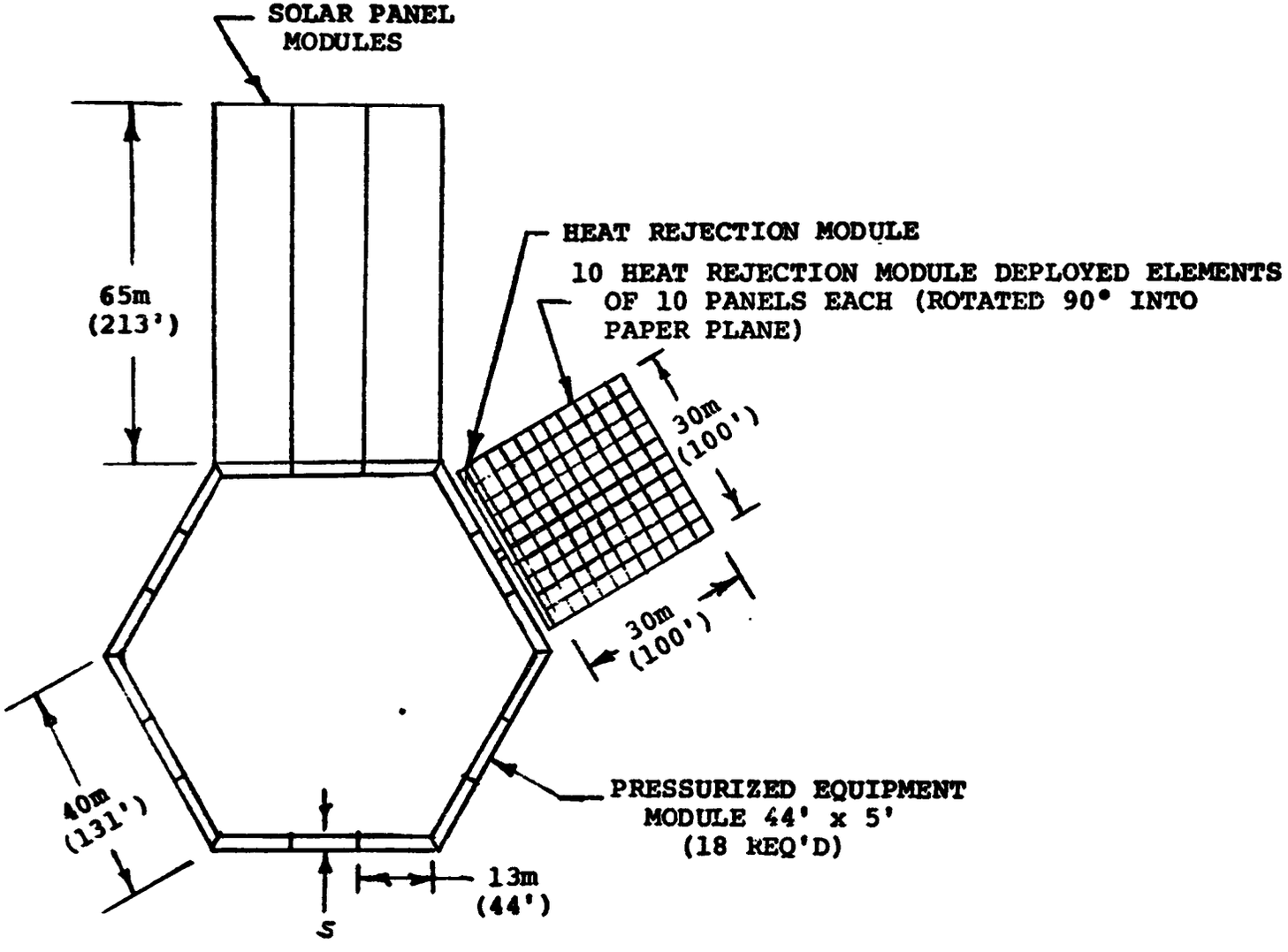

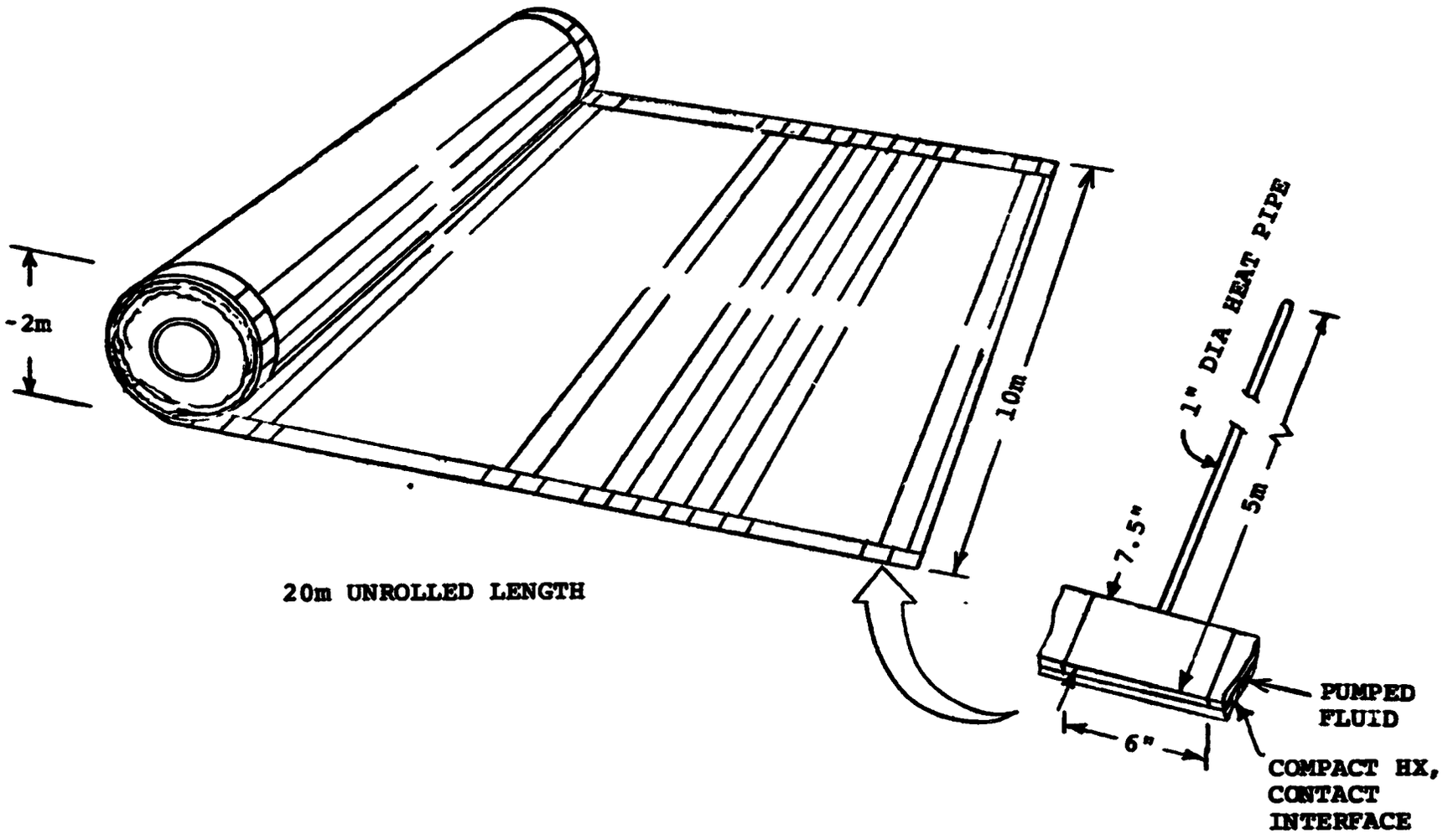

FIGURE 17

BLANKET RADIATOR SUBMODULE

TUBE-FIN

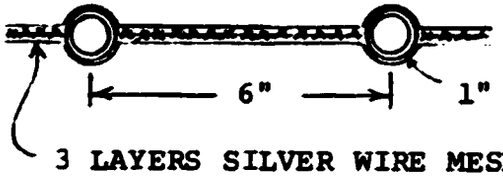

3 LAYERS SILVER WIRE MESH/TEFLON, HEAT BONDED

η_F = .43 , RADIATES FROM BOTH SIDES

HEAT PIPE

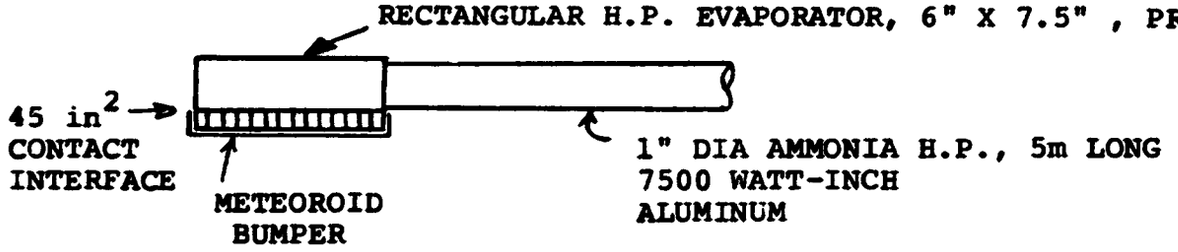

COMPACT HX MANIFOLD/CONTACT INTERFACE

0.014" Al CORE
ΔT FLUID-WALL < 1°F
ΔP (20m) = 7 PSI
F-21 @ 2200 pph
FILLED SILICONE ELASTOMER (CHOMERICS X-4044-3)
.017" LAYER
1-5 PSI CONTACT (OVERCENTER LATCH, NOT SHOWN)
ΔT CONTACT = 2.5°F

FIGURE 18 BLANKET RADIATOR PANELS

FIGURE 19 CONCEPT FOR RADIATOR BLANKET INTEGRATED WITH LARGE STRUCTURE (SPACE ASSEMBLY)

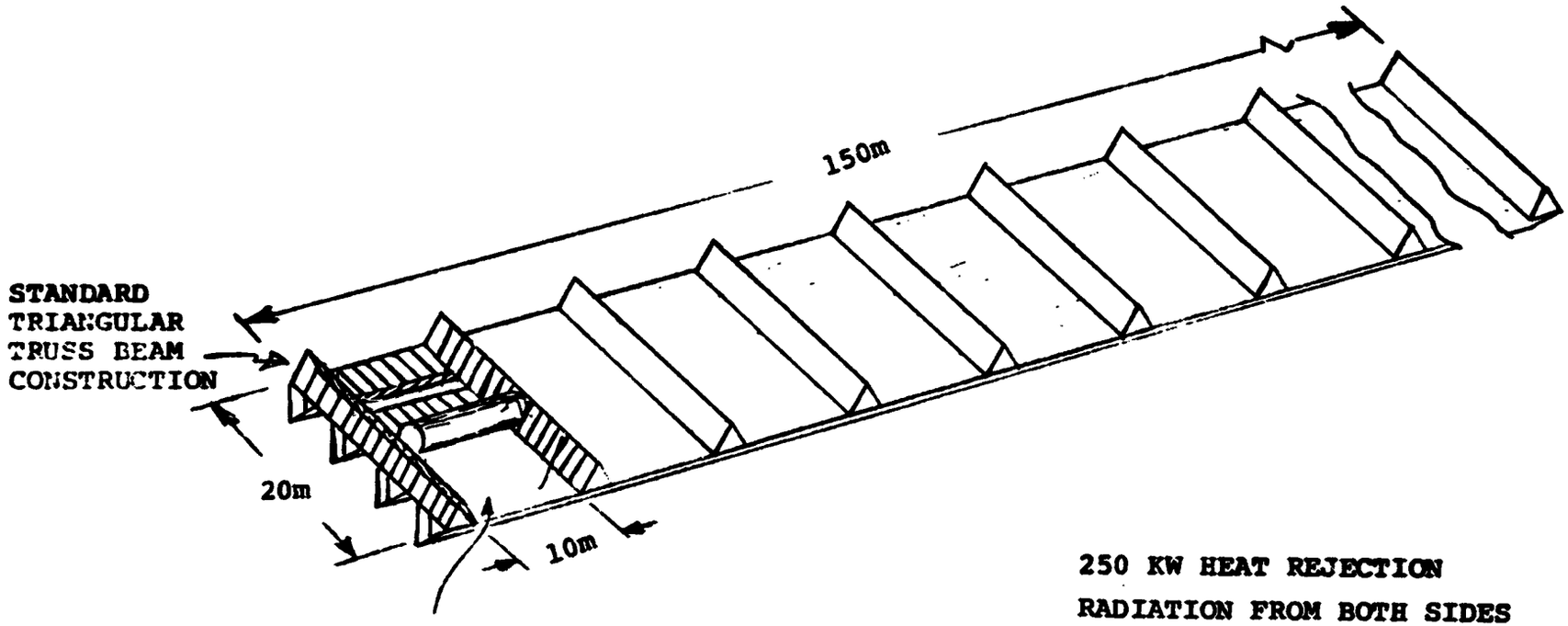

250 KW HEAT REJECTION

RADIATION FROM BOTH SIDES

FLEXIBLE RADIATOR FINS, RIGID TUBES

- 3 x CURRENT FIN THICKNESS
- PUMPED FLUID MANIFOLD
- 6" SPACING OF HEAT PIPES
- CONTACT INTERFACE WITH MANIFOLD

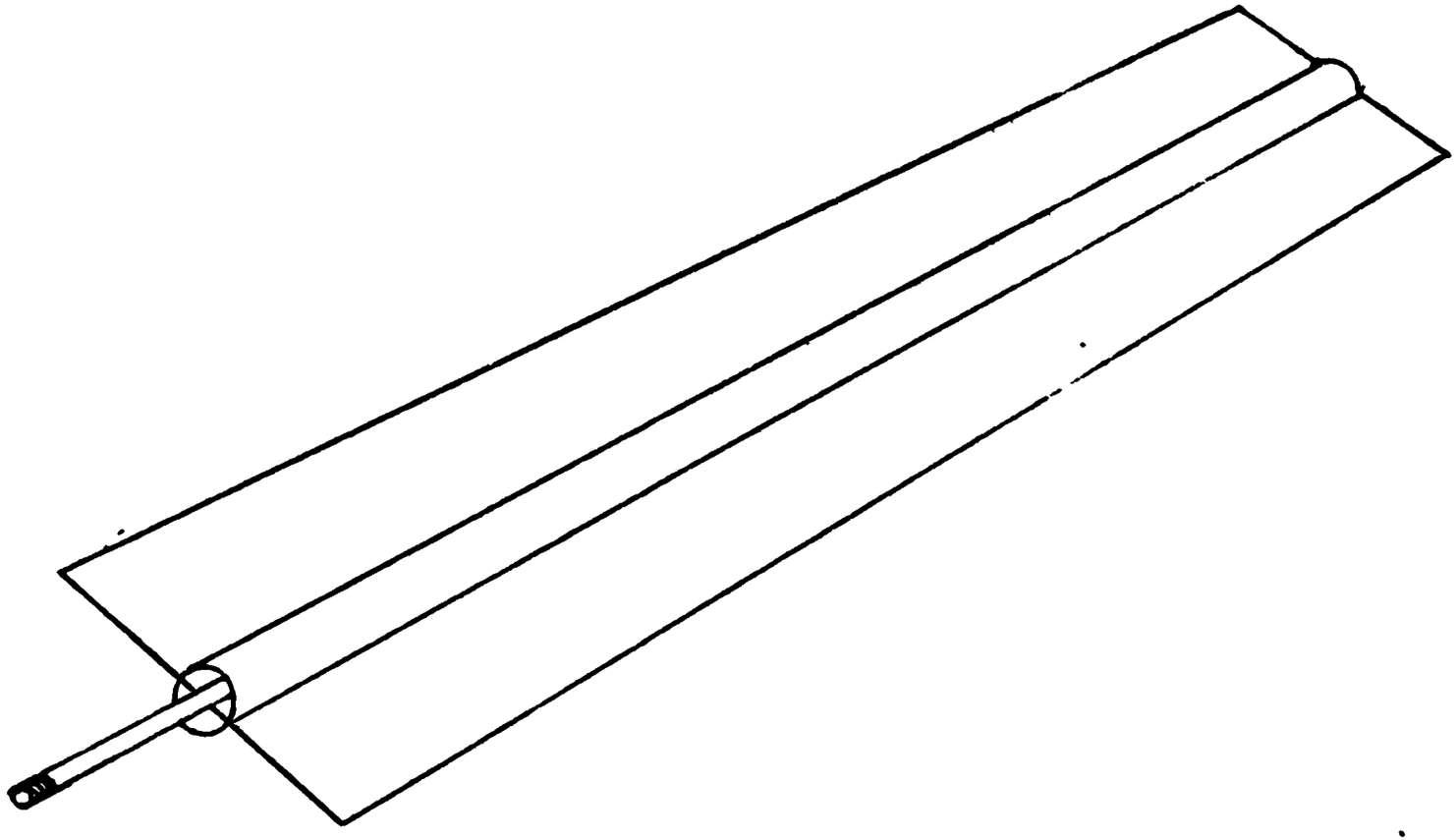

FIGURE 20 ELEMENTAL HEAT PIPE RADIATOR

small heat rejection requirements the heat pipes may be tied directly to the heat source, whereas for large heat rejection requirements, the heat pipes may be connected to the heat source through a transport fluid loop as shown in Figure 21. The end of the heat pipe is specially formed to facilitate joining the element to the heat source as is shown in Figure 22, for example. Series of elements may be connected together as shown in Figures 23 and 24 to form large radiating surfaces. Typical design details for the elements are given in Figure 25. Advantages of this approach are listed in Table XVIII.

3.4 Extended Life Flexible Radiator

The extended life flexible radiator, shown in Figure 26, is a variation of the flexible radiator previously developed under this contract, and could be built using existing technology. It achieves an extended operating life by employing metal tubing in place of the Teflon tubing of the soft tube flexible radiator. The deployment retraction system is also modified for long life. It retains many of the advantages of the soft tube flexible radiator in that it may be developed and qualified independent of its mission, can be stowed in a compact volume, is deployable and retractable, and has wide heat load capacity. It is compatible with most transport fluids, and has a broader operating temperature range than the existing flexible radiator.

3.5 Condensing Radiator

In future applications where electrical power can be obtained for weight penalties on the order of 100 lb_m/KW, and mission durations are relatively long so that micrometeoroid protection for the radiator is a problem, or radiating surface area must be minimized, a condensing radiator system such as is illustrated in Figure 27 will have advantages over conventional radiators. Some of the operating features of the system are listed in Figure 27. Vought has developed technology for fabricating this system under the Self Contained Heat Rejection Module program sponsored by NASA-JSC (NAS9-14408).

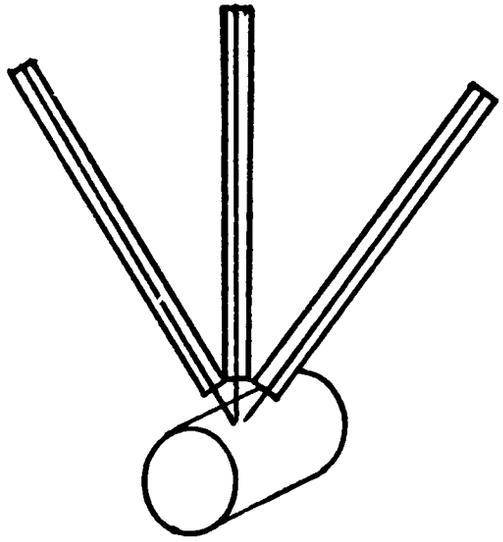

SMALL HEAT LOAD

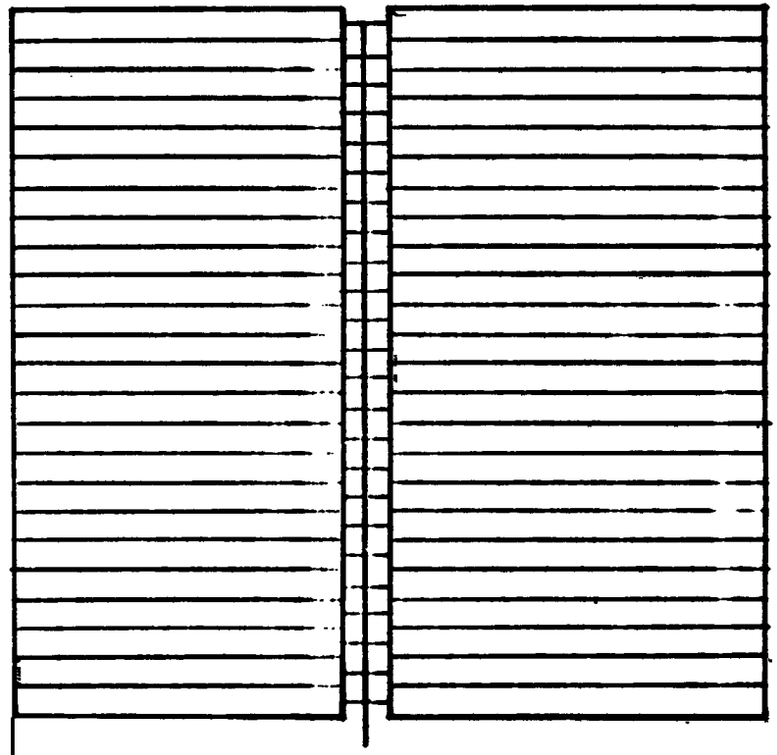

LARGE HEAT LOAD

FIGURE 21 ADAPTABLE TO VARIED PAYLOAD REQUIREMENTS

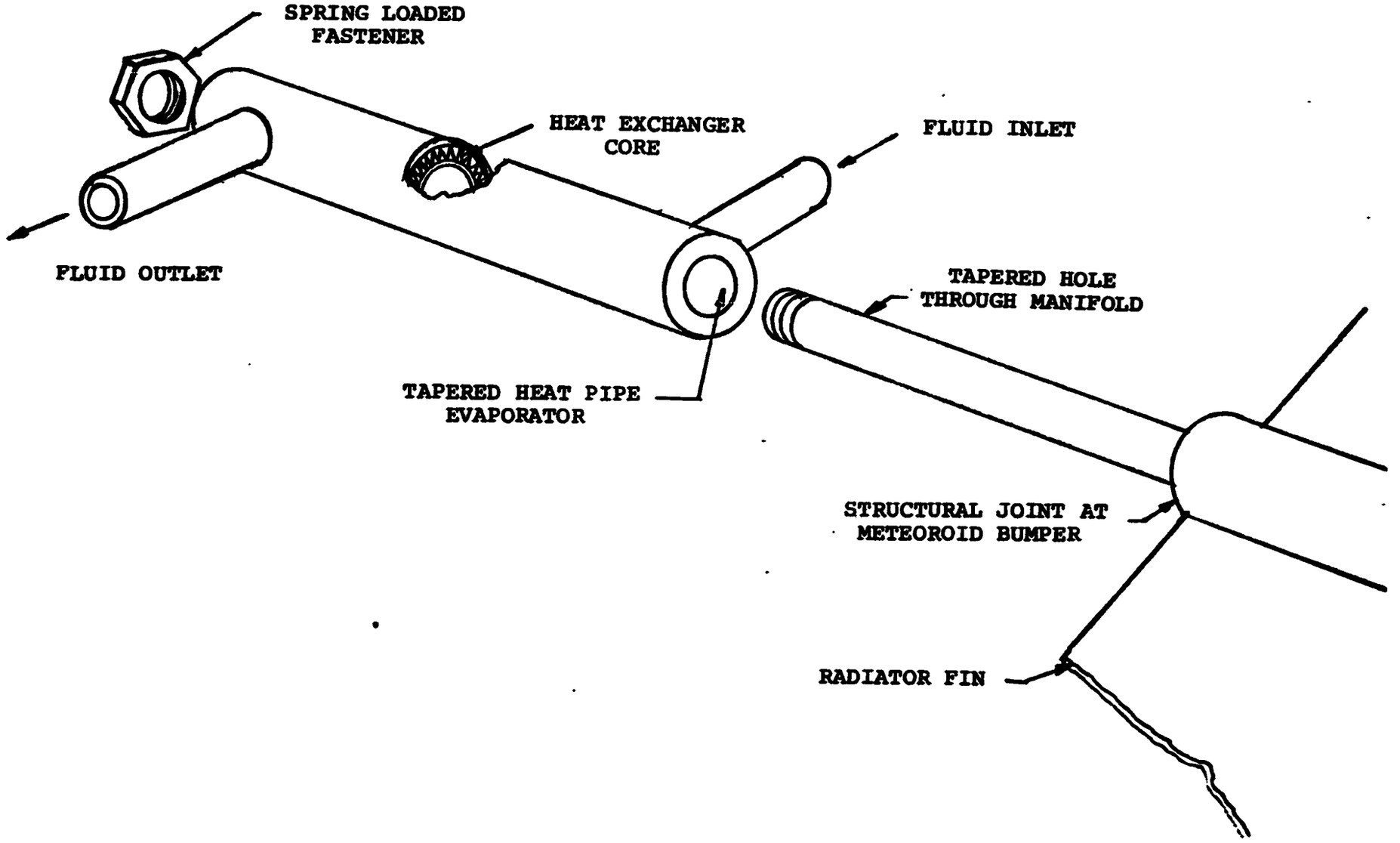

FIGURE 22

ELEMENTAL HEAT PIPE RADIATOR MANIFOLD ATTACHMENT DETAIL

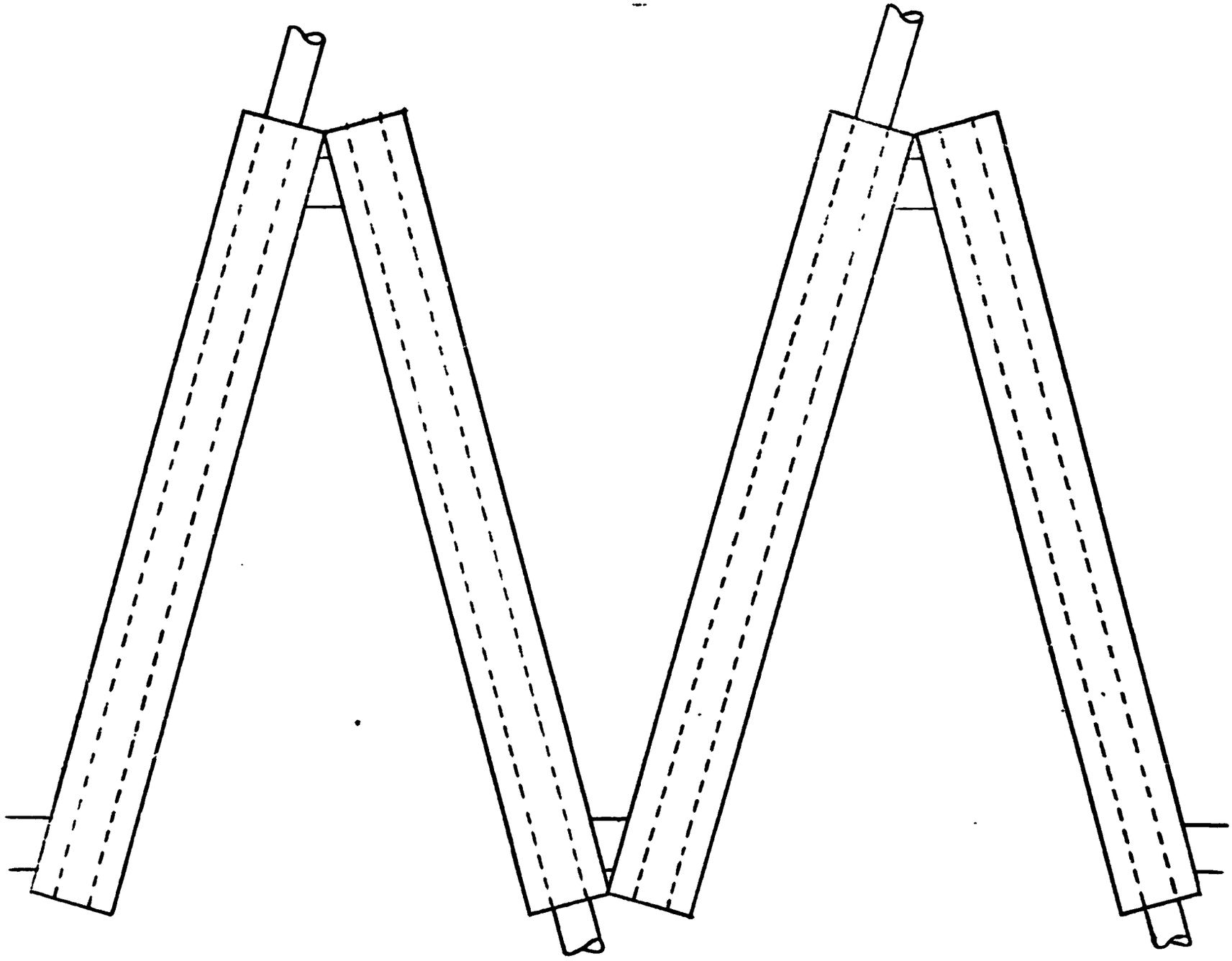

FIGURE 23 MANIFOLD DETAIL FOR RIGID PANEL RADIATOR

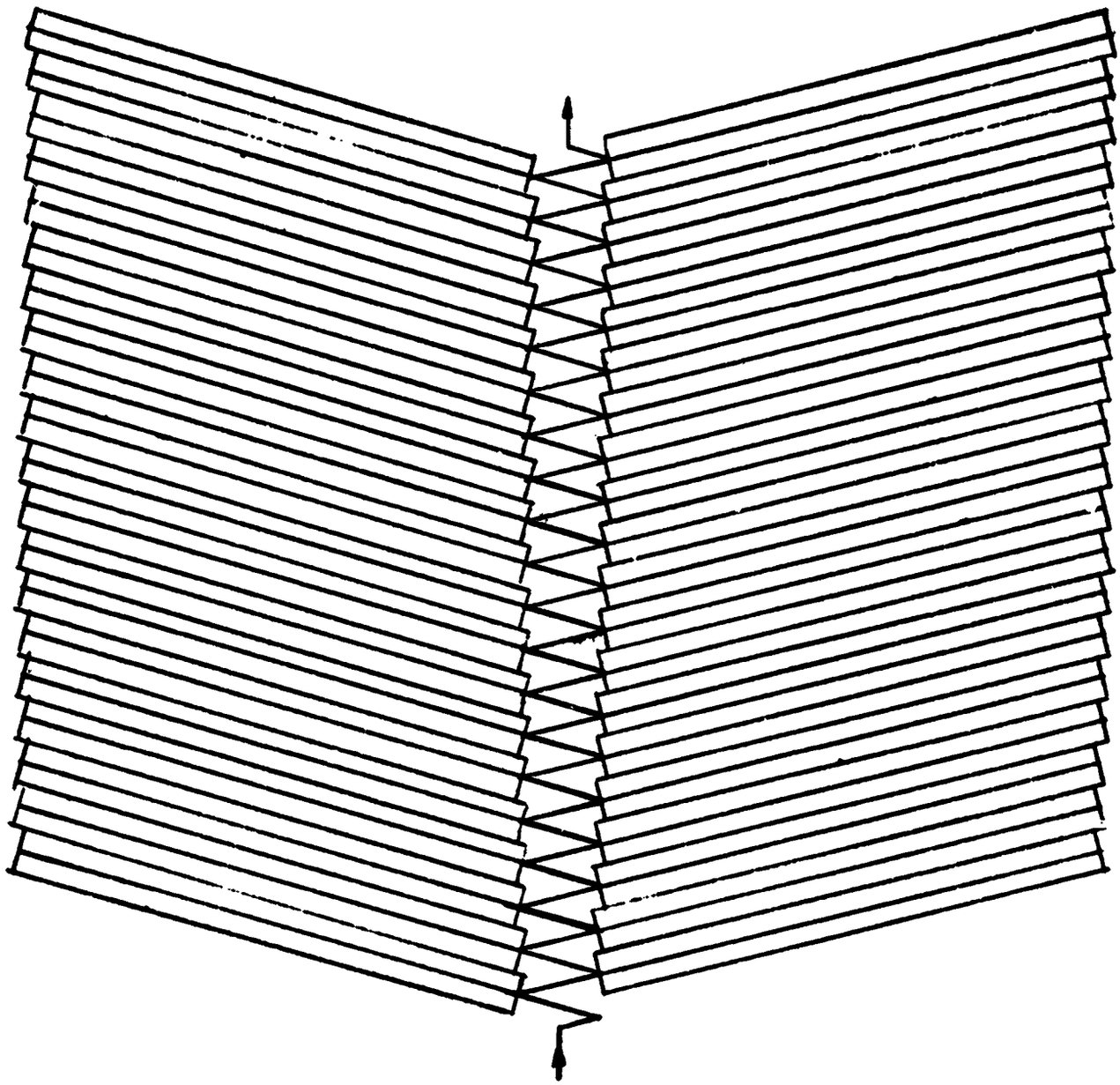

FIGURE 24

RIGID PANEL CONSTRUCTED FROM ELEMENTAL
HEAT PIPE RADIATORS

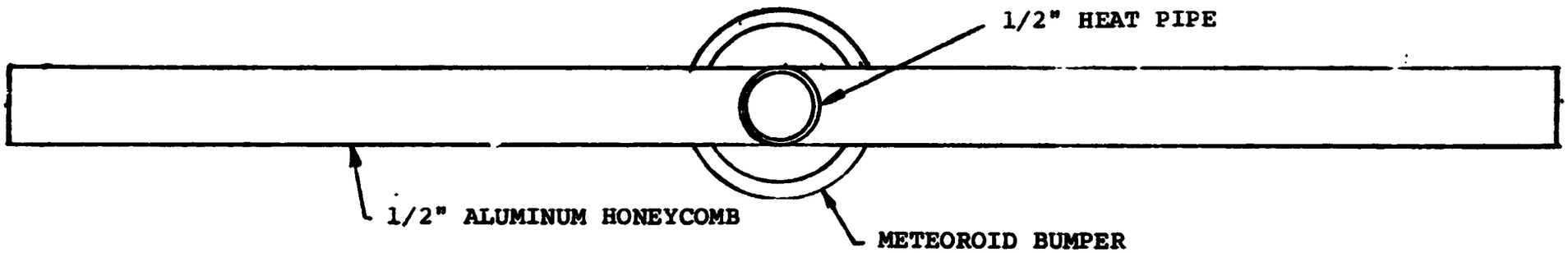

WIDTH = 1'
LENGTH = 8'
HEAT REJECTION = 175 WATTS
WEIGHT = 10.3 lb_m (1.29 lb_m/ft^2)
10 YEAR SURVIVAL PROBABILITY = 0.99

WEIGHT SUMMARY

HONEYCOMB	4.03
FACESHEET	2.88
METEOROID BUMPER	0.90
COATING	0.89
HEAT PIPE	1.60
	10.30 lb_m

FIGURE 25
TYPICAL ELEMENTAL HEAT PIPE RADIATOR PROPERTIES

TABLE XVIII

ELEMENTAL HEAT PIPE RADIATOR ADVANTAGES

- DEVELOP AND QUALIFY INDEPENDENT OF MISSION
- APPLICABLE TO LARGE OR SMALL SYSTEMS
- STOW IN COMPACT VOLUME
- LARGE SYSTEMS ASSEMBLED IN SPACE
- REPAIR OR REPLACE WITHOUT OPENING PUMPED FLUID LOOP
- LARGE NUMBER OF IDENTICAL ELEMENTS REDUCE COST
- NO BRAZING OF HEAT PIPE REQUIRED
- SIMPLE HEAT PIPE GEOMETRY
- LOW THERMAL RESISTANCE AT JOINT
- USES EXISTING TECHNOLOGY

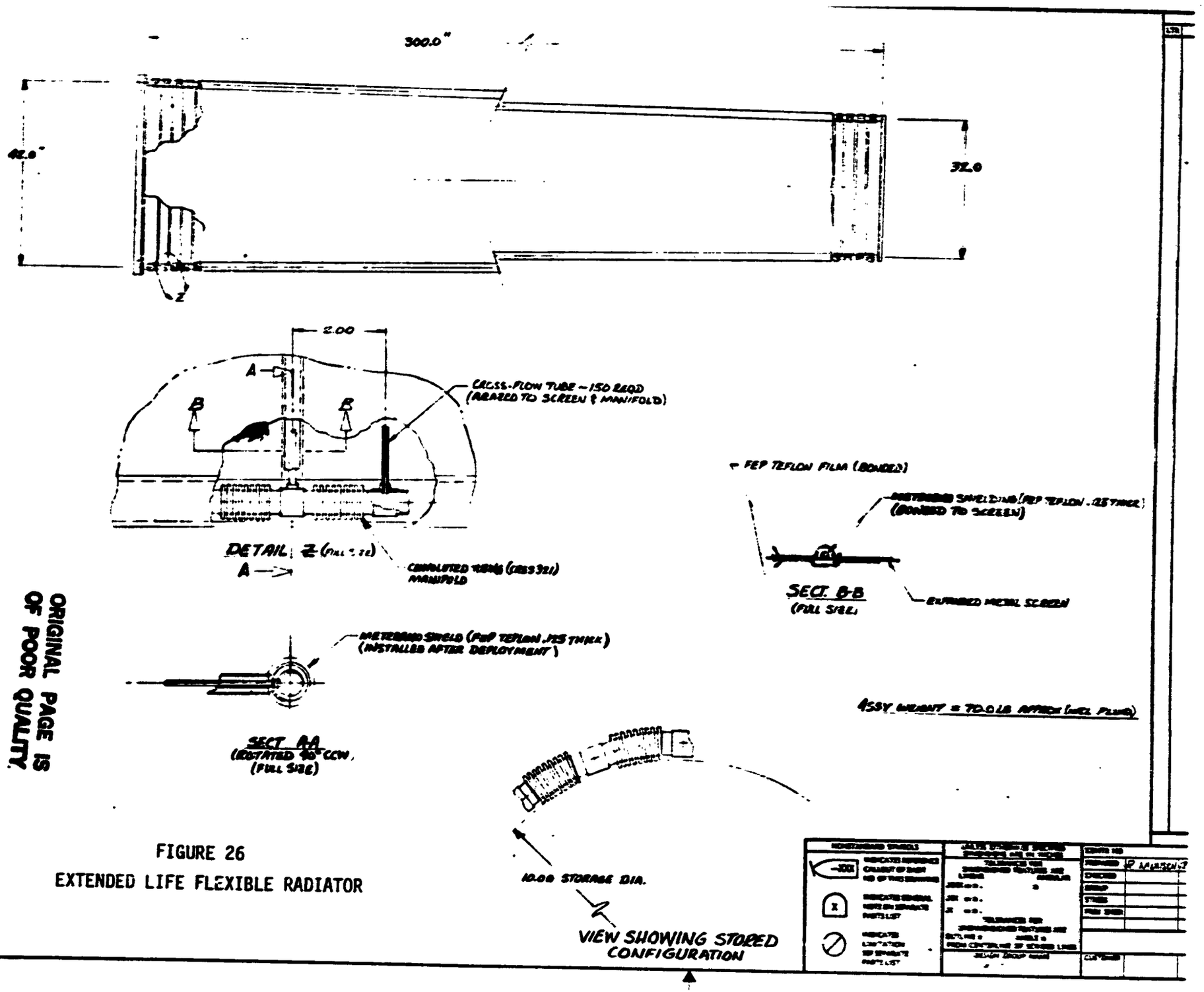

FIGURE 26

EXTENDED LIFE FLEXIBLE RADIATOR

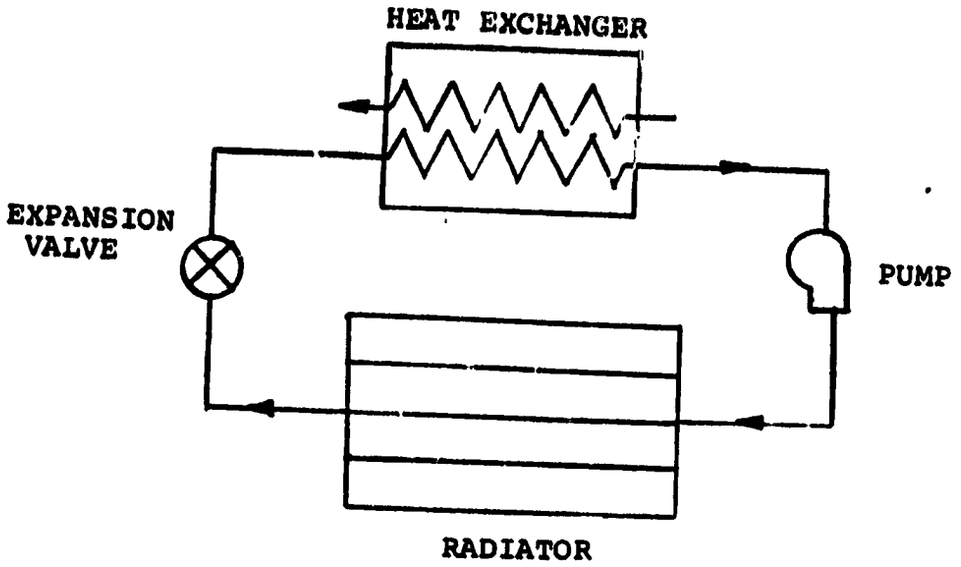

- RADIATOR AREA REDUCED BY 50%
- PUMP POWER IS 20% OF TOTAL HEAT LOAD
- EXPANSION VALVE PROVIDES HEAT LOAD CONTROL
- HEAT PIPE RADIATOR
- CYCLES OTHER THAN VAPOR COMPRESSION NEED STUDY

FIGURE 27

CONDENSING RADIATOR SYSTEM

4.0 LARGE LONG LIFE RADIATORS

The optimization of large heat rejection systems involves the selection of components for reliability, weight, and performance; and the evaluation of alternative arrangements of these components with redundancy and/or oversizing to achieve a prescribed capacity and probability of mission success with minimum weight and cost.

Because of the number of components required in large space heat rejection systems, and the failure rates of the components, redundant elements or subsystems are essential to high system reliability. Figure 28 illustrates how redundancy improves the probability of maintaining full operating capacity throughout a mission. In this example, each subsystem has a 90% probability of surviving the mission. With one redundant subsystem (a total of two subsystems) the probability that one or the other of the subsystems will fail is 18%, and the probability that both systems will fail is 1%. Thus the probability that one of the two subsystems will remain functional is P = 1 - P(2) = 99%. For double redundant systems the probability that one of the three loops will remain functional is P = 1-P(3) = 99.9%.

If, in the example with three subsystems, two of the systems must remain functional to maintain full system capacity, the probability of success is P = 1 - P(2) - P(3) = 97.2%. This illustrates how large systems can be constructed from modules with oversizing to achieve high probabilities of success.

There are several ways to provide redundancy. With full redundancy, each system element has a redundant element capable of performing the same function. With selective redundancy, system elements are selectively grouped with a redundant identical group performing the same function. With simple redundancy, the basic system has a redundant system capable of performing the same function. In addition there are several ways to activate the redundant components. Table XIX gives advantages and disadvantages of alternative approaches.

When constructing large heat rejection systems, there are cost and manufacturing advantages in building up the system from a number of identical modules as described in Section 2.0. Thus the system would be based on simple redundancy although the modules themselves might employ selective redundancy

FIGURE 28 EXAMPLE CALCULATIONS OF RELIABILITY IMPROVEMENTS WITH REDUNDANCY

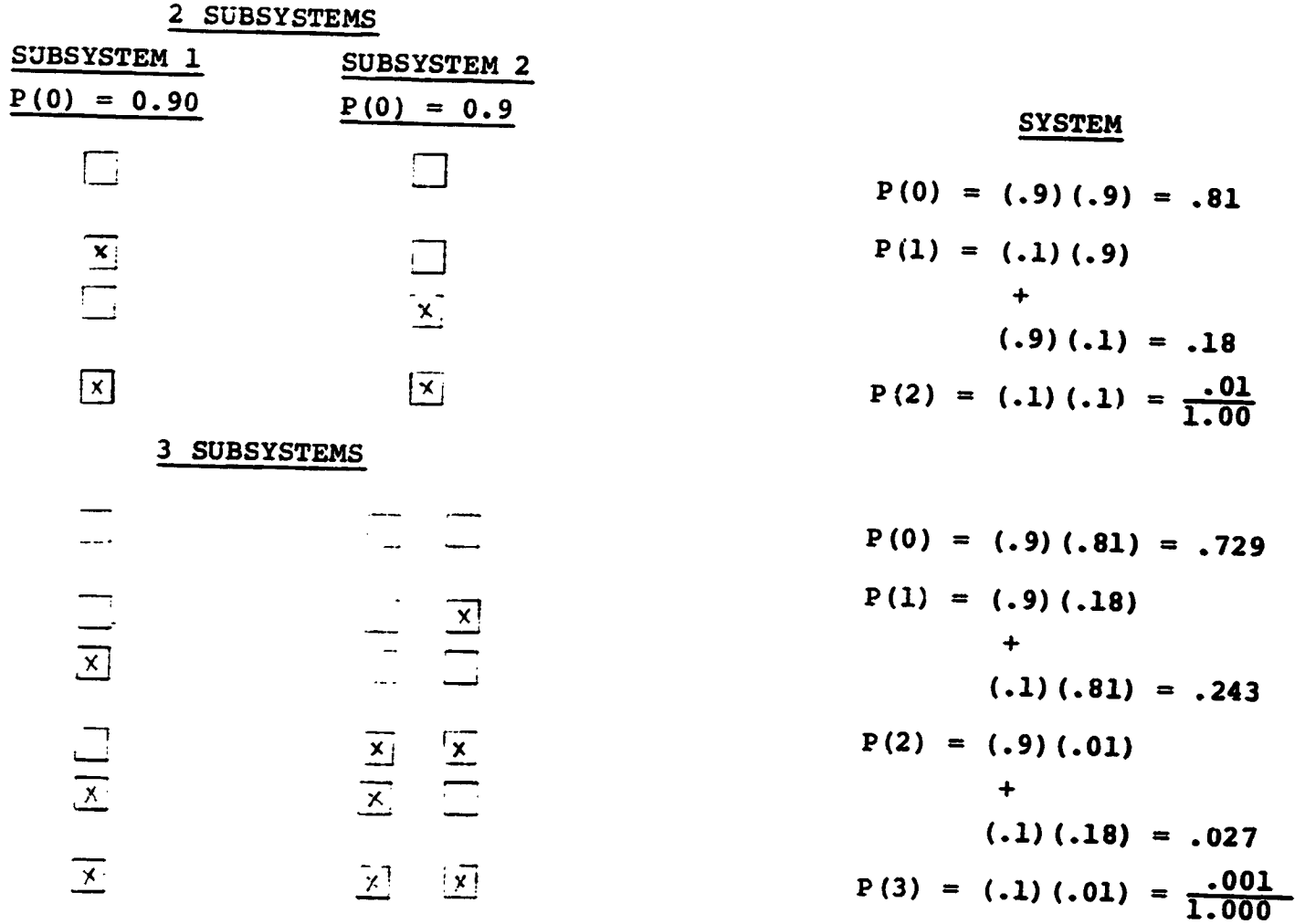

TABLE XIX REDUNDANCY ACTIVATION APPROACHES

TYPES	MERITS
• ACTIVE REDUNDANCY – THAT REDUNDANCY WHEREIN ALL REDUNDANT ITEMS ARE OPERATING SIMULTANEOUSLY RATHER THAN BEING SWITCHED ON WHEN NEEDED.	PRO: • DOES NOT REQUIRE MALFUNCTION SENSING OR SWITCHING OF FUNCTIONS CON: • REQUIRES MORE POWER • INCREASES LIKELIHOOD OF FAILURE • CAN DEGRADE PRIMARY SYSTEM RELIABILITY
• STANDBY REDUNDANCY – THAT REDUNDANCY WHEREIN THE ALTERNATIVE MEANS OF PERFORMING THE FUNCTION IS INOPERATIVE UNTIL NEEDED AND IS SWITCHED ON UPON FAILURE OF THE PRIMARY MEANS OF PERFORMING THE FUNCTION.	PRO: • REQUIRES NO MORE POWER THAN THE "NO-REDUNDANCY" SYSTEM • INCREASES LIKELIHOOD OF FAILURE OVER THE "NO-REDUNDANCY" SYSTEM BUT IS LESS THAN THE "ACTIVE" CASE CON: • REQUIRES MALFUNCTION SENSING AND SWITCHING OF FUNCTIONS • CAN DEGRADE PRIMARY SYSTEM RELIABILITY (E.G. MALFUNCTION OF THE SENSOR/SWITCH FUNCTION)
• GRACEFUL DEGRADATION – A FORM OF ACTIVE REDUNDANCY WHICH PERMITS CONTINUED (BUT DEGRADED) SYSTEM OPERATION IN THE EVENT OF AN ELEMENT FAILURE, E.G. HEAT PIPE CONCEPT.	PRO: • PERMITS SYSTEM OPERATION FOLLOWING ELEMENT LOSS • CAN OVERDESIGN SYSTEM TO PERMIT LOSS OF SEVERAL ELEMENTS BEFORE REDUCTION OF SYSTEM CAPABILITY TO 100% OF THAT REQUIRED CON: • COULD REQUIRE MORE POWER, WEIGHT WEIGHT AND VOLUME THAN THE SYSTEM DESIGNED TO THE 100% REQUIREMENT • INCREASES LIKELIHOOD OF ELEMENT FAILURE

for components with poor reliabilities. Example calculations are given below to illustrate how the system's probability of remaining functional varies with the number of modules and the probability that each module will survive the mission.

Figure 29 shows results obtained from analyses such as are illustrated in Figure 28, for a system constructed from 10 independent modules. The figure shows the probability of the loss of subsystems as it affects the total radiating area of the system. The most probable percentage of area loss increases as the probability of survival of the subsystems decreases. If the system is oversized so that part of the radiating area can be lost without affecting the system's capacity to perform at the required level, the systems survivability will exceed that of its subsystems. In this case the systems probability of survival is computed by summing the probabilities of all possible combinations of subsystem failures which will result in more area loss than is allowable. This is analogous to computing the areas under the curves in Figure 29 past the point corresponding to the amount of system oversize. Figure 30 gives typical results computed for a system with 20 subsystems. The figure shows that if a system survivability of 98% is required (.02 probability of loss of more area than oversized), the system must be oversized by 9% if the probability of survival of the subsystems is 0.99, by 13% if the subsystem survivability is 0.95, and by 28% if the subsystem survivability is 0.90. This means the system having 0.99 survivability modules must be designed to operate with 18 subsystems; the system having 0.95 modules with 16 subsystems; and the system having 0.90 modules with 14 subsystems. Thus the size of the modules must increase as the probability of survival decreases.

In some cases the allowable radiating area oversizing may be limited. Thus Figure 31 shows how the probability of survival of a system with 20% oversizing depends on the number and survivability of its subsystems. This figure was generated from cross-plots of curves such as are given in Figure 30. The results show, for example, that a 98% probability of success can be obtained by a system of 20 modules, each having 95% survivability; or by a system with 10 modules, each having 98% survivability. Which system is better depends on properties such as weight, cost, and complexity.

Figure 32 compares the weights computed for a large pumped fluid radiator system having variable numbers of subsystems and subsystem survivabilities.

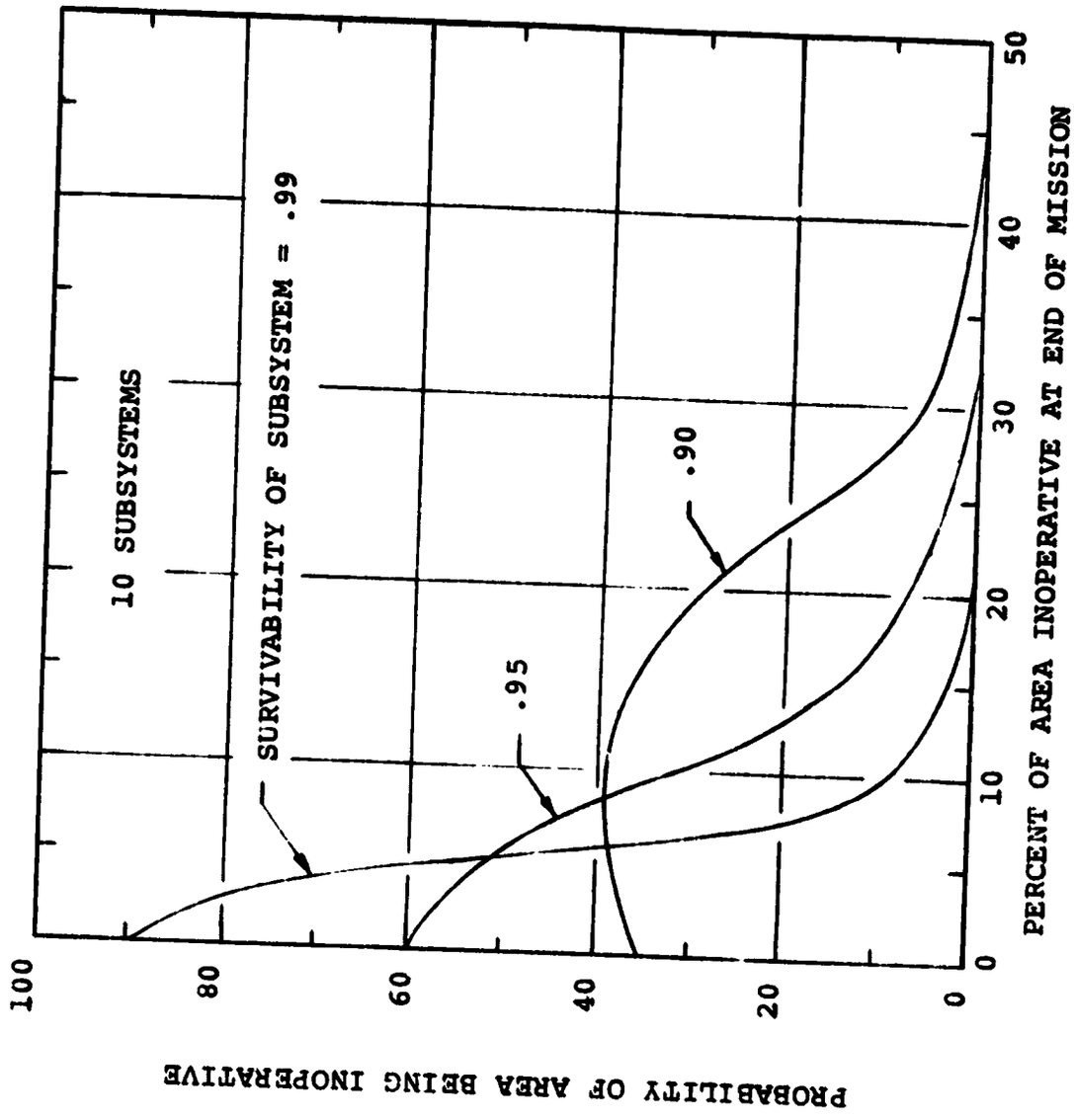

FIGURE 29

EFFECT OF SUBSYSTEM SURVIVABILITY ON MOST PROBABLE LOSS OF RADIATING AREA

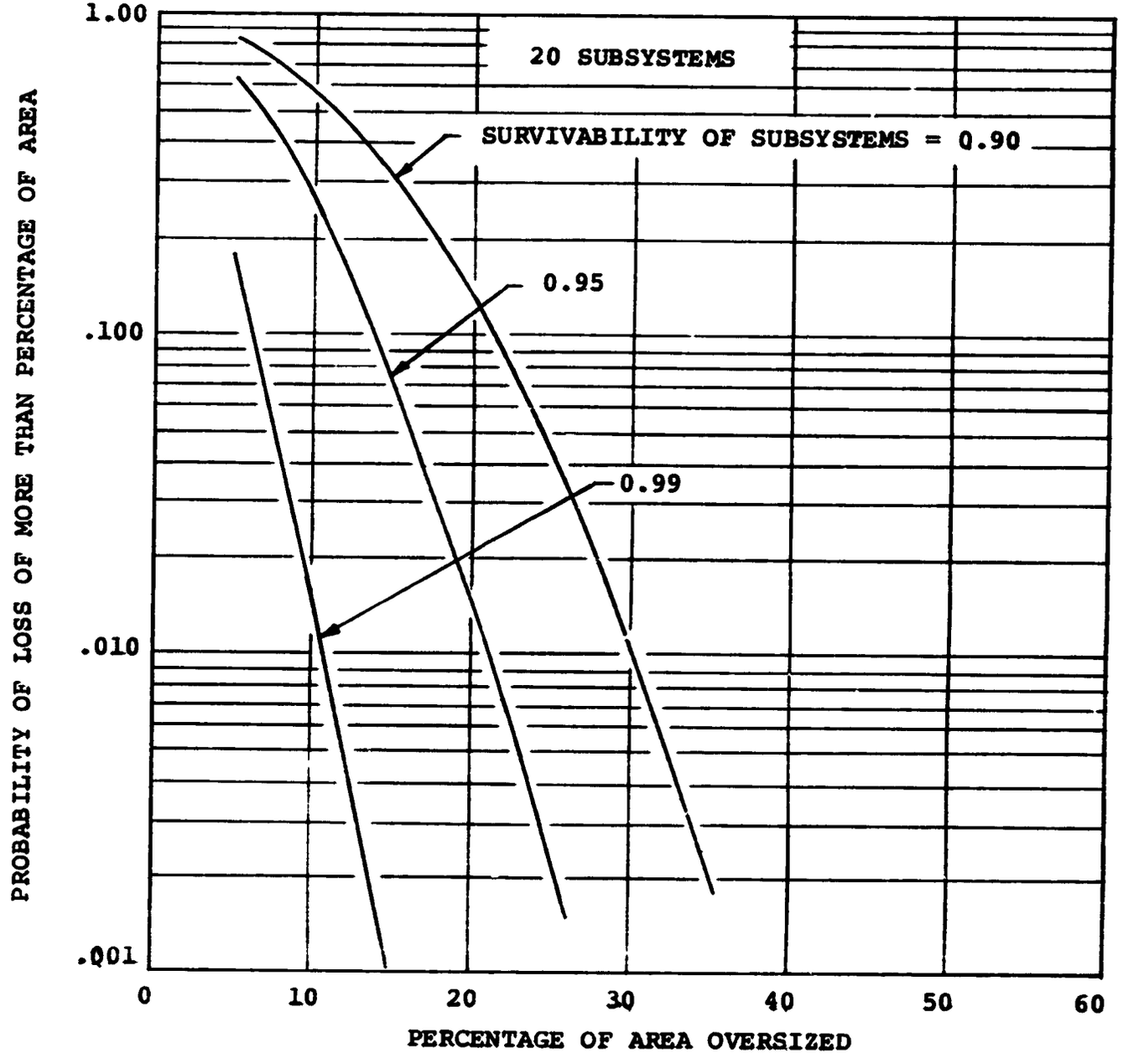

FIGURE 30 EFFECT OF OVERSIZING ON PROBABILITY OF MAINTAINING REQUIRED SYSTEM CAPACITY

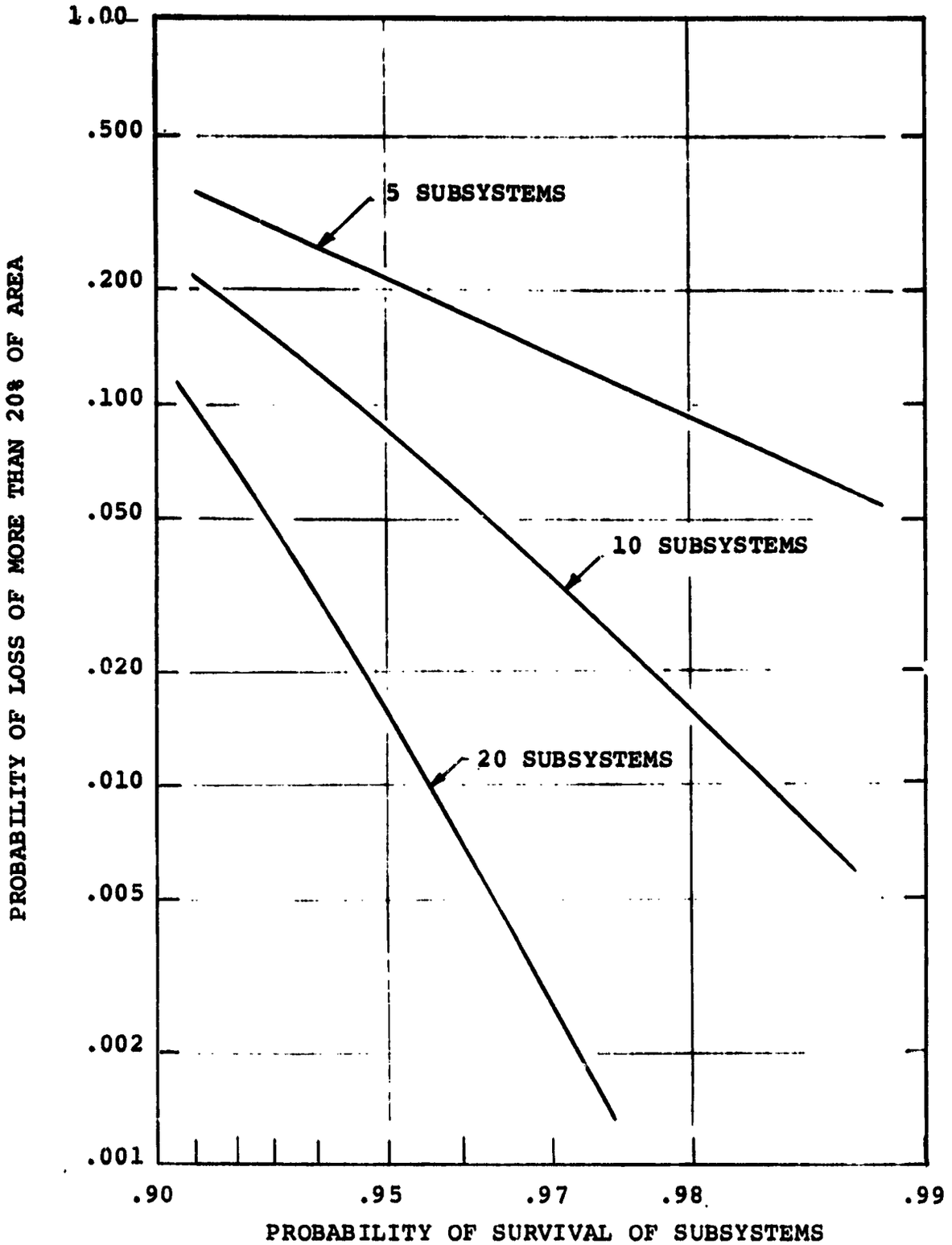

FIGURE 31 SYSTEM SURVIVABILITY WITH LIMITED OVERSIZING

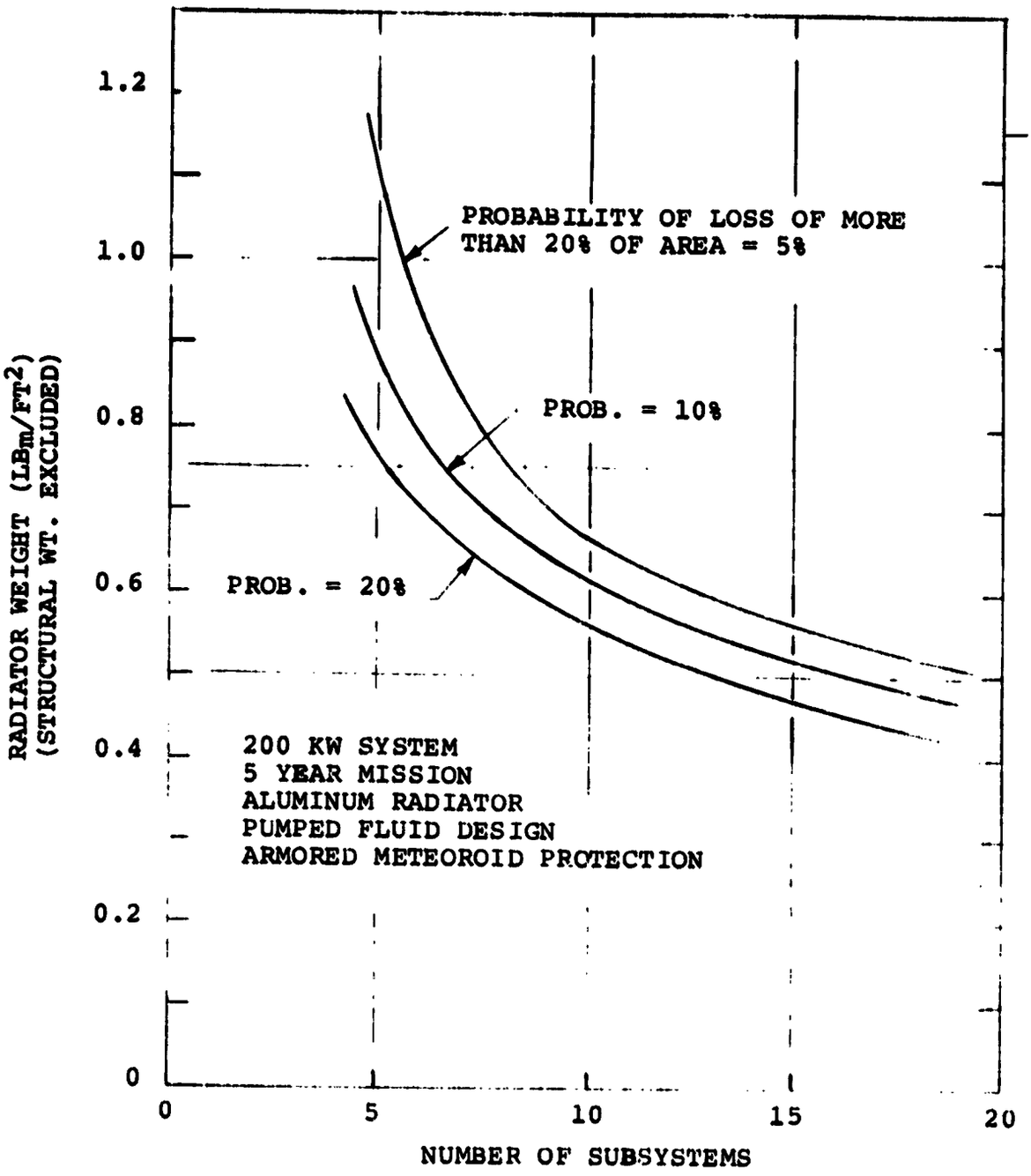

FIGURE 32

WEIGHT OF ALTERNATIVE PUMPED FLUID RADIATOR SYSTEMS

The figure shows that the weight of the radiators decreases as the number of modules increases for a fixed probability of maintaining full system capacity. Cost and other vehicle component weights might increase for large numbers of modules, so that the system design cannot be selected based on the radiator weight alone. However, the figure shows that significant weight savings are possible if the system is constructed from 10 or more modules. This number does not seem unreasonable for a system of 200 KW capacity.

General Comparisons of Pumped Fluid and Hybrid Heat Pipe/Pumped Fluid Radiators

In this section the weights of radiator panels with and without heat pipes are compared for various heat rejection loads and mission durations to determine whether the heat pipes reduce the radiator weight. Optimum designs of each type of radiator are compared. Several types of heat pipe radiator manifold/evaporator designs are considered to determine the effect of various degrees of added complexity on the total radiator weight. Meteoroid bumper and meteoroid armor protection designs are also studied. In addition, alternative ways of constructing large systems from variable numbers of subsystems are considered for each type of design. Redundant flow passages attached to a common radiator fin are not considered. Redundant flow passages complicate the manifold/evaporator design of heat pipe based radiators so as to increase the temperature drop between the fluid loop and the radiating fin. Therefore, to avoid complicating the comparative evaluation of radiators with and without heat pipes, redundant flow loops are not considered.

Redundant flow loops are considered in the more specific and detailed case study documented in the next section, where it is shown that the weight of pumped fluid radiators can be reduced below the values reported here in some cases. The purpose of this section is to determine whether there are applications where heat pipes offer advantages when redundant flow loops on a common radiating surface cannot be considered. This a valid question for some potential future applications where redundant elements must be physically separated. Such requirements might be necessary to minimize the threat of damage to the heat rejection system by laser attacks, or gross wreckage by manipulators, etc.

Figure 33 gives the radiator weights, including pumping power penalty for several designs for a 20 KW system with 99% probability of not being incapacitated by micrometeoroids in a 5 year mission. The heat pipe radiator entries are for the lightest weight of several heat pipe manifold/evaporator designs considered. This is a proprietary concept generated under Vought funding. Other manifold/evaporator designs such as are common in the open literature are considerably heavier.

The overall system probability of surviving 5 years in a micrometeoroid environment is at least 99% for each design represented in Figure 33. For the designs with only one subsystem, the subsystem must have a 99% probability of survival. With two subsystems, each having a 90% chance of surviving, the probability that one of the two subsystems will survive is 99%. The wall thicknesses of the 90% subsystems are less than for the 99% subsystems, but the weight of two 90% subsystems is more than the weight of one 99% subsystem, so that there is no advantage in such designs. The pumped fluid based designs with five subsystems, requiring three for full capacity, are weight competitive with the single subsystem designs, but the weight advantage is insufficient justification for the added complexity. The designs with 10 or more subsystems have greater weight advantages, but probably would not be selected for a 20 KW system unless there were other reasons such as a need for redundant pump loop components to improve the total heat rejection system reliability.

Thus, for the 20 KW heat rejection requirement, the best system appears to be a single subsystem pumped fluid design with meteoroid bumpers. The best heat pipe based radiator is lighter than the armor protected pumped fluid panel, but weighs more than the bumper protected design. Figure 34 shows radiating fin cross sections of the three designs as determined from the computer routines described in Section 2. The weights shown in Figure 33 includes the weights of the basic radiator panel components shown in Figure 34 plus the weights of the transport fluid, radiator coatings, manifolds, headers, pumping power penalty weight, and an additional structural weight. The additional structural weight accounts for honeycomb or other equivalent panel stiffening structure, and is assumed to be independent of the panel design. Figure 35 gives the weight break-down for the three types of radiators. Figure 36 gives radiator weights for a 160 KW system. Here the heat pipe based radiators weighs

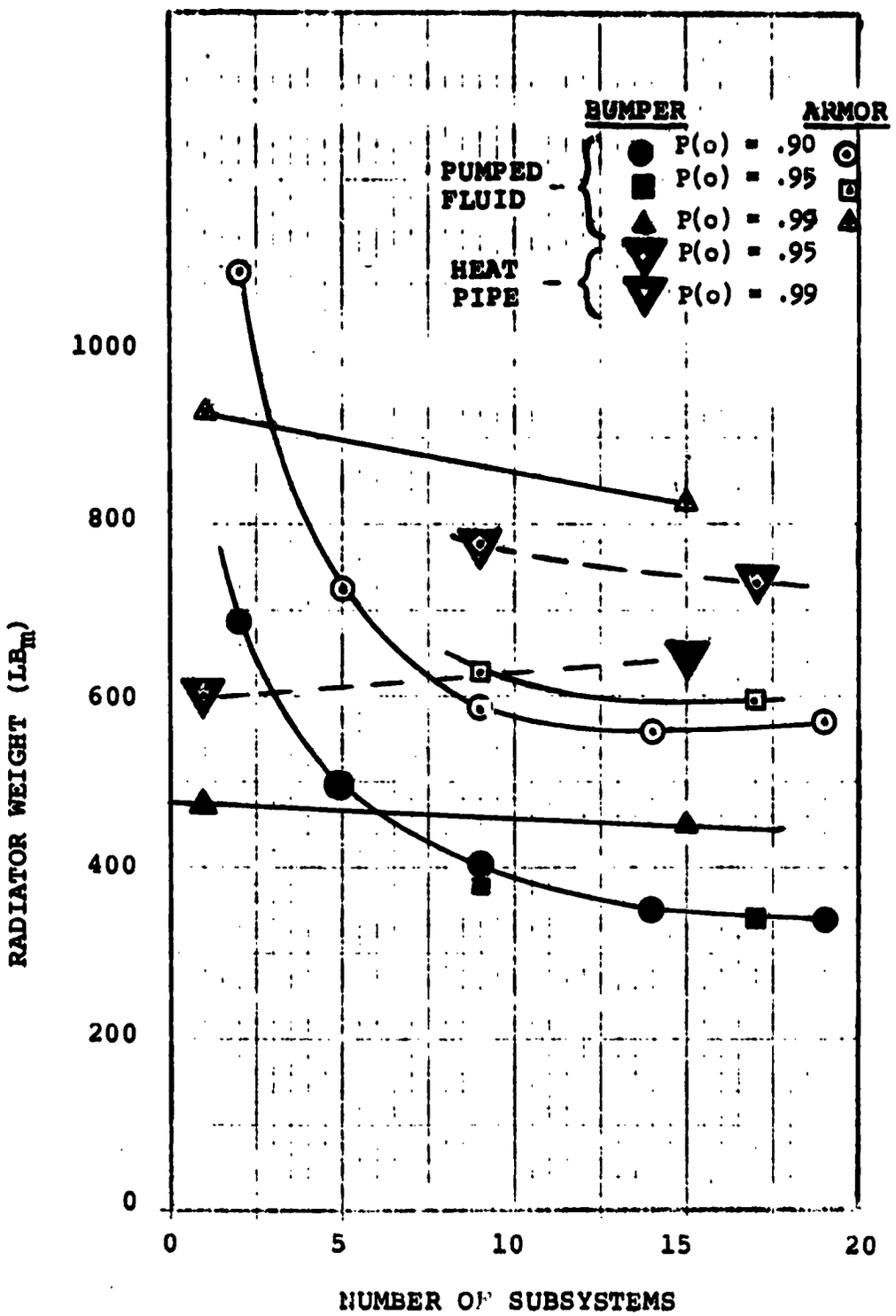

FIGURE 33

RADIATOR DESIGN COMPARISONS, 20 kW SYSTEM,
5 YEARS, P(o) = 0.99

FIGURE 34 20 KW RADIATOR DESIGN COMPARISONS, P(o) = 0.99, 5 YEARS

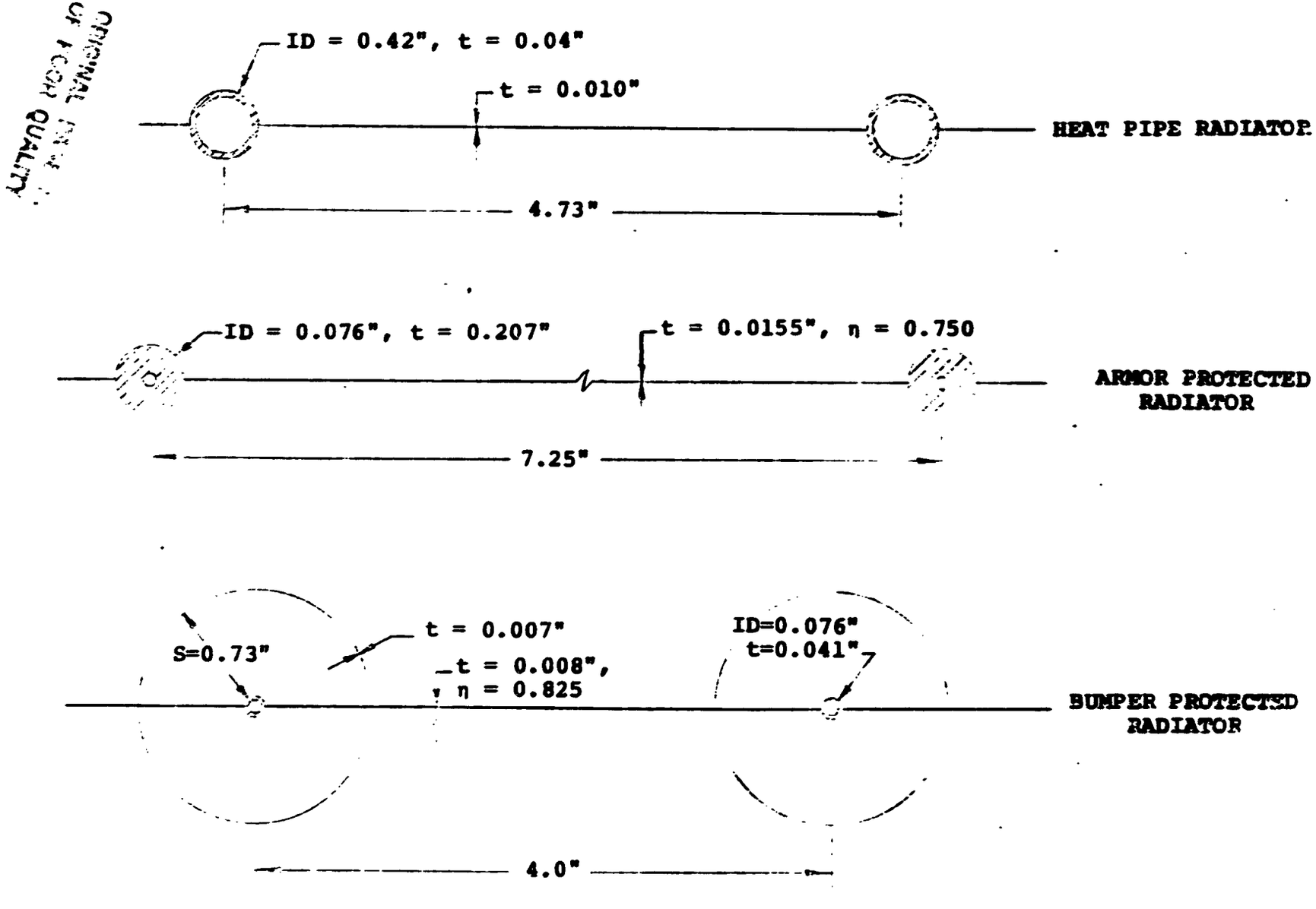

FIGURE 35 COMPONENT WEIGHTS - 20 kW RADIATOR, Po = 0.99, TIME = 5 YEARS

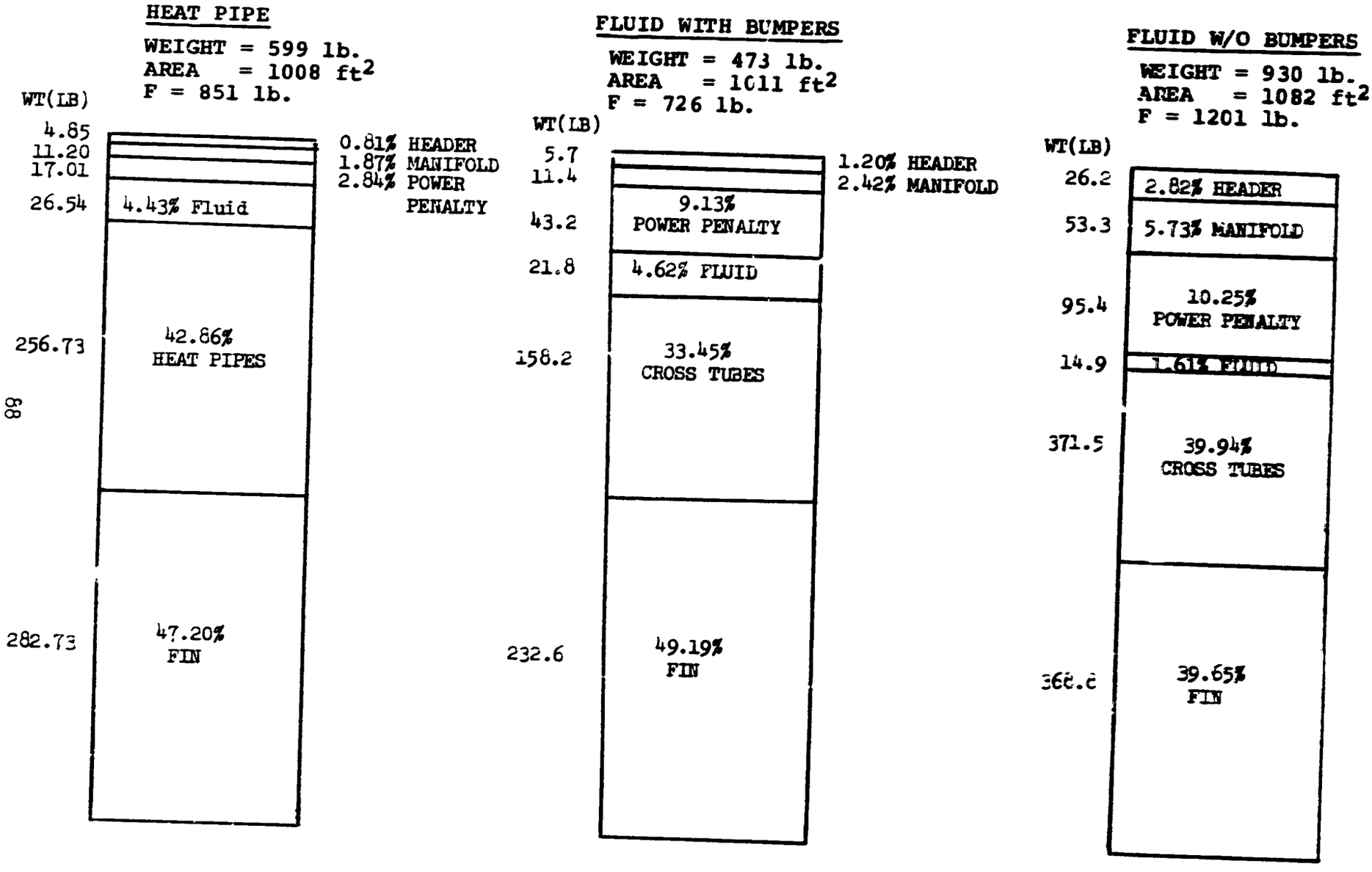

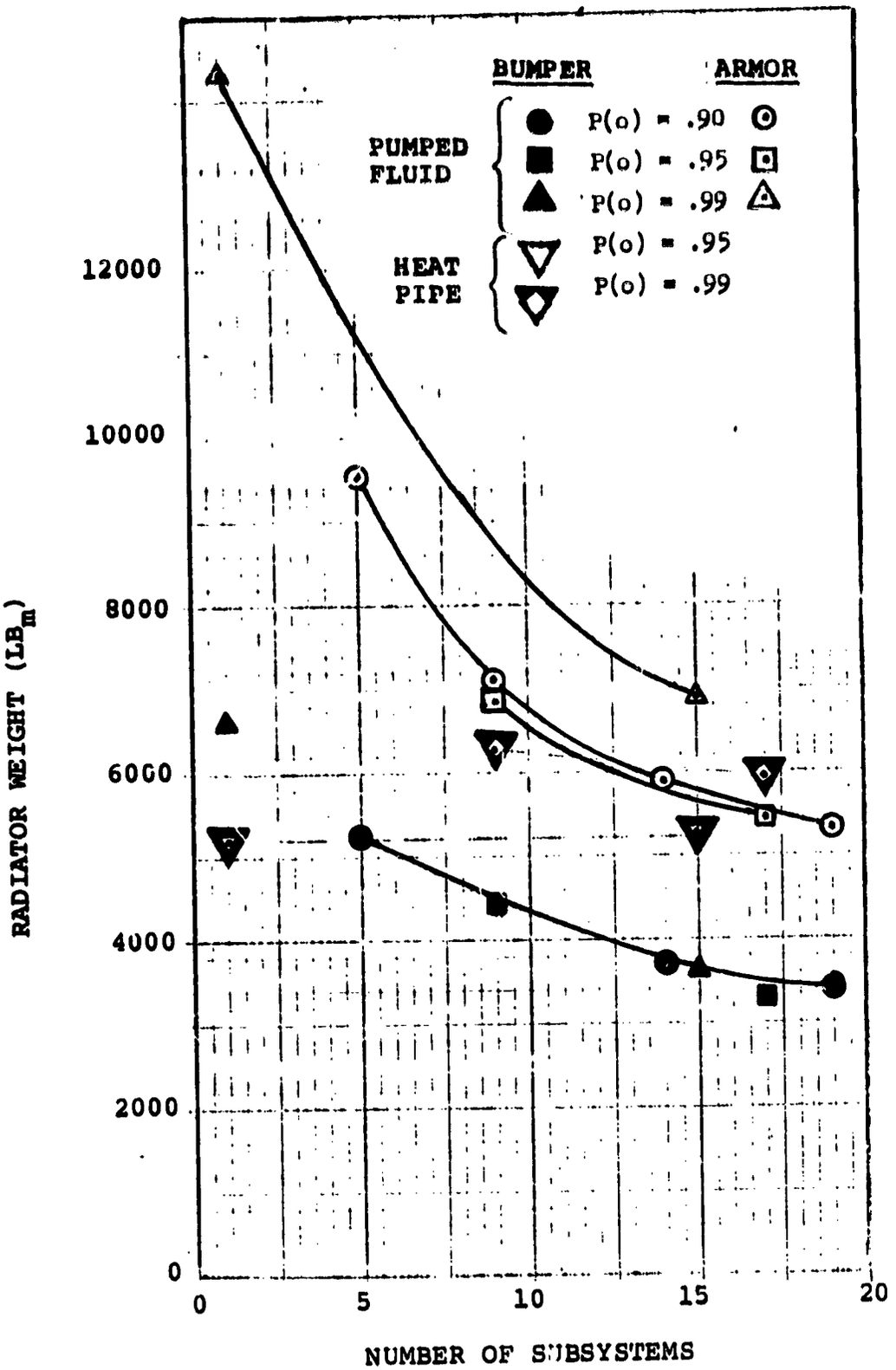

FIGURE 36 160 kW SYSTEM, 5 YEARS, P(o) = .99

less than either the bumper or armor protected designs unless the system is built up from 5 or more subsystems. However, significant weight savings are possible if the system is constructed from 10 or more pumped fluid radiators. Similarly, the data for the 250 KW system in Figure 37 shows that large weight savings are possible if the system is constructed from subsystems of 10-20 KW capacity.

Radiator weights and surface areas are plotted in Figures 38-43 for systems with 95% probability of surviving five years. The results are similar to those for the 0.99 probability system discussed above except that there are no cases where heat pipe based designs offer weight advantages.

Thus, the results show that heat pipes are best suited for large single subsystem designs with high probabilities of surviving long periods of time on orbit (.99 for 5 years or more). For cases where the system can be built up from modules of 10-20 KW capacity, pumped fluid designs are lighter weight.

C-2

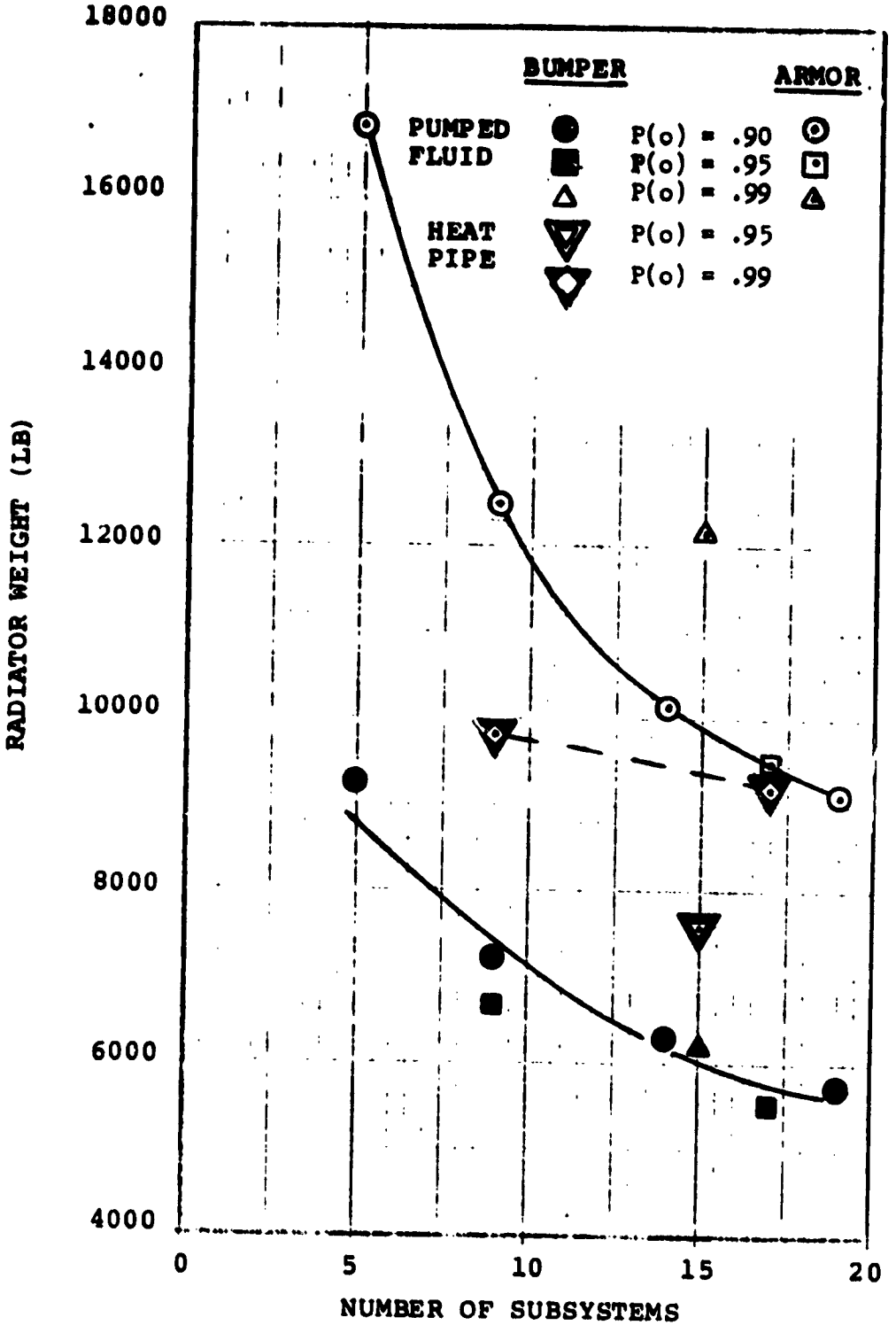

FIGURE 37 250 kW SYSTEM, 5 YEARS, P(o) = .99

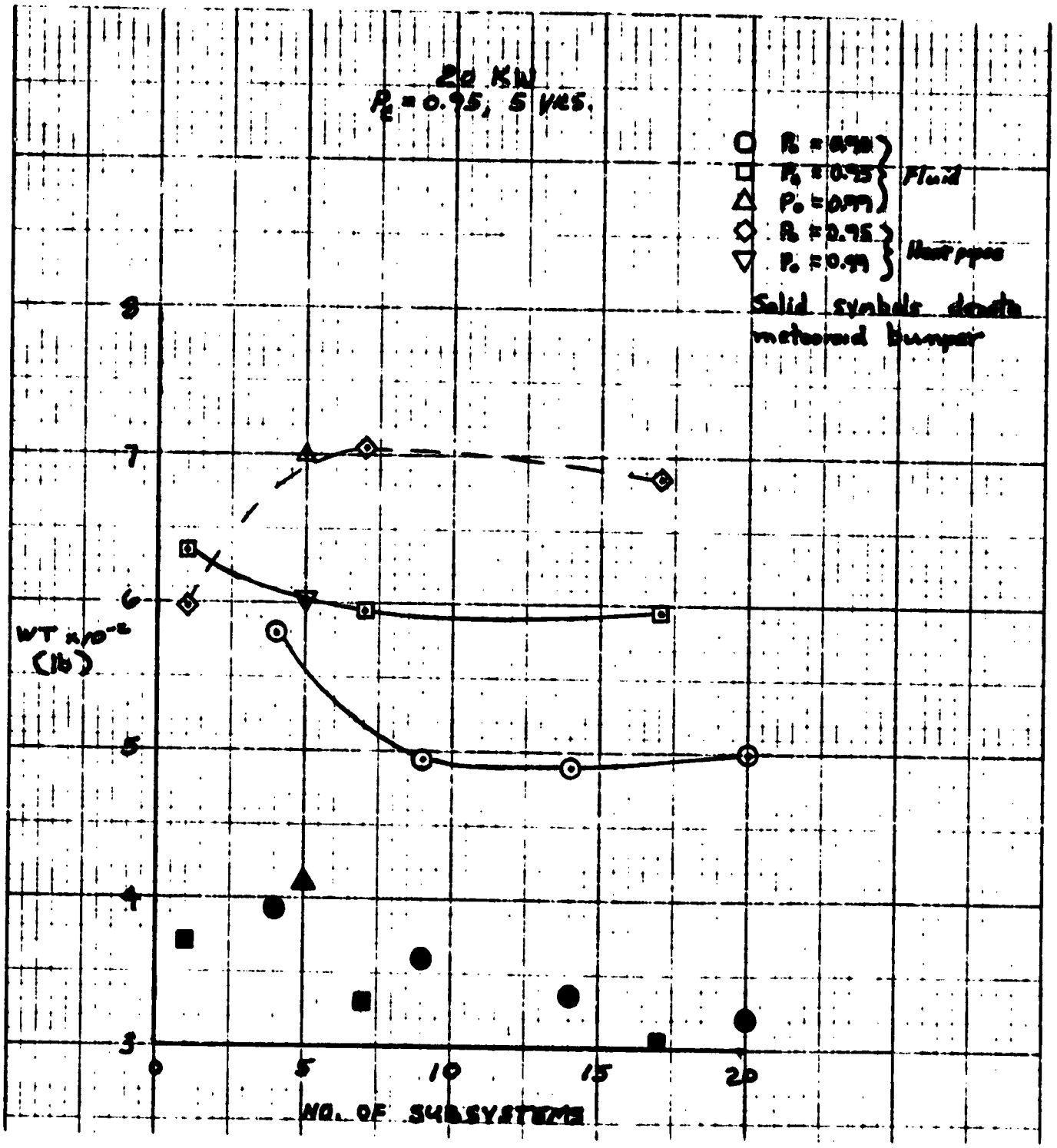
20 KW
P_t = 0.95, 5 YRS.
Solid symbols denote
meteoroid bumper
WT x10⁻²
(lb)
NO. OF SUBSYSTEMS

FIGURE 38

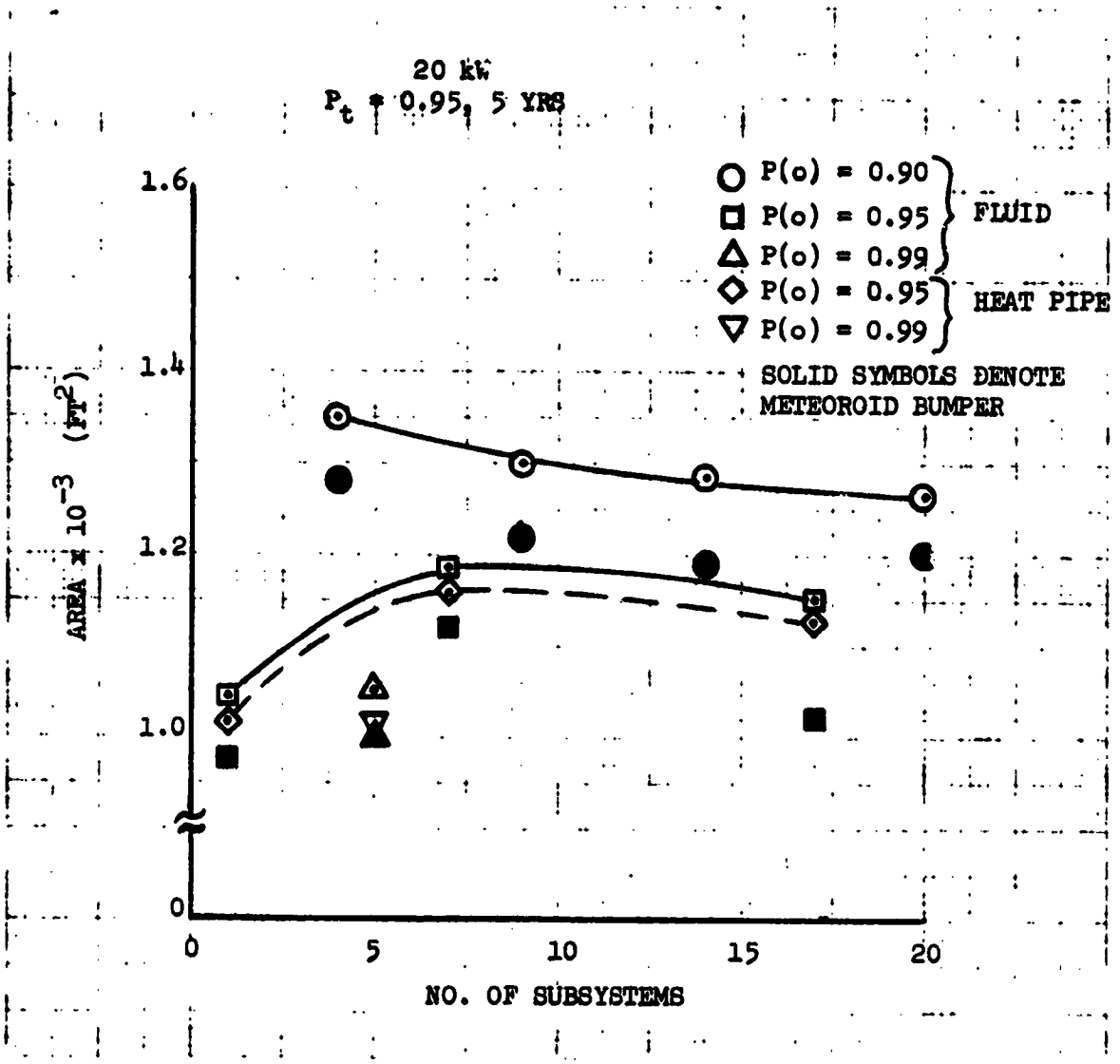

FIGURE 39

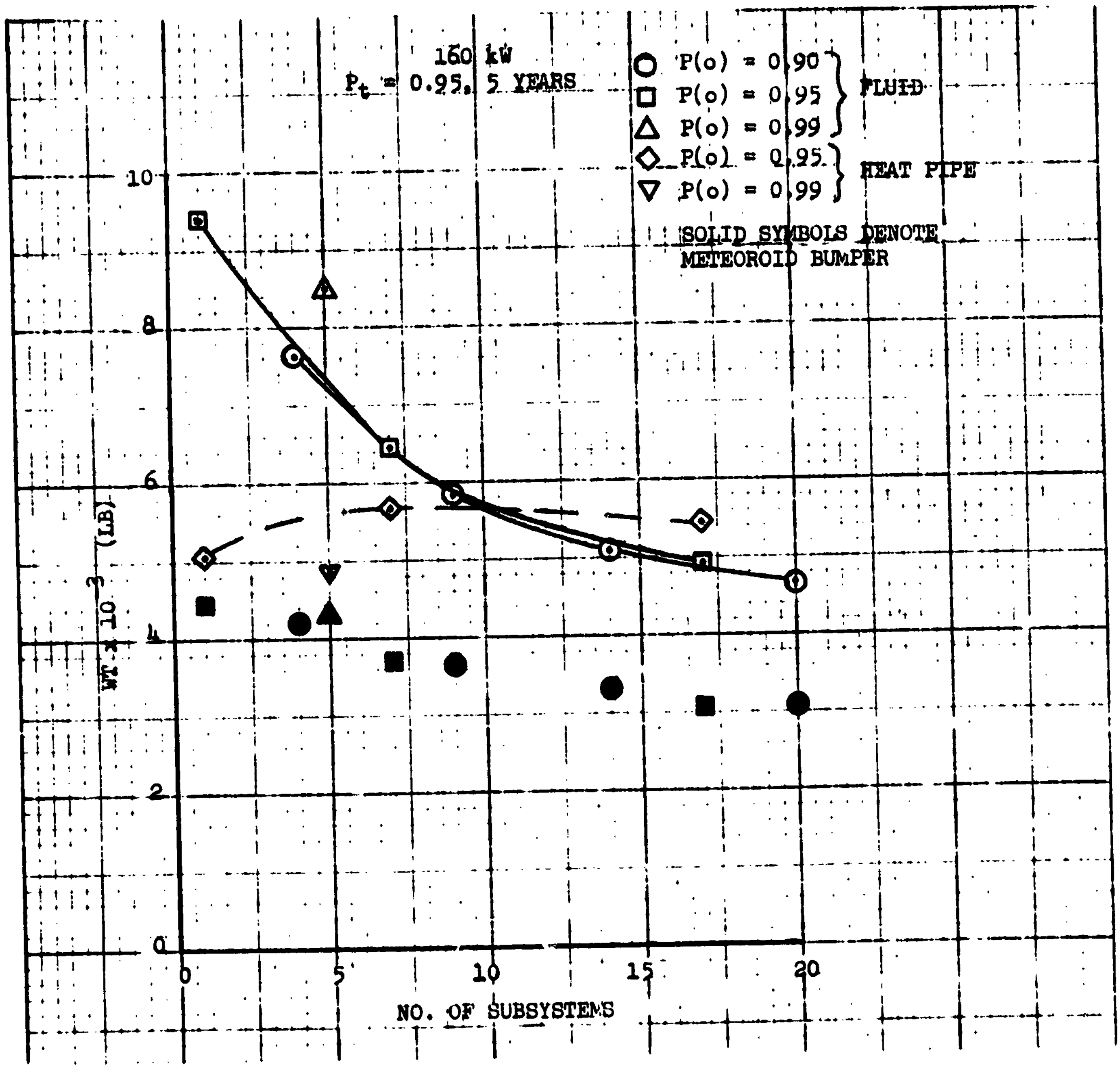
160 kW
P_t = 0.95, 5 YEARS
P(o) = 0.90
P(o) = 0.95
P(o) = 0.99
FLUID
P(o) = 0.95
P(o) = 0.99
HEAT PIPE
SOLID SYMBOLS DENOTE
METEOROID BUMPER
WT x 10^3 (LB)
0
2
4
6
8
10
0
5
10
15
20
NO. OF SUBSYSTEMS

FIGURE 40

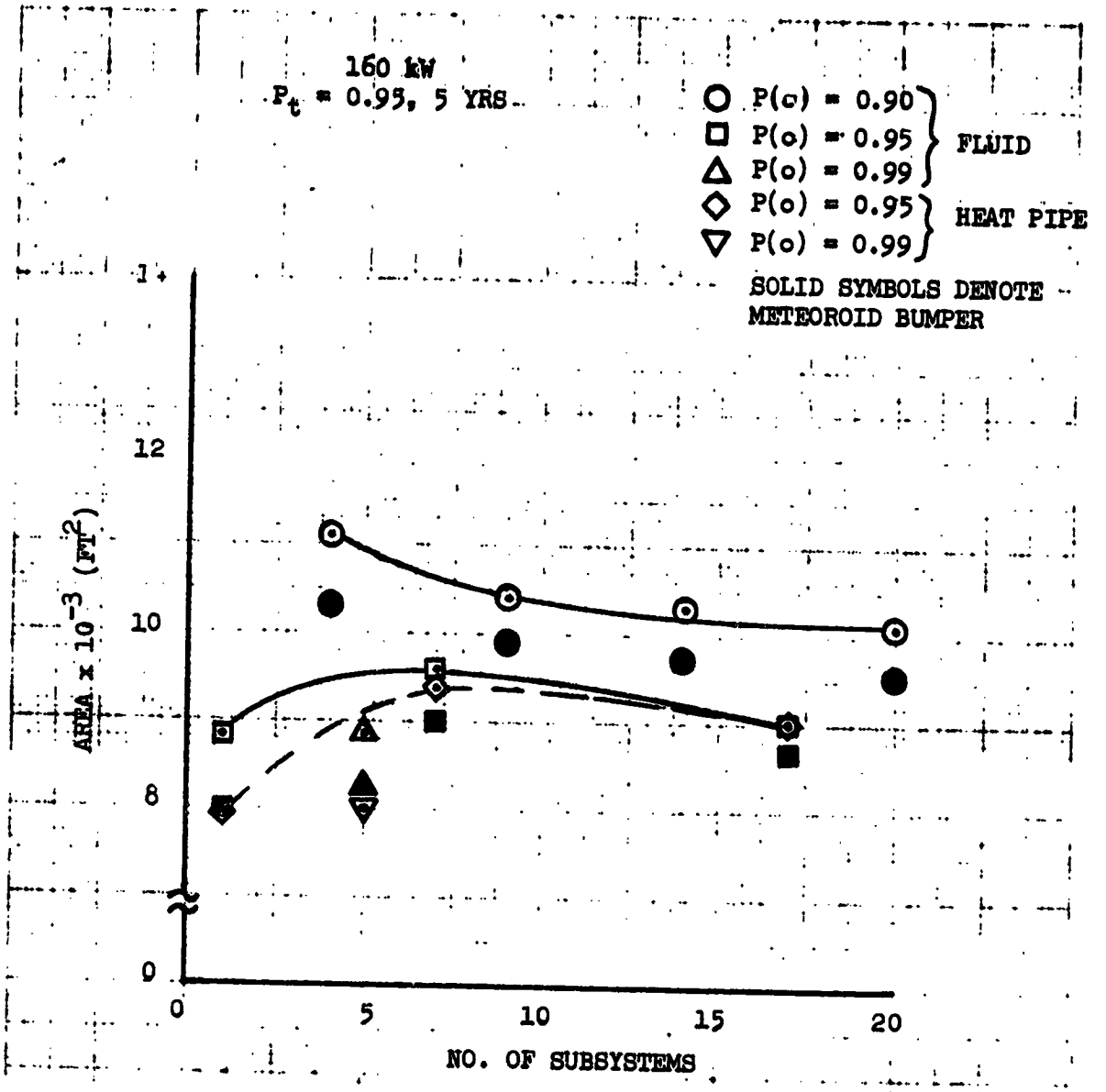
160 kW
P_t = 0.95, 5 YRS
P(o) = 0.90
P(o) = 0.95
P(o) = 0.99
FLUID
P(o) = 0.95
P(o) = 0.99
HEAT PIPE
SOLID SYMBOLS DENOTE METEOROID BUMPER
AREA x 10^{-3} (FT^2)
14
12
10
8
0
0
5
10
15
20
NO. OF SUBSYSTEMS

FIGURE 41

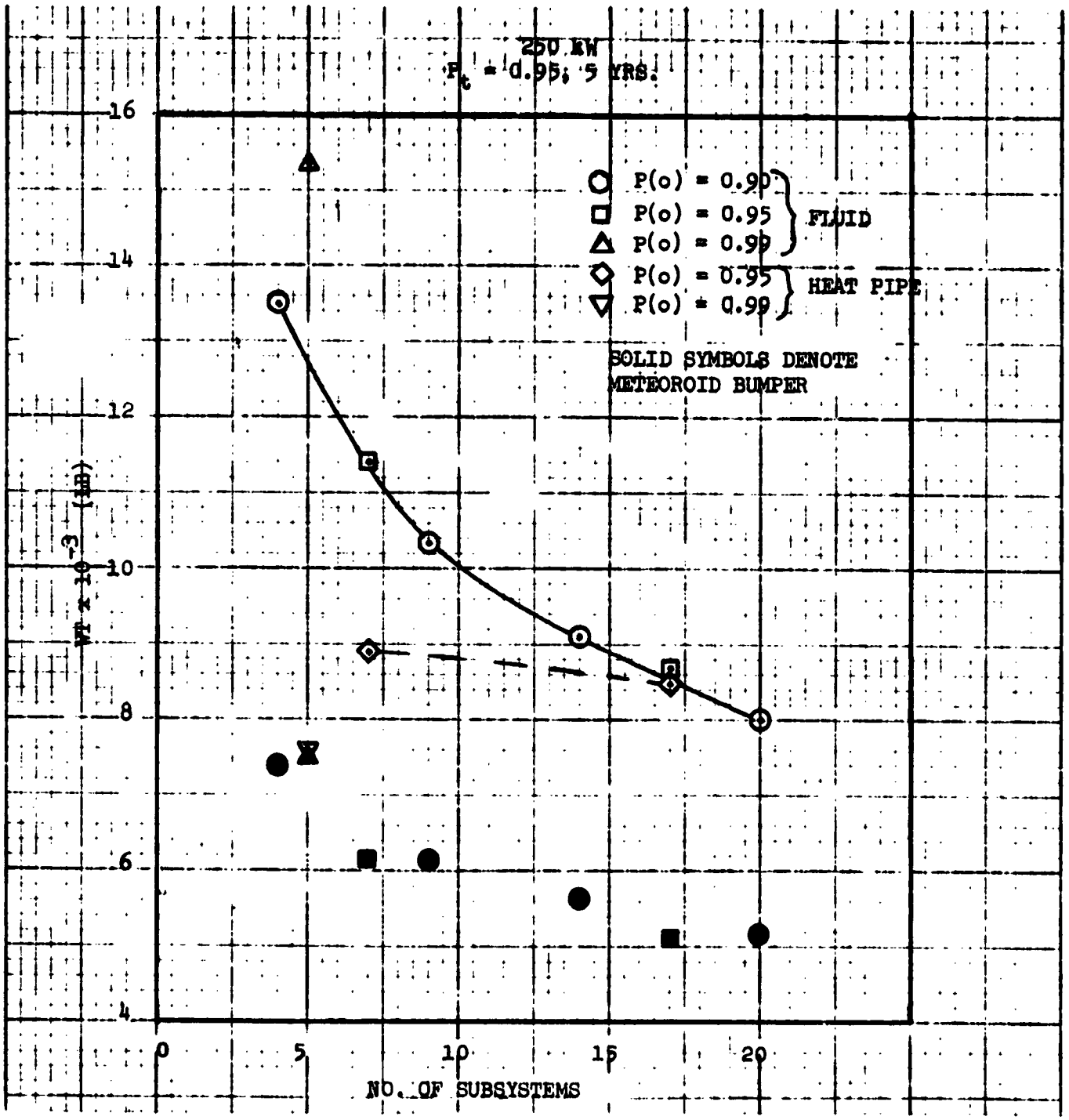

FIGURE 42

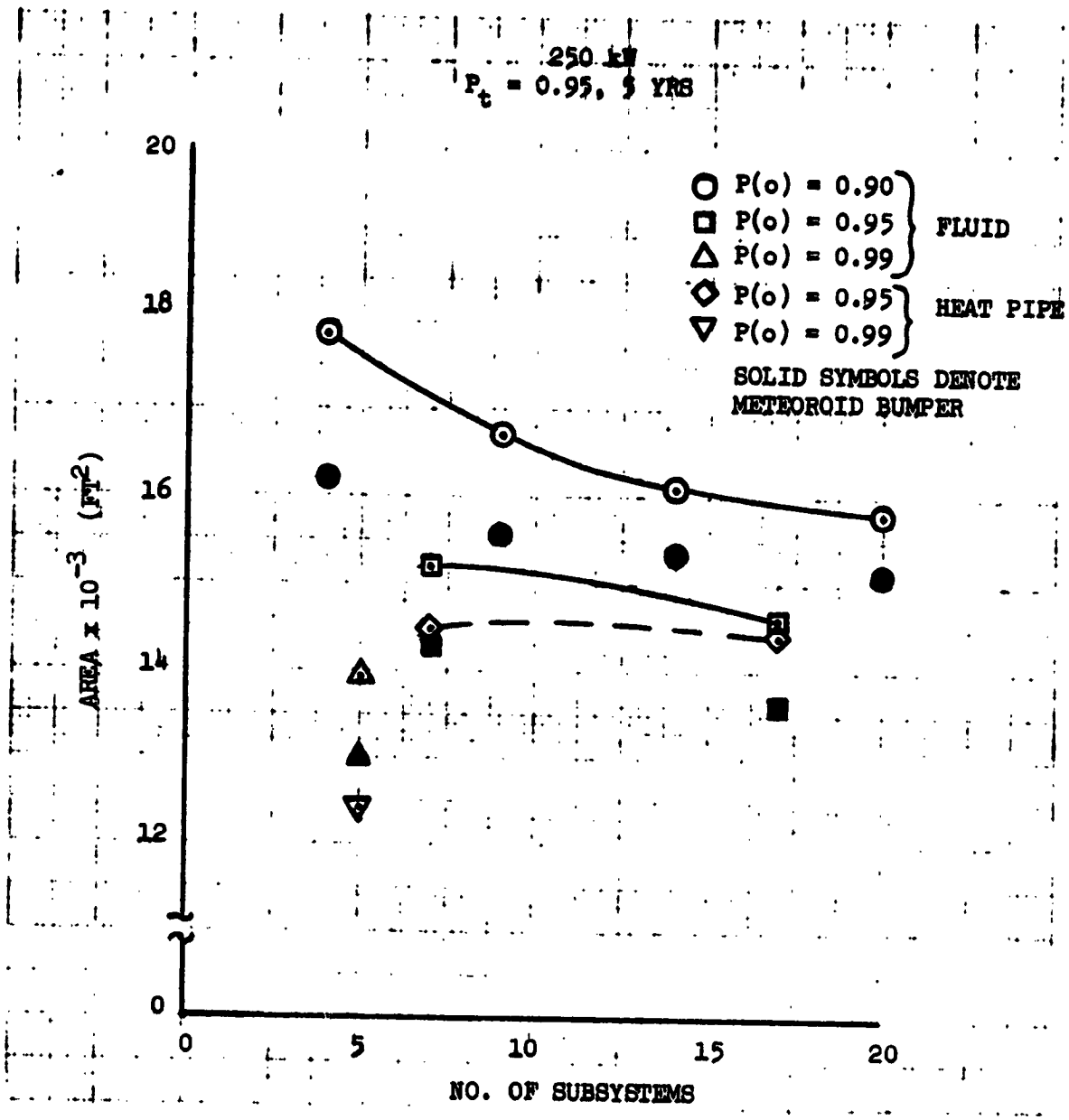

FIGURE 43

5.0 DESIGN OF A 50 KW HEAT REJECTION SYSTEM

In this section a complete heat rejection system consisting of radiators and transport loop components is analyzed to determine how the radiator design impacts the total system weight and reliability. The majority of the trade studies in this section were performed in conjunction with concurrent related projects, and is summarized here to illustrate application of the techniques developed in the previous sections. The system is made up of two radiators (for symmetrical mass distribution) and associated hardware such as flexlines and fittings, fluid lines connecting the radiators to the heat load, pumps, motors, inverters, check valves, accumulator, filter, fill and drain valves, temperature sensors, thermal control valves, and heat exchangers. Two fluid swivels are included for each radiator to permit continuous rotation of the radiators relative to the spacecraft. The system weight includes a power penalty of 200 lb/KW and a 0.65 lb/ft^2 penalty for structural support of the radiator.

Figure 44 shows typical radiator dimensions computed for this system. Since the radiator panel is relatively large, provisions are made for folding each panel in three places to facilitate stowage. Thus, with no redundant loop, the heat pipe based panel shown in Figure 44 would require 12 flex lines (3 on each manifold). A pumped fluid radiator would require only two manifolds (or 6 flex lines) per panel. Extra manifolds are required in the heat pipe design because the lengths of the heat pipes are constrained by watt-inch limitations.

Table XX gives failure rate data for state-of-the-art spacecraft heat rejection system components. Table XXI illustrates how the failure rates data is used to determine the probability that the system will not fail in a 5 year mission. For this example each independent fluid loop contains a redundant pump, and the radiator is designed so that the probability of no meteoroid puncture is 77% for each loop. The probability that the system will remain operational ranges from 64% to 68% depending on the number of flex lines required. Table XXII gives additional data showing how the system weight and reliability varies with the radiator construction, the probability of no meteoroid puncture, and the number of independent flow loops.

There are a few components in Table XXI whose relatively high failure rates add up so as to lower the reliability of the total system. Therefore, improvements in the system's probability of survival depend on whether these components can be improved or backed up by redundant counterparts. The failure rate of radiators due to micrometeoroid impact can be lowered from

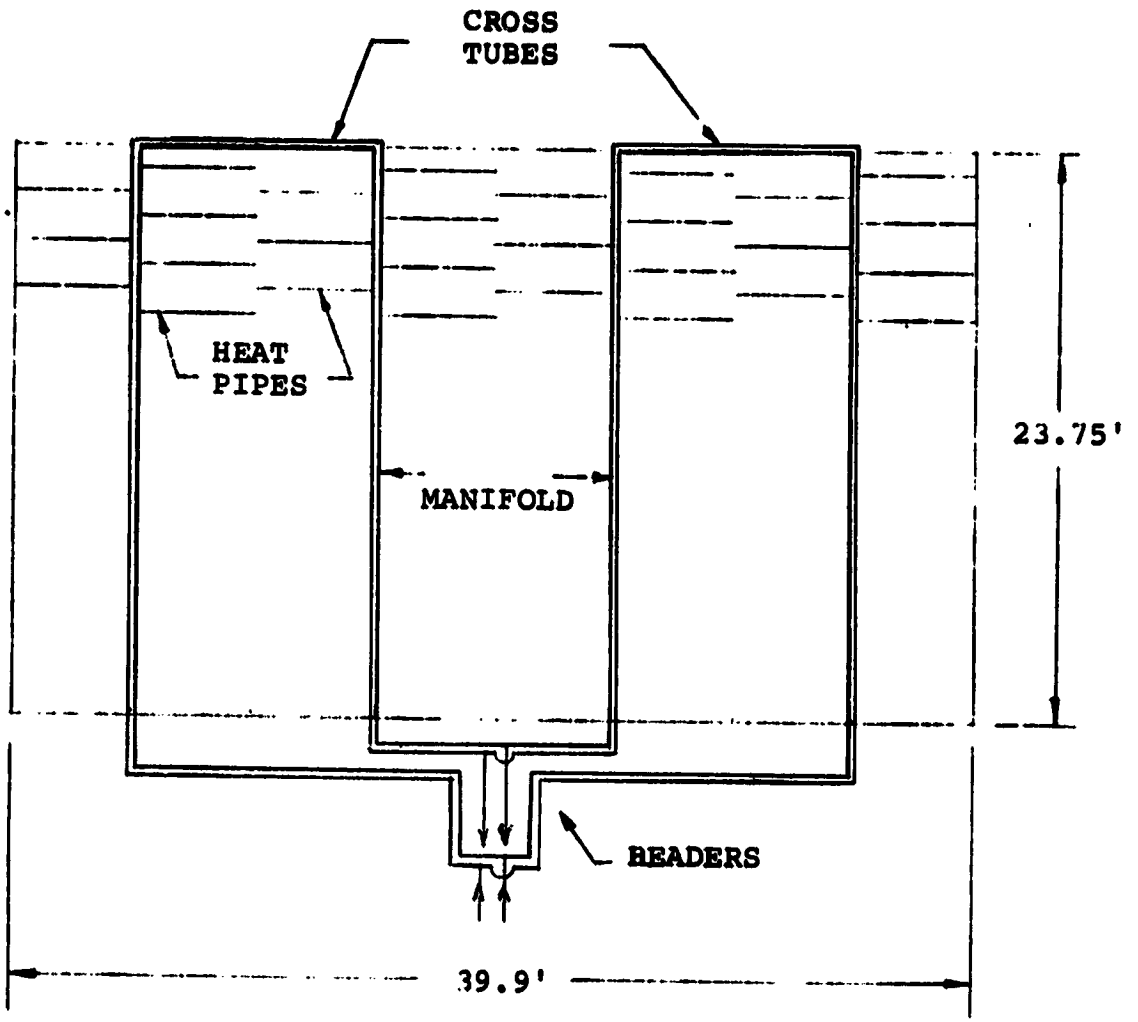

FIGURE 44

HEAT PIPE (HYBRID) 25 kW RADIATOR - 2 REQ'D
WITH REDUNDANT LOOP

TABLE XX

FAILURE RATE SOURCES FOR ANALYSES

ELEMENT	G.E.*	SUNSTRAND**	AIRESEARCH**	ESTIMATE	OTHER	ASSIGNED RATE (x 10^6 HOURS)
RADIATOR	X	-	-	X	-	0.2/PANEL
FLEX LINES, PAIR	-	-	-	X	-	0.1
TEMPERATURE CONTROL VALVE						
• ELECTRICAL	-	-	-	X	-	2.00
• SELF-CONTAINED	-	X	X	-	-	0.52
SENSORS, TEMPERATURE	X	-	-	-	-	1.5
PUMP/MOTOR	-	X	X	-	-	2.0
ACCUMULATOR/FILTER	-	-	X	-	-	0.30
SWIVEL, FLUID	-	-	-	X	-	0.5
LINES/FITTINGS	X	-	-	-	-	0.05
FILL/DRAIN VALVE	X	-	-	-	-	0.05
HEAT PIPES						
• PANEL PIPE OR HEADER	-	-	-	-	HUGHES***	0.25
• CONTROL	-	-	-	X	-	0.50
DEPLOY/LOCK	-	-	-	X	-	0.1
SPECIAL GEAR/BEARING/DRIVE	-	-	-	X	-	5.0
ELECTRONICS	-	-	-	X	SPACE SHUTTLE	0.50
INVERTER	-	-	X	-		0.24
FLEX BELLOWS (PAIR)	-	-	-	X	-	0.1

*INFORMATION FOR RELIABILITY PREDICTION REV. I, G.E., SEPT. 1964

**TELECON WITH RELIABILITY PERSONNEL 7/17/78

***HUGHES REPORT RP-E130600, DATED 5/6/76

TABLE XXI
PROBABILITY OF SUCCESS FOR 50 KW POWER MODULE
THERMAL CONTROL SYSTEM

		HEAT PIPE				PUMPED FLUID		
		$\lambda \times 10^6$	N	$N\lambda \times 10^6$		N	$N\lambda$	
A	PUMP/MOTOR	2.0	1	2.0		1	2.0	
	CHECK VALVE	0.1	1	0.1		1	0.1	
				2.1	$P_A = 0.912$		2.1	
B	INVERTER	.24	1	.24		1	.24	
	ACCUMULATOR/FILTER	.30	1	.30		1	.30	
	THERMAL CONTROL VALVE	2.0	1	2.0		1	2.0	
	FILL/DRAIN VALVE	.05	2	.10		2	.10	
	FLEX LINES	.10	36	3.6		24	2.4	
	RADIATOR TUBING	.20	2	.40		2	.40	
	METEOROID PROTECT. (RAD)	5.79	1	5.79		1	5.79	
	METEOROID PROTECT. (LINES)	1.17	1	1.17		1	1.17	
	TEMPERATURE SENSORS	1.50	2	3.0		2	3.0	
	LINES/FITTINGS	.05	40	2.0		26	1.30	
	DEPLOY/LOCK MECH.	.10	2	.20		2	.20	
	FLUID SWIVELS	.50	4	2.0	20.8	4	2.0	18.9
					$P_B = .402$			$P_B = .437$

$$P_1 = P_B(P_A^2 + 2\,Q_A P_A)$$

$$= .402(.992)$$

$$P_1 = .399$$

$$P_2 = P_1^2 + 2\,Q_1 P_1$$

$$\boxed{P_2 = 0.64}$$

$$P_1 = .437(.992)$$

$$P_1 = .434$$

$$P_2 = P_1^2 + 2\,Q_1 P$$

$$\boxed{P_2 = 0.68}$$

TABLE XXII

50 KW RADIATOR SYSTEM COMPARISONS

TYPE OF RADIATOR	NO. OF LOOPS	METEOROID SURVIVABILITY (EACH LOOP)	SYSTEM SURVIVABILITY (EACH LOOP)	SYSTEM SURVIVABILITY	RADIATOR WEIGHT (LB)	SYST WEIG (LB
HEAT PIPE	2	0.95	0.488	0.738	2481	366
	2	0.77	0.399	0.639	2394	357
	1	0.95	0.468	0.488	2409	300
PUMPED FLUID, BUMPER	2	0.95	0.531	0.780	2229	341
	2	0.77	0.434	0.580	2060	324
	1	0.95	0.531	0.531	2016	260
PUMPED FLUID, ARMOR	2	0.95	0.531	0.780	3244	442
	2	0.77	0.434	0.580	2652	383
	1	0.95	0.531	0.531	2744	333

$5.8 \cdot 10^{-6}$ to $0.22 \cdot 10^{-6}$ by increasing the wall thickness of transport loop passages so that the probability of meteoroid penetration increases from 77% to 99%. Similarly, the failure rate associated with meteoroid penetrations of connecting lines can be reduced significantly by increasing the tubing wall thickness. Redundant thermal control valves and temperature sensors can also be provided without seriously impacting the cost or complexity of the system. Complete redundant flow loops are required to avoid the limitations of flex lines or fluid swivels.

Figure 45 shows how the systems probability of failure can be reduced at the expense of added system complexity. Each of the flow loops for the systems represented in Figure 45 contains redundant elements for all components having high failure rates. Thus the system represented by the hexagonal symbols is the same as that of Table XXII except that redundant thermal control valves and temperature sensors have been added. The other systems have at least three independent transport loops for added redundancy of critical elements.

Figure 45 shows that the heat pipe based radiators and pumped fluid radiators with meteoroid bumpers have practically the same weight. However, the analyses assume that redundant flow loops can be added to the heat pipe designs without increasing the temperature drop between the fluid loop and the heat pipes. It is probable that when a design has been worked out to incorporate redundant flow loops in heat pipe radiators that some increase in radiating area and consequently weight, will be required to off-set the added thermal resistance between the transport fluid and radiating fin. Thus the weights of the heat pipe based systems in Figure 45 are probably optimistic. Additional costs for heat pipes and radiator panel fabrication would be another factor against the heat pipe design. Table XXIII summarizes some of the other factors that should be considered in trade studies for selecting a radiator design.

In summary, the design analyses for a typical 50 KW heat rejection system show that reliability problems inherent in pump loop components are more serious than those associated with the radiator panels. Unless redundant flow loops are employed, there is no justification for designing the radiator with more than 90% probability of surviving in the micrometeoroid environment. With redundant components the radiators should be designed for 95-99% survivability. Flex lines and fluid swivels should be avoided whenever possible. There is no apparent justification for employing heat pipes in a 50 KW radiator.

FIGURE 45 SYSTEM FAILURE PROBABILITIES AND WEIGHTS 50 kW POWER MODULE

- ⬡ 2 - 25 kW RADIATOR PANELS, 2 - 50 kW FLUID LOOPS, Po = 0.99
- ○ 2 - 25 kW RADIATOR PANELS, 4 - 25 kW FLUID LOOPS, Po = 0.99
- ▽ 2 - 25 kW RADIATOR PANELS, 6 - 25 kW FLUID LOOPS, Po = 0.95
- ◇ 2 - 25 kW RADIATOR PANELS, 3 - 50 kW FLUID LOOPS, Po = 0.99
- △ 4 - 25 kW RADIATOR PANELS, 4 - 25 kW FLUID LOOPS, Po = 0.99
- □ 2 - 25 kW RADIATOR PANELS, 6 - 25 kW FLUID LOOPS, Po = 0.99

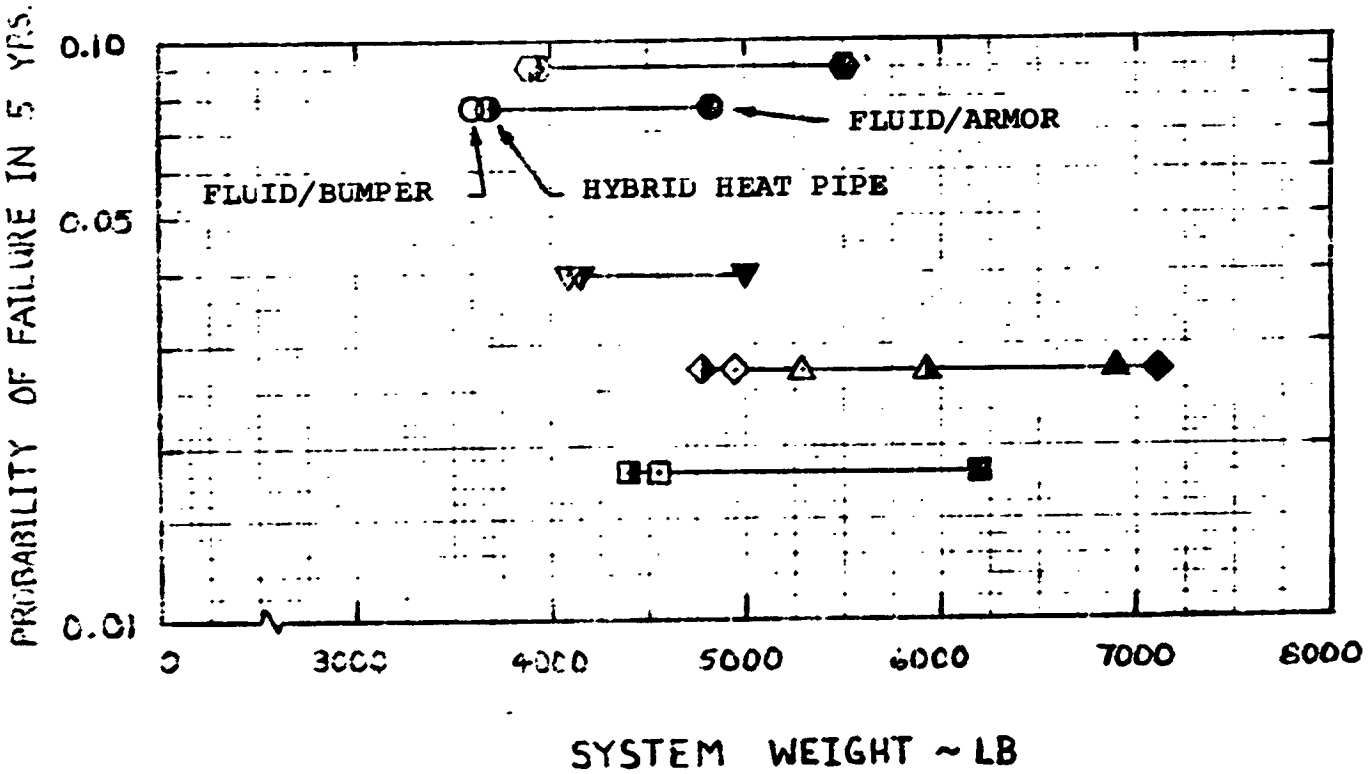

NOTE: HEAT PIPE RADIATORS NOT OVERSIZED

TABLE XXIII

COMPARISON OF PUMPED FLUID AND HEAT PIPE RADIATORS

(50 KW HEAT LOAD, REDUNDANT LOOP, 5 YEAR MISSION)

DESIGN VARIABLE	PUMPED FLUID RADIATOR (BUMPER)	PUMPED FLUID RADIATOR (ARMOR)	HEAT PIPE RADIATOR (BUMPER)
Probability of No Meteoroid Penetration of Each Fluid Loop	0.95	0.95	0.95
Weight (Excluding Structural Support)	0.58 lb/ft^2	1.05 lb/ft^2	0.66 lb/ft^2
Structural Weight (Estimated)	0.65 lb/ft^2	0.65 lb/ft^2	0.65 lb/ft^2
Armor Thickness	~	0.15 inch	~
Area Required (Optimum Design)	1756 ft^2	1887 ft^2	1921 ft^2
Potential Fabrication Problems	None	None	Manifold
Reliability Problem Areas	Fluid Loop	Fluid Loop	Fluid Loop + Manifolds + Heat Pipes
Radiator Cost Considerations	Panel Fab	Panel Fab	Panel Fab + Manifolds + Heat Pipes + Δ Engineering
Structural Requirements	Impacts Panel Design		Impact Panel + Manifolds
Impact of Redundant Flow Loop	Extra Manifold		Manifold Redesig Inefficient Heat Transfer

6.0 REFERENCES

(1) Dietz, J. B., et.al., "Basic Subsystem Module Space Radiator Study", Report No. 00977, LTV Aerospace Corp., Dallas, Texas, Aug. 1967.

(2) Leach, J. W., "Flow Instabilities in Spacecraft Radiators", Vought Report No. T169-56, Dallas, Texas, November 1974.

(3) R. W. Kurland, Private Communications, 11 October 1977

(4) Telecon between Dr. Bill Lehn of AFML, Wright Patterson Air Force Base, and Dr. J. W. Leach of Vought Corporation, 12 October 1977.

(5) NASA Contract NAS8-31906, Space Stable Thermal Control Coatings, between IIT Research Institute and NASA Marshall Space Flight Center

(6) Rittenhouse, J. B., "Meteoroids", Space Materials Handbook, 3rd ed., Addison-Wesley, Reading, Mass., 1968.

(7) Leont'ev, L. V., Tarasov, A. V., and Tereshkin, I. A., "Some Results of Research on High Velocity Impacts", NASA TT F-13, 740, August 1971.

(8) Henry, G. R., and Rand, J. L., Private Communication, Texas A&M University, Bryan, Texas, January 1977.

(9) Cour-Palais, B. G., "Meteoroid Environment Model, Near Earth to Lunar Space", NASA SP-8013, March 1969.

(10) DiBattista, J. D., and Humes, D. H., "Multi-material Lamination As A Means of Retarding Penetration and Spallation Failures in Plates", NASA TN D-6989, November 1972.

(11) R. Madden, Ballistic Limit of Double-Walled Meteoroid Bumper Systems, NASA-TN-D-3916, Langley Research Center, Langley Station, Hampton, Va., April 1967.

(12) Maiden, C. J., Gebring, J. W., McMillan, A. R., and Sennett, R. E., Experimental Investigation of Simulated Meteoroid Damage to Various Spacecraft Structures; Summary Report, NASA TR 65-48, 1965

(13) Cour-Palais, B. G., "Meteoroid Protection by Multiwall Structures", AIAA Paper No. 69-372, presented at AIAA Hypervelocity Impact Conference, Cincinnati, Ohio, April 1969.

(14) C. Robert Nysmith, "An Experimental Investigation of Aluminum Double-Sheet Structures", AIAA Paper No. 69-375, presented at AIAA Hypervelocity Impact Conference, Cincinnati, Ohio, April 1969.

(15) R. J. Arenez, "Influence of Hypervelocity Projectile Size and Density on the Ballistic Limit of Dual Sheet Structures", AIAA Paper No. 69-376, Presented at AIAA Hypervelocity Impact Conference, Cincinnati, Ohio, April 1969.

(16) A. R. McMillan, "Experimental Investigation of Simulated Meteoroid Damage to Various Spacecraft Structures", NASA-CR-915, General Motors Corp., Santa Barbara. California, Jan. 1968.

(17) DiBattista, John D. and D Humes, "Multimaterial Lamination as A Means of Retarding Penetration and Spallation Failure in Plates", NASA TN D-6989, Langley Research Center, Hampton, Va., November 1972.

(18) Lieblein, S., "Analysis of Temperature Distribution and Radiant Heat Transfer Along a Rectangular Fin of Constant Thickness", NASA TN D-196, November 1959.

(19) J. A. Oren and C. L. Wiggins, "Design Analysis for Surveillance Satellite Thermal Control Systems," AFFDL-TR-3009, Vought Corporation, February 1979.

APPENDIX A

LISTING OF COMPUTER PROGRAM FOR OPTIMIZATION OF PUMPED FLUID RADIATORS WITH ARMOR PROTECTION FOR MICROMETEOROIDS

```
      PROGRAM RADB(INPUT,OUTPUT,TAPE5=INPUT,TAPE6=OUTPUT)
      DIMENSION FLUID (2)
  503 FORMAT(3F5.3)
  504 FORMAT(F7.3,F6.1,2F6.3)
  505 FORMAT(2A10)
  506 FORMAT(1H1,18H  RADIATOR FLUID =,2A10,/)
  510 FORMAT(I2,2F6.3)
  600 FORMAT(//,8H  Q(KW)=,F7.2,14H  TIME(YEARS)=,F7.3,7H  P(I)=,F6.3)
  605 FORMAT(52H     TBC        SC        TBM        SM        TBH        SH)
  610 FORMAT(10H  T IN(F)=,F7.2,11H  T OUT(F)=,F7.2,11H  T AMB(F)=,F7.2)
  615 FORMAT(34H     TBS        SS        TS        SM)
  620 FORMAT(43H  DELTA P (MANIFOLD)/DELTA P (CROSS TUBE) =,F6.3)
  630 FORMAT(30H  PUMP POWER PENALTY (LB/KW) =,F7.3)
  635 FORMAT(19H  PUMP EFFICIENCY =,F6.3)
  640 FORMAT(50H  AREA FACTOR IN OPTIMIZATION PARAMETER (LB/FT2) =,F8.4)
  650 FORMAT(8H  E BAR=,F7.4,7H  ZE.4=,F7.4,13H  : COATING =,F8.5)
  655 FORMAT(5H  MU=,F8.3,15H LB/FT/HR  RHO=,F8.3,11H LB/FT3  K=,F8.4,15
     1H B/HR/FT/F  CP=,F7.4,7H B/LB/F)
  660 FORMAT(7(1X,F8.4))
  665 FORMAT(1X,F8.1,4(1X,F8.4),/)
  670 FORMAT(63H MAN DIA  HEAD DIA   WALL T   FIN T   DELTA P  RE/1000
     1   WT/A)
  680 FORMAT(52H    WT M      WT CT     WT H      WT F      WT FL     WT P)
  690 FORMAT(42H      A         EFF        W          NL         NS)
  730 FORMAT(4X,3HL/W,5X,5HN FIN,6X,1HS,8X,1HD,8X,1HL,6X,5HM DOT,6X,1HF)
      READ(5,505) FLUID
      READ(5,504) XMU,RHO,XK,CP
      READ(5,500) Q,TIME,P0
      READ(5,500) TIN,TOUT,TAMB
      READ(5,500) XK1,XK2,XK3
      READ(5,500) XE,Z,TC
      READ(5,500) XNP
      READ(5,510) NQ
      SIG=.1714/(10.**8)
      PR=(CP*XMU/XK)**.33333
      RHOM=173.
      RM=SQRT(RHOM/62.4)
      XKM=10.
      PI=3.14159
      CW=RHOM*PI/144.
      CR=1./PI/XK
      CRE=.8./PI/XMU
      PL=ALOG(P )
      TI=TIN+460.
      TO=TOUT+460.
      TA=TAMB+460.
      D1=ALOG((TI-TA)*(TO+TA)/(TI+TA)/(TO-TA))
      D2=ATAN(TI/TA)-ATAN(TO/TA)
      DL=ALOG((TI**4-TA**4)/(TO**4-TA**4))
      D4=(D1/4.-D2/2.)/TA**3
      CF=3.*SIG*XE*(((TI+TO)/2.)**3.)/XKM
      Q=Q/2.
      DO 100 MQ=1,NQ
```

ORIGINAL PAGE IS
OF POOR QUALITY

```
      Q=2.*Q
      WRITE(6,506) FLUID
      WRITE(6,655) XMU,RHO,XK,CP
      WRITE(6,660) Q,TIME,PJ
      WRITE(6,610) TIN,TOUT,TAMB
      WRITE(6,620) XK1
      WRITE(6,630) XK2
      WRITE(6,635) XNP
      WRITE(6,640) XK3
      WRITE(6,650) XE,Z,TC
      WRITE(6,730)
      WRITE(6,670)
      WRITE(6,605)
      WRITE(6,615)
      WRITE(6,680)
      WRITE(6,690)
      XNL=0.
      DO 100 INL=1,4
      XNL=XNL+1.
      F4=100.
      XN=.7
      DXN=.05
      DO 99 I=1,2
    1 XN=XN+DXN
      CN=XN*XE*SIG
      Y=1.-XN
      X=(.0307+.7925*Y+.705*Y*Y)*SQRT(Y)
      S=2.
      DS=1.
      F3=100.
      DO 96 J=1,3
    3 S=S+DS
      IF(S.GE.0.) GO TO 103
      DS=DS/2.
      S=-DS
  103 SF=S/12.
      DELTA=CF*((SF/X)**2.)
      F2=100.
      D=.02
      DD=.01
      DO 93 K=1,4
    4 D=D+DD
      IF(D.GE.0.) GO TO 104
      DD=DD/2.
      D=-DD
  104 CD=.336/RHO/((10.*D)**5)
      XM=100.*D
      DXM=XM/2.
      F1=100.
      DO 90 L=1,5
    5 XM=XM+.X4
      IF(XM.GE.0.) GO TO 105
```

```
      DXM=DXM/2.
      XM=-DXM
  105 RE=CRE*XM/D
      IF(RE-2300.) 10,10,20
   10 XNU=4.
      XF=64./RE
      DR=.00357*RE**.8
      GO TO 50
   20 IF(RE-6000.) 30,30,40
   30 XNU=.116*(RE**.6857-125.)*PR
      XF=.184/(RE**.2)
      DR=1.234
      GO TO 50
   40 XNU=.023*RE**.8*PR
      XF=.184/(RE**.2)
      DR=1.234
   50 R=CR/XNU
      D3=CN*SF*R*DL
      CT=(TI-TO)/(C4+D3)
      A=3414.*Q/CN/CT
      XL=XM*CP*(TI-TO)/CT/CN/SF
      CAPL=XNL*XL
      W=A/CAPL
      YLW=CAPL/W
      DR=(DR*W**2.6/(XK1*SF**1.8*XL))**.2083
      DF=CD*XM*XM*XL*XF
      DIAM=DR*D
      IF(XNL-3.) 51,51,52
   51 DIAM=DIAM
      GO TO 53
   52 DR=(((CAPL-XL)**1.8)*(CAPL+4.6*XL)/XK1/W/(XL**1.8))**.2083
      DIAM=.5146*DIAM*DR
   53 AF=L/SF+.IAM*(XNL+.544)/CAPL+2.*DIAM*(CAPL-XL)/A
      T=.1388*((-Z*TIME*A*AR/PL)**.29)/SQRT(RHOM)
      DIAS=.772*DIAM
      DM=.2866*((-Z*TIME*AR*A/PL)**.2748)
      TS=.01*TM
      IF(TS.LT.0.005) TS=.005
      TX=TS/DM
      C1=-2.*TX
      C2=.1741*RM*(TX**1.528)
      C3=-16.522/RM/(TX**.528)
      C4=2.39*C2
      C5=1.39*C3
      C6=-.5*DM*C3
      C7=DM*((-C3/2.)**.7194)
      SX=10.
      YD=D/DM
      DO 2 I=1,4
  201 SX=SX*(YD-C1-C2*SX**2.39-C3/SX**1.39)/(C4*SX**1.39-C5/SX**2.79)
      TBC=C6/(SX**1.39)
      SX=20.
```

```
      YC=DIAM/DM
      DO 2.2 IS=1,4
  202 SX=SX+(YC-C1-C2*SX**2.39-C3/SX**1.39)/(C4*SX**1.39-C5/SX**2.39)
      TBM=C6/(SX**1.39)
      SX=2J.
      YC=DIAS/DM
      DO 203 IS=1,4
  203 SX=SX+(YC-C1-C2*SX**2.39-C3/SX**1.39)/(C4*SX**1.39-C5/SX**2.39)
      TBS=C6/(SX**1.39)
      SX=20.
      YC=DIAH/DM
      DO 2.4 IS=1,4
  204 SX=SX+(YC-C1-C2*SX**2.39-C3/SX**1.39)/(C4*SX**1.39-C5/SX**2.39)
      TBH=C6/(SX**1.39)
      IF(TBC.LT.0.02) TBC=.02
      IF(TBM.LT.0..2) TBM=.02
      IF(TBH.L .0.02)  BH=.02
      IF(TBS.LT.0.02) TBS=.02
      SC=C7/((TBC/DM)**.7194)
      SM=C7/((TBM/DM)**.7194)
      SH=C7/((TBH/DM)**.7194)
      SS=C7/((TBS/DM)**.7194)
      WP=.00005423*XK2*XM*CP/RHO/SF/XL/XNP
      WCT=CW*(TBC*(D+TBC)+TS*(D+2.*(TBC+SC)+TS))/SF
      WM=CW*(TBM*(DIAM+TBM)+TS*(DIAM+2.*(TBM+SM)+TS))*(XNL-1.)
      WM=(WM+2.*CW*(TBS*(LIAS+ BS)+TS*(DIAS+2.*(TBS+SS)+TS)))/CAPL
      WH=CW*(TBH*(DIAH+TBH)+TS*(DIAH+2.*(TBH+SH)+TS))*2.*(1./W-XL/A)
      WF=RHOM*(TC+DELTA)/12.
      WFL=DIAM*DIAM*(1./XL+.544/CAPL)+DIAH*DIAH*2.*(1./W-XL/A)+D*D/S
      WFL=RHO*F1*WFL/576.
      WT=WM+WCT+WH+WF+WFL+WP
      WT=WT+WM+WCT+WH+WFL
      XEF=XN/(1.+U3/D4)
      F=(W. +XK3)/XEF
      IF(F1-F) 80,70,70
   70 F1=F
      GO TO 5
   80 F1=F
   9: DXM=-DXM/2.
      IF(F2-F) 92,91,91
   91 F2=F
      GO TJ 4
   92 F2=F
   93 DD=-DD/2.
      IF(F3-F) 95,94,94
   94 F3=F
      GO TJ 3
   95 F3=F
   96 DS=-DS/2.
      IF(F4-F) 98,97,97
   97 F4=F
      GO TJ 1
```

```
 98 F4=F
 99 DXN=-DXN/2.
    RRE=RE/1 .?.
    XLL=A/W/XL
    XSS=A/SF
    WRITE(6,603) YLW,XN,S,D,XL,XM,F
    WRITE(6,65 ) DIAM,DIAH,T,DELTA,DP,RRE,WT
    WRITE(6,60 ) TBL,SC,T3M,SM,,BM,SH
    WRITE(6,6  ) TBS,SS,TS,DM
    WRITE(6,660) WM,WCT,WH,WF,WFL,WP
    WRITE(6,665) A,XEF,W,XLL,XSS
100 CONTINUE
    STOP
    END
```

APPENDIX B

LISTING OF COMPUTER PROGRAM FOR OPTIMIZATION OF PUMPED FLUID RADIATORS WITH BUMPER PROTECTION FOR MICROMETEOROIDS

```
      PROGRAM RADD(INPUT,OUTPUT,TAPE5=INPUT,TAPE6=OUTPUT)
      DIMENSION FLUID (2)
  500 FORMAT(5F6.3)
  504 FORMAT(F7.2,F6.1,2F6.3)
  505 FORMAT(2A10)
  506 FORMAT(1H1,18H  RADIATOR FLUID =,2A10,/)
  510 FORMAT(I2,2F6.3)
  600 FORMAT(//,8H  Q(KW) =,F7.2,14H  TIME(YEARS)=,F7.3,7H  P(0)=,F6.3)
  610 FORMAT(1H  T IN(F) =,F7.2,11H  T OUT(F)=,F7.2,11H  T AMB(F)=,F7.2)
  620 FORMAT(43H  DELTA P (MANIFOLD)/DELTA P (CROSS TUBE) =,F6.3)
  630 FORMAT(34H  PUMP POWER PENALTY (LB/KW) =,F7.3)
  635 FORMAT(19H  PUMP EFFICIENCY =,F6.3)
  640 FORMAT(54H  AREA FACTOR IN OPTIMIZATION PARAMETER (LB/FT2) =,F8.4)
  650 FORMAT(8H  E BAR=,F7.4,7H  ZETA=,F7.4,13H  T COATING =,F8.5)
  655 FORMAT(5H  MU=,F8.5,15H LB/FT/HR  RHO=,F8.3,11H LB/FT3  K=,F8.4,15
     1H B/HR/FT/F  CP=,F7.4,7H B/LB/F)
  660 FORMAT(7(1X,F8.4))
  665 FORMAT(1X,F9.1,4(1X,F8.4),/)
  670 FORMAT(63H MAN DIA  HEAD DIA   WALL T   FIN T   DELTA P  RE/1000
     1   WT/A)
  680 FORMAT(52H   WT M     WT CT     WT H      WT F      WT FL     WT P)
  690 FORMAT(42H      A        EFF       W         NL         NS)
  730 FORMAT(4X,3H_/W,5X,5HN FIN,6X,1HS,8X,1HD,8X,1HL,6X,5HM DOT,6X,1HF)
      READ(5,505) FLUID
      READ(5,504) XMU,RHO,XK,CP
      READ(5,500) Q,TIME,P0
      READ(5,500) TIN,TOUT,TAMB
      READ(5,500) XK1,XK2,XK3
      READ(5,504) XE,Z,TC
      READ(5,500) XNP
      READ(5,510) NQ
      SIG=.1714/(10.**8)
      PR=(CP*XMU/XK)**.33333
      RHOM=170.
      XKM=100.
      PI=3.14159
      CW=RHOM*PI/144.
      CR=1./PI/XK
      CRE=49./PI/XMU
      PL=ALOG(P0)
      TI=TIN+460.
      TO=TOUT+460.
      TA=TAMB+460.
      D1=ALOG((TI-TA)*(TO+TA)/(TI+TA)/(TO-TA))
      D2=ATAN(TI/TA)-ATAN(TO/TA)
      DL=ALOG((TI**4-TA**4)/(TO**4-TA**4))
      D4=(DL/4.-D2/2.)/TA**3
      CF=3.*SIG*XE*(((TI+TO)/2.)**3.)/XKM
      Q=Q/2.
      DO 10. MQ=1,NQ
      Q=2.*Q
      WRITE(6,506) FLUID
      WRITE(6,655) XMU,RHO,XK,CP
```

```
      WRITE(6,603) Q,TIME,P0
      WRITE(6,611) TIN,TOUT,TAMB
      WRITE(6,620) XKA
      WRITE(6,630) XN2
      WRITE(6,635) XNP
      WRITE(6,640) XKB
      WRITE(6,650) XE,Z,TC
      WRITE(6,700)
      WRITE(6,670)
      WRITE(6,680)
      WRITE(6,690)
      F5=100.
      XNL=0.
  101 XNL=XNL+1.
      F4=100.
      XN=.7
      DXN=.05
      DO 99 I=1,2
    1 XN=XN+DXN
      CN=XN*XE*SIG
      Y=1.-XN
      X=(.99907+.7925*Y+.75*Y*Y)*SQRT(Y)
      S=2.
      DS=1.
      F3=100.
      DO 96 J=1,3
    3 S=S+DS
      IF(S.GT.0.) GO TO 103
      DS=DS/2.
      S=-DS
  103 SF=S/12.
      DELTA=CF*((SF/X)**2.)
      F2=100.
      D=0.9
      DD=.1
      DO 95 K=1,4
    4 D=D+DD
      IF(D.GT.0.) GO TO 104
      DD=DD/2.
      D=-DD
  104 CD=.336/R40/((1.-D)**5)
      XM=100.*D
      DXM=XM/2.
      F1=1.0.
      DO 9( L=1,5
    5 XM=XM+DXM
      IF(XM.GT.0.) GO TO 105
      DXM=DXM/2.
      XM=-DXM
  105 RE=CRE*XM/3
      IF(RE-2300.) 10,10,2.
   10 XNU=4.
      XF=64./RE
```

```
      DR=.0[illegible]57*RE**.8
      GO TO 5
    2 IF(RE-6000.) 30,30,4
    3 XNU=.116*(RE**.6667-125.)*PR
      XF=.184/(RE**.2)
      DR=1.234
      GO TO 5
    4 XNU=.023*RE**.8*PR
      XF=.184/(RE**.2)
      DR=1.234
    5 R=DR/XNU
      D3=CN*SF*R*D
      CT=(TI-TO)/(D4+D3)
      A=3414.*Q/CN/CT
      XL=XM*CP*(TI-TO)/CT/CN/SF
      CAPL=XNL*XL
      H=A/CAPL
      YLW=CAPL/H
      DR=(DR*W**2.8/(XK1*SF**1.8*XL))**.2083
      DP=CD*XM*XM*XL*XF
      DIAM=DR*D
      IF(XNL-3.) 51,51,52
   51 DIAH=DIAM
      GO TO 53
   52 DR=(((CAPL-YL)**1.8)*(CAPL+4.6*XL)/XK1/W/(XL**1.8))**.2083
      DIAH=.5146*DIAM*DR
   53 AR=D/SF+DIAM*(XNL+.544)/CAPL+2.*DIAH*(CAPL-XL)/A
      F=.1388*((-Z*TIME*A*AR/PL)**.29)/SQRT(RHOM)
      WP=.0000[illegible]5423*XK2*XM*DP/RHO/SF/XL/XNP
      WM=CW*T*(T*(XNL+1.)+DIAM*(XNL+.544))/CAPL
      WCT=CW*T*(T+D)/SF
      WF=RHOM*(TC+DELTA)/12.
      WH=CW*T*(DIAH+T)*2.*(1./W-XL/A)
      WFL=DIAM*DIAM*(1./XL+.544/CAPL)+DIAH*DIAH*2.*(1./W-XL/A)+D*D/S
      WFL=RHO*PI*WFL/576.
      WT=WM+WCT+WH+WF+WFL+WP
      XEF=XN/(1.+D3/D4)
      F=(WT+XK3)*XEF
      IF(F1-F) 90,70,70
   70 F1=F
      GO TO 5
   80 F1=F
   90 DXM=-DXM/2.
      IF(F2-F) 92,91,91
   91 F2=F
      GO TO 4
   92 F2=F
   93 DD=-DD/2.
      IF(F3-F) 95,94,94
   94 F3=F
      GO TO 3
   95 F3=F
```

```
   96 DS=-DS/2.
      IF(F4-F) 98,97,97
   97 F4=F
      GO TO 1
   98 F4=F
   99 DXN=-DXN/2.
      RRE=RE/1000.
      XLL=A/W/X.
      XSS=W/SF
      WRITE(6,660) YLW,XN,S,D,XL,XM,F
      WRITE(6,660) DIAM,DIAH,T,DELTA,DP,RRE,WT
      WRITE(6,660) WM,WCT,WH,WF,WFL,WP
      WRITE(6,663) A,XEF,W,XLL,XSS
      IF(F5-F) 106,106,102
  102 F5=F
      GO TO 101
  106 F5=F
      IF(XNL.LT.4.5) GO TO 101
  100 CONTINUE
      STOP
      END
```

APPENDIX C

HEAT PIPE LENGTH OPTIMIZATION

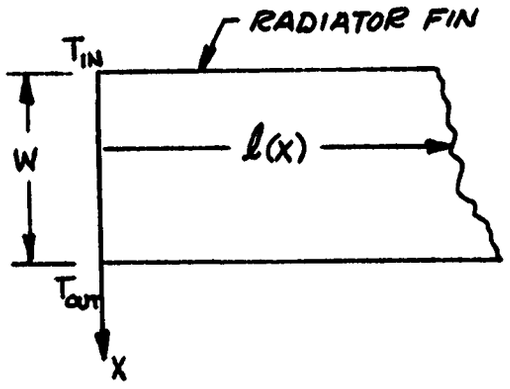

T_{IN}, T_{OUT}, W FIXED

DETERMINE $\ell(x)$ TO MINIMIZE A.

$$A = \int_0^W \ell \, dx = \int_{T_{IN}}^{T_{OUT}} \frac{\ell}{\left(\frac{dT}{dx}\right)} dT$$

$$\frac{dT}{dx} = \frac{-\varepsilon \eta \bar{\varepsilon} \sigma \ell}{\dot{m} c_p} \left(T^4 - T_\infty^4\right)$$

$$\varepsilon \equiv \frac{1}{1 + \frac{4 \eta \bar{\varepsilon} \sigma \ell T^3}{u_o \ell_e}}$$

$$A = \int_{T_{IN}}^{T_{OUT}} \frac{-\ell \dot{m} c_p \, dT}{\varepsilon \eta \bar{\varepsilon} \sigma \ell \left(T^4 - T_\infty^4\right)} = \frac{-\dot{m} c_p}{\eta \bar{\varepsilon} \sigma} \int_{T_{IN}}^{T_{OUT}} \frac{dT}{\varepsilon \left(T^4 - T_\infty^4\right)}$$

$$A = \frac{\dot{m} c_p}{\eta \bar{\varepsilon} \sigma} \left\{ \int_{T_{OUT}}^{T_{IN}} \frac{dT}{\left(T^4 - T_\infty^4\right)} + \frac{4 \eta \bar{\varepsilon} \sigma}{u_o \ell_e} \int_{T_{OUT}}^{T_{IN}} \frac{\ell T^3 dT}{\left(T^4 - T_\infty^4\right)} \right\}$$

CONSTRAINT

$$W = \int dx = \int_{T_{IN}}^{T_{OUT}} \frac{dT}{\left(\frac{dT}{dx}\right)} = \frac{\dot{m} c_p}{\eta \epsilon \sigma} \left\{ \int_{T_{OUT}}^{T_{IN}} \frac{dT}{\ell (T^4 - T_\infty^4)} + \frac{4 \eta \epsilon \sigma}{u_o \ell_e} \int_{T_{OUT}}^{T_{IN}} \frac{T^3 dT}{(T^4 - T_\infty^4)} \right\}$$

LET

$$F = \frac{1 + \frac{4 \eta \epsilon \sigma}{u_o \ell_e} \ell T^3}{T^4 - T_\infty^4}$$

$$G = \frac{1 + \frac{4 \eta \epsilon \sigma}{u_o \ell_e} \ell T^3}{\ell (T^4 - T_\infty^4)}$$

$H = F + \lambda G$ where λ = Lagrange multiplier

EULERS EQUATION

$$\frac{d}{dT}\left(\frac{\partial H}{\partial \ell}\right) - \frac{\partial H}{\partial \ell} = 0$$

$$\frac{\partial H}{\partial \ell} = \frac{\frac{4 \eta \epsilon \sigma}{u_o \ell_e} T^3}{T^4 - T_\infty^4} + \lambda \left(\frac{-1}{\ell^2 (T^4 - T_\infty^4)} \right) = 0$$

$$\ell^2 = \frac{\lambda}{\frac{4\eta\bar{\epsilon}\sigma}{u_o A_e} T^3} \quad ; \quad \ell = C T^{-3/2} \tag{1.}$$

$$W = \frac{\dot{m} c_p}{\eta\bar{\epsilon}\sigma}\left\{\frac{1}{C}\int_{T_{OUT}}^{T_{IN}} \frac{T^{3/2}\,dT}{T^4 - T_\infty^4} + \frac{\eta\bar{\epsilon}\sigma}{u_o \ell_e} \ln\left(\frac{T_{IN}^4 - T_\infty^4}{T_{OUT}^4 - T_\infty^4}\right)\right\}$$

$$W - \frac{\dot{m} c_p}{u_o \ell_e} \ln\left(\frac{T_{IN}^4 - T_\infty^4}{T_{OUT}^4 - T_\infty^4}\right) = \frac{\dot{m} c_p}{\eta\bar{\epsilon}\sigma}\,\frac{1}{C}\int_{T_{OUT}}^{T_{IN}} \frac{T^{3/2}\,dT}{T^4 - T_\infty^4}$$

$$C = \frac{\frac{\dot{m} c_p}{\eta\bar{\epsilon}\sigma}\int_{T_{OUT}}^{T_{IN}} \frac{T^{3/2}\,dT}{T^4 - T_\infty^4}}{W - \frac{\dot{m} c_p}{u_o \ell_e} \ln\left(\frac{T_{IN}^4 - T_\infty^4}{T_{OUT}^4 - T_\infty^4}\right)} \tag{2}$$

$$\frac{\ell\,(40°F)}{\ell\,(100°F)} = \left(\frac{560}{500}\right)^{3/2} = 1.185$$

FOR ℓ = CONSTANT = $\bar{\ell}$

$$W = \frac{\dot{m} c_p}{\eta\bar{\epsilon}\sigma}\left\{\frac{1}{\bar{\ell}}\int_{T_{OUT}}^{T_{IN}} \frac{dT}{T^4 - T_\infty^4} + \frac{\eta\bar{\epsilon}\sigma}{u_o \ell_e} \ln\left(\frac{T_{IN}^4 - T_\infty^4}{T_{OUT}^4 - T_\infty^4}\right)\right\}$$

$$W = \frac{\dot{m} c_p}{\eta \bar{\varepsilon} \sigma} \left\{ \frac{1}{C} \int_{T_{OUT}}^{T_{IN}} \frac{T^{3/2}\, dT}{T^4 - T_\infty^4} + \frac{\eta \bar{\varepsilon} \sigma}{u_o \ell_e} \ln\left(\frac{T_{IN}^4 - T_\infty^4}{T_{OUT}^4 - T_\infty^4} \right) \right\}$$

$$\frac{1}{C} \int_{T_{OUT}}^{T_{IN}} \frac{T^{3/2}\, dT}{T^4 - T_\infty^4} = \frac{1}{\bar{\ell}} \int_{T_{OUT}}^{T_{IN}} \frac{dT}{T^4 - T_\infty^4}$$

$$\frac{C}{\bar{\ell}} = \frac{\displaystyle\int_{T_{OUT}}^{T_{IN}} \frac{T^{3/2}\, dT}{T^4 - T_\infty^4}}{\displaystyle\int_{T_{OUT}}^{T_{IN}} \frac{dT}{T^4 - T_\infty^4}}$$

$$\frac{A(\ell)}{A(\bar{\ell})} = \frac{\displaystyle\int_{T_{OUT}}^{T_{IN}} \frac{dT}{(T^4 - T_\infty^4)} + \frac{4\eta \bar{\varepsilon} \sigma}{u_o \ell_e} \int_{T_{OUT}}^{T_{IN}} \frac{C\, T^{3/2}\, dT}{(T^4 - T_\infty^4)}}{\displaystyle\int_{T_{OUT}}^{T_{IN}} \frac{dT}{(T^4 - T_\infty^4)} + \frac{4\eta \bar{\varepsilon} \sigma}{u_o \ell_e} \frac{C \displaystyle\int_{T_{OUT}}^{T_{IN}} \frac{dT}{T^4 - T_\infty^4}}{\displaystyle\int_{T_{OUT}}^{T_{IN}} \frac{T^{3/2}\, dT}{T^4 - T_\infty^4}} \int_{T_{OUT}}^{T_{IN}} \frac{T^3\, dT}{T^4 - T_\infty^4}}$$

$$\frac{A(\ell)}{A(\bar{\ell})} = \frac{1 + \dfrac{4\eta\bar{\epsilon}\sigma C}{u_o \ell_e} \dfrac{\displaystyle\int_{T_{OUT}}^{T_{IN}} \frac{T^{3/2}\,dT}{(T^4 - T_\infty^4)}}{\displaystyle\int_{T_{OUT}}^{T_{IN}} \frac{dT}{(T^4 - T_\infty^4)}}}{1 + \dfrac{4\eta\bar{\epsilon}\sigma C}{u_o \ell_e} \dfrac{\displaystyle\int_{T_{OUT}}^{T_{IN}} \frac{T^{3}\,dT}{(T^4 - T_\infty^4)}}{\displaystyle\int_{T_{OUT}}^{T_{IN}} \frac{T^{3/2}\,dT}{(T^4 - T_\infty^4)}}}$$

$$\frac{A(\ell)}{A(\bar{\ell})} = \frac{1 + \dfrac{4\eta\bar{\epsilon}\sigma \bar{\ell}}{u_o \ell_e} \left[\dfrac{\displaystyle\int_{T_{OUT}}^{T_{IN}} \frac{T^{3/2}\,dT}{(T^4 - T_\infty^4)}}{\displaystyle\int_{T_{OUT}}^{T_{IN}} \frac{dT}{(T^4 - T_\infty^4)}}\right]^2}{1 + \dfrac{4\eta\bar{\epsilon}\sigma \bar{\ell}}{u_o \ell_e} \dfrac{\displaystyle\int_{T_{OUT}}^{T_{IN}} \frac{T^{3}\,dT}{(T^4 - T_\infty^4)}}{\displaystyle\int_{T_{OUT}}^{T_{IN}} \frac{dT}{T^4 - T_\infty^4}}}$$

$$\int_{T_{OUT}}^{T_{IN}} \frac{dT}{T^4 - T_\infty^4} = \frac{1}{4T_\infty^3} \ln\left[\left(\frac{T_{OUT} + T_\infty}{T_{OUT} - T_\infty}\right)\left(\frac{T_{IN} - T_\infty}{T_{IN} + T_\infty}\right)\right]$$

$$+ \frac{1}{2T_\infty^3}\left[\tan^{-1}\left(\frac{T_{OUT}}{T_\infty}\right) - \tan^{-1}\left(\frac{T_{IN}}{T_\infty}\right)\right]$$

$$\int_{T_{OUT}}^{T_{IN}} \frac{T^3 dT}{T^4 - T_\infty^4} = \frac{1}{4} \ln\left(\frac{T_{IN}^4 - T_\infty^4}{T_{OUT}^4 - T_\infty^4}\right)$$

$$\int_{T_{OUT}}^{T_{IN}} \frac{T^{3/2} dT}{T^4 - T_\infty^4} = \text{NUMERICAL SOLUTION}$$

SIMPSONS RULE: $\int_{x_0}^{x_2} f(x)\,dx = \frac{h}{3}\left[f(x_0) + 4f(x_1) + f(x_2)\right]$

$$\int_{40}^{100} \frac{T^{3/2} dT}{T^4 - T_\infty^4} = \frac{10}{3}\left(688.8 \times 10^{-8}\right) = 2.296 \times 10^{-5}$$

$$\int_{40}^{100} \frac{T^3 dT}{T^4 - T_\infty^4} = \frac{1}{4} \ln\left[\frac{535.704}{177.254}\right] = 0.27650$$

$$\int_{40}^{100} \frac{dT}{T^4 - T_\infty^4} = \frac{10^{-6}}{2(97.336)}\left[\frac{1}{2}\ln\left[\left(\frac{960}{40}\right)\left(\frac{100}{1020}\right)\right] + \left[\tan^{-1}\left(\frac{500}{460}\right) - \tan^{-1}\left(\frac{560}{460}\right)\right]\right]$$

$$= 1.9096 \times 10^{-9}$$

FOR $\varepsilon = 0.7 = \frac{1}{1.42857}$; $\frac{4\eta\bar{\varepsilon}\sigma\bar{l}}{u_o l_e}(510)^3 = 0.42857$

$$\frac{4\eta\bar{\varepsilon}\sigma l}{u_o A_e} = \frac{0.42857}{(510)^3} = 3.2308 \times 10^{-9}$$

$$\frac{A(l=\text{variable})}{A(l=\bar{l})} = \frac{1 + 3.2308\times10^{-9}\left[\frac{2.296\times10^{-5}}{1.9096\times10^{-9}}\right]^2}{1 + 3.2308\times10^{-9}\left[\frac{0.27680}{1.9096\times10^{-9}}\right]} = \frac{1.467056}{1.467802} = 0.99949$$